Thermal Modeling of an Electric Vehicle Soft Magnetic Composite Permanent Magnet Synchronous Motor

Muhammet Talha Mercan

A Thesis

In The Department

of

Electrical and Computer Engineering

Presented in Partial Fulfillment of the Requirements

for the Degree of

Master of Applied Science (Electrical and Computer Engineering) at

Concordia University

Montréal, Québec, Canada

November 2023

CONCORDIA UNIVERSITY
SCHOOL OF GRADUATE STUDIES

This is to certify that the thesis prepared

By: Muhammet Talha Mercan

Entitled: Thermal Modeling of an Electric Vehicle Soft Magnetic Composite Permanent Magnet Synchronous Motor

and submitted in partial fulfillment of the requirements for the degree of

Master of Applied Science (Electrical and Computer Engineering)

complies with the regulations of this University and meets the accepted standards with respect to originality and quality.

Signed by the final examining committee:

_____ Chair
Dr. Chunyan Lai

_____ Internal Examiner
Dr. Rabindranath Raut

_____ Supervisor
Dr. P. Pillay

Approved by: _____
Dr. Yousef R. Shayan, Chair
Department of Electrical and Computer Engineering

_____
Dr. Mourad Debbabi, Dean,
Faculty of Engineering and Computer Science

ABSTRACT

Thermal Modeling of an Electric Vehicle Soft Magnetic Composite Permanent Magnet Synchronous Motor

Muhammet Talha Mercan

Today, with the increasing impacts of the climate change, sustainable solutions are being searched for in many areas. Demand is increasing in the fields of energy, health, housing and transportation to meet the needs of developing economies and growing populations. In these areas, studies are being carried out to reduce the use of fossil fuels and for renewable solutions. Various solutions are being worked on for the transportation sector, which is the second biggest factor in terms of carbon emissions. One of the most important steps is electric vehicles. Electric vehicle density is increasing day by day both to reduce dependence on fossil fuels and for an environmental solution.

One of the most important steps of this evolution in transportation is the types of motors used in vehicles. The replacement of internal combustion engines by electric motors has brought about various research topics. Today, Permanent Magnet Synchronous Motors have become one of the most preferred models with the many advantages they provide for electric vehicles. With its high-power density, high efficiency, ability to reach high speeds and compact size, it has become a suitable motor for electric vehicles. In addition to all these benefits, there are also some challenges that need to be solved. Thermal design is crucial to avoid the negative effects of temperature rise for high power generating motors in small sizes. In order to perform all these analyses, it is necessary to design thermal modeling to determine the temperature limits and design the cooling system.

In this thesis, the thermal equivalent models of two different PMSMs were analyzed and proposed by using the Lumped Parameter Network Method to predict temperature rise during operation. In addition, the motors were tested with real-time experiments and supported by simulation results. The thermal models analyzed for the two different motors were analyzed to compare the temperature differences and to analyze the geometry in terms of temperature distribution and suitability.

ACKNOWLEDGEMENTS

I would like to express my deepest gratitude to my supervisor Dr. Pragasen Pillay, who provided me with all kinds of support throughout my master's education, guided me in my studies, showed me light on an unfamiliar path and gave me the opportunity to work with him. In addition to his supervision, I would like to express my endless gratitude for acting like a friend and a father and making me feel like I was in a family environment.

Also, I would like to present my deepest gratitude to the Ministry of National Education of Türkiye and the Ministry of Energy and Natural Resources of Türkiye for sponsoring all my expenses during my education life, for providing me with one of the best education opportunity thousands of kilometers away from my country, and to the Republic of Türkiye for giving me this opportunity.

I would like to send my heartfelt feelings to my brother Tolga, who has shared many experiences, offered me his friendship inside and outside the school and has been my companion for two years.

I would like to thank my colleague Amir, who has been my partner throughout my work and provided me with all kinds of support, for being with me on this challenging path. I would like to express my sincerest regards to Dr. Akrem and Dr. Mathews who observed us in all my experiments and ensured that our work proceeded safely.

I also would like to sincerely thank my colleagues in the PEER group lab. Nazanin, Mohanraj, Tamamwe, Neetusha, Bassam, Rao, Gael and Soliha.

Finally, I would like to wholeheartedly express my appreciation to my wife Tugce, who has always supported me and held my hand on this path of spiritual ups and downs.

Table of Contents

List of Figures

List of Tables

Nomenclature

BEV	Battery Electric Vehicle
BLDC	Brushless DC
CFD	Computational Fluid Dynamics
DAQ	Data Acquisition
DC	Direct Current
EV	Electric Vehicle
FCEV	Fuel Cell Elektric Vehicle
FEA	Finite Element Analysis
HEV	Hybrid Electric Vehicle
ICE	Internal Combustion Engine
IPMSM	Inset Permanent Magnet Synchronous Motor
LPTN	Lumped Parameter Network Method
PHEV	Plug-in Hybrid Electric Vehicle
PMSM	Permanent Magnet Synchronous Motor
R&D	Research and Development
SMC	Soft Magnetic Composite
SPMSM	Surface Permanent Magnet Synchronous Motor
SRM	Switched Reluctance Motor
WTW	Well to Wheel

1. INTRODUCTION

Our ecosystem, environment, and general quality of life have been seriously threatened by the growing worldwide worry that is titled climate change and global warming. It is currently one of the most urgent problems facing the entire planet [1]. Both indirect and direct temperature consequences, influences of extreme weather events like droughts, floods, and storms, effects of the spread of diseases that are sensitive to the climate, effects of inadequate quality of air, and other impacts on the health of people can all be categorized as climate change's effects on human wellness [2]. Also, economy as well as nature and humanity are impacted by global warming [3]. While there are many causes of global warming, the transportation sector, which includes a variety of modes of transportation such as light heavy and light duty applications, vehicles, trucks, ships, planes, buses, and trains, is a significant cause of this concern. With the guidance of the transportation industry, societies are able to connect, commute, and conduct global trade. However, the dependence of fossil fuels like petrol and diesel has had a negative impact on the ecosystem. The burning of fossil fuels in vehicles results large atmospheric emissions of carbon dioxide (CO2), methane (CH4), and nitrous oxide (N2O). These heat-trapping greenhouse gases cause global warming and other environmental problems. Research shows that the transportation sector is the second most influential category in global carbon dioxide emissions after the power sector [4]. In addition, researchers predict that the vehicle numbers will grow rapidly in the next decades due to a growing population, a booming economy, and the development of the transportation sector [5]. Also economically, the price of fossil fuels is increasing day by day and governments are planning to reduce fuel consumption by introducing new taxes. All these developments have pushed the transportation sector to find sustainable solutions. Reducing carbon emissions is seen as one of the most important steps to minimize the effects of global warming. Consequently, due to electrically powered vehicles' eco-friendly zero CO2 emission qualities, the number of light duty vehicles depending on fossil fuels, such as oil, petrol, etc., needs to be replaced in order to avoid the rise in CO2 emissions [6]. This is why one of the newest study areas nowadays is the development of electrically dominated vehicle drive systems. Additionally, governments, automakers, and customers worldwide are increasingly promoting electric vehicles due to a sharp shift in the climate and concerns over other environmental issues [7]. Despite its disadvantages, electric vehicles can bring a sustainable solution to the

transportation sector as they have renewable options and provide sustainable alternative solutions. One of the details that make electric vehicles clean and sustainable is their electric motors. These motors, which have been used in different areas of the industry for a long time, continue to be developed for traction applications today. The most common type of electric motors used in various types of electric vehicle applications today is the Permanent Magnet Synchronous Motors. PMSM motors have become one of the most important parts of electric vehicles with their torque, speed, power density and efficiency advantages. On the other hand, it has brought some challenges due to its compact structure. Due to its ability to provide high power in small sizes and its complex structure, heating problems have arisen. In order to solve all these problems, a suitable cooling system must be designed. In order to design this system, it is necessary to predict the temperature parameters before the production phase and apply cooling according to these temperature limits. If an inadequate cooling system is integrated, the motor may experience problems due to high temperatures. Theoretical approaches for various thermal analyses have been made in the literature. In this thesis, the Lumped Parameter Network Method, which is an analytical method, is studied. Temperature parameters of two different motors with almost the same power rating are analyzed by applying the LPTN method. In addition, simulations and real-time experiments are compared with the simulation and real-time experiments to investigate the applicability of the analytical model to simple and complex motors.

1.1. Sustainable Solution for Transportation: Electric Vehicles

Numerous significant issues and difficulties have been brought due to the increasing usage of fossil fuels in transportation, both locally and globally, such as air pollution, energy dependency, sustainability challenges and depletion of energy resources [8]. As a solution to all these problems, one of the issues that is growing in popularity today is the innovative solutions offered by electrified vehicles [9]. In terms of preventing climate change and developing a more sustainable transportation system, electric vehicles are an essential aspect [10]. A vehicle type known as an Electric Vehicle (EV) is one that operates on electricity for transportation rather than internal combustion engines that burn gasoline or diesel fuel [11]. These vehicles do not need conventional internal combustion engines that burn fossil fuels because they are powered by electricity stored in large batteries. The outcome is a more sustainable, cleaner type of transportation with a number of important advantages. Electric vehicles have no emissions,

making them a green mode of transportation. So, people can get a chance to reduce their carbon footprint by driving an electric vehicle. In addition, the carbon footprint of electric vehicles is directly related to the source of electricity. The use of renewable energy resource reduces emissions from vehicles that obtain cleaner energy from the grid compared to internal combustion engines, which are less efficient and lose an important amount of energy as heat, they transfer a higher percentage of the energy from the power source to generate power at the wheels. Also, EVs are becoming more accessible and useful as technology develops. Expanding the network of chargers makes it easier to charge EVs at home, at work, and while on the go. In addition, the use of various types of electric vehicles has been paved with the developing technology. In addition to being fully electric, hybrid electric vehicles have also been developed. Electric vehicles can be used directly with an electric motor, or they can be used in hybrid form with conventional engines [12]. There are four electric vehicle types. These are Battery Electric Vehicles (BEVs), Hybrid Electric Vehicles (HEVs), Plug-in Hybrid Electric Vehicles (PHEVs) and Fuel-cell Electric Vehicles (FCEVs). Electric vehicles have the potential to completely change our method of travel. EVs are desirable alternatives to conventional cars due to their improved fuel efficiency and minimal emissions. Overall, electric vehicles offer a cleaner, quieter, and more energy-efficient way to get from point A to point B while assisting in protecting our planet for future generations. They also represent a sustainable and forward-thinking solution to our transportation needs.

- Battery Electric Vehicles (BEVs): Fully electric cars are known as BEVs since they only use power that has been stored in powered lithium-ion or other types of batteries. They have no emissions generated by the exhaust system and only use facilities for charging [13].
- Plug-in Hybrid Electric Vehicles (PHEVs): PHEVs combine an internal combustion engine with an electric motor. They have a limited all-electric range and can be charged from a power source. They switch to the gasoline engine or another fuel source when the battery runs out, providing more flexibility while decreasing reliance on fossil fuels [14].
- Hybrid Electric Vehicles (HEVs): HEVs have an electric motor in addition to an internal combustion engine. They cannot be plugged in to charge, but they do use the IC engine and regenerative braking to charge a small battery that helps the car accelerate and enhances fuel economy [15].

- Fuel Cell Electric Vehicles (FCEVs): In a fuel cell stack, hydrogen is chemically transformed into electricity by FCEVs as a fuel source. The car is then driven by an electric motor using this electricity [16].

1.2. Comparison of Electric Vehicles & Conventional Vehicles

The decision between conventional petrol or diesel-powered cars and electric vehicles (EVs) has grown in importance for consumers in the age of environmental consciousness and sustainable living [17]. It is critical to fully understand the distinctions between these two categories of vehicles as global worries over climate change and air quality grow. First, from an environmental point of view, the effect that your vehicle choice will have on the environment is one of the most important factors. Internal combustion engines that burn fossil fuels like petrol or diesel to power conventional cars release pollutants and greenhouse gases into the atmosphere. On the other side, electric cars use electricity that has been stored in batteries and have no emissions from their tailpipes. Because of this important contrast, EVs are a better option for lowering carbon footprints and improving air quality, especially in cities [18]. In terms of fuel consumption, electric cars usually use less energy than their gasoline-powered equivalents. The high level of heat loss during the energy conversion of fossil fuel engines causes a serious decrease in their efficiency [19]. The most important detail in the efficiency of electric vehicles is that they use electric machines. These motors have high efficiency in energy conversion [20]. Therefore, compared to conventional cars, EVs often have more effective energy efficiency and can go further on a unit of energy. Additionally, long-term operational costs for EVs often are lower. They cost less to maintain and repair since they contain fewer moving parts [21]. The cost of fuel is often lower with electricity than with petrol or diesel [22]. On the other hand, the range for driving of EVs on a single charge is a common source of worry. Range may still be a concern for people who routinely drive long distances, despite recent significant improvements. However, this particular issue is being addressed by the development of infrastructure for charging globally [23]. In addition to the growing number of public chargers, many EV owners now use normal electrical outlets or faster home charging equipment to recharge their vehicles at home [24]. Also, in terms of simplicity of fueling up, traditional cars have a long-standing advantage. Refueling facilities for petrol and diesel are numerous and practically everywhere. EV drivers, on the other hand, might need to plan their travels around charging outlets, which may be less common, especially in rural locations. However, this problem is being addressed by the development of

charging infrastructure globally. Also, long charging times are another disadvantage [25]. While conventional vehicles can fill their tanks in a short time, electric vehicles can take a long time to charge. It is important to develop fast charging stations to eliminate this disadvantage. Today, charging stations have been developed with the capacity to fill the battery in less than 30 minutes [26]. These developments may soon eliminate this problem for electric vehicles. One of the most important issues of nowadays is that when connected to the grid, electric vehicles can function as mobile energy storage units, increasing grid stability and allowing the use of vehicle batteries for energy storage during periods of peak demand [27]. While there are many benefits to using electric vehicles, it's crucial to remember that there are also drawbacks, including a lack of sufficient charging infrastructure, concern about range, and the negative effects of battery manufacturing and recycling on the environment. However, these benefits make electric vehicles a key technology in the search for more sustainable, effective, and environmentally friendly transportation. All these comparisons are with pros and cons, electric cars have become known for their quick acceleration and quiet, smooth ride because to their instant torque delivery. Conventional vehicles adjust to various driving preferences with a wide range of engine types and performance levels. A strong V8 engine may still be preferred by some enthusiasts, but many find the EV's quiet operation and quick response to be an advantage.

1.3. The Global Electric Vehicle Numbers

The use of electric vehicles is increasing day by day due to advancing technology, increased production, access to raw materials and technology, and decreasing prices. The most important factors that electric vehicle users consider when choosing an electric vehicle are the range, power and price performance of the vehicle [28]. The development of the production range and the increase in the variety of vehicles has enabled all kinds of users to find the vehicle they need. From scooters to three-wheelers, from cars to buses, from trucks to trains, and even in airplanes, electric motors have started to be used [29]. According to the International Energy Agency, between 2017 and 2022, sales of electric vehicles increased nearly 9 times, from around 1.3 million to around 10.3 million. In 2023, electric vehicle sales are projected to increase by around 40 percent compared to the previous year, reaching 13.9 million. USA, where nearly one million electric vehicles have been sold, ranks third. In the rest of the world, around 0.6 million vehicles were sold, suggesting that other countries should give more attention to this issue. The highest rate of electric vehicle sales was recorded in Norway. Almost 88 percent of the vehicles sold

were electric vehicles. Around 60 percent of the electric vehicles registered in 2022 are in China [30]. The number of electric vehicles globally reached almost 30 million last year, with nearly half of these vehicles in China. According to the data, the number of electric vehicles almost doubles every year compared to the previous year. If the trend continues, we will see more than a hundred million electric vehicles on the road in the next five years.

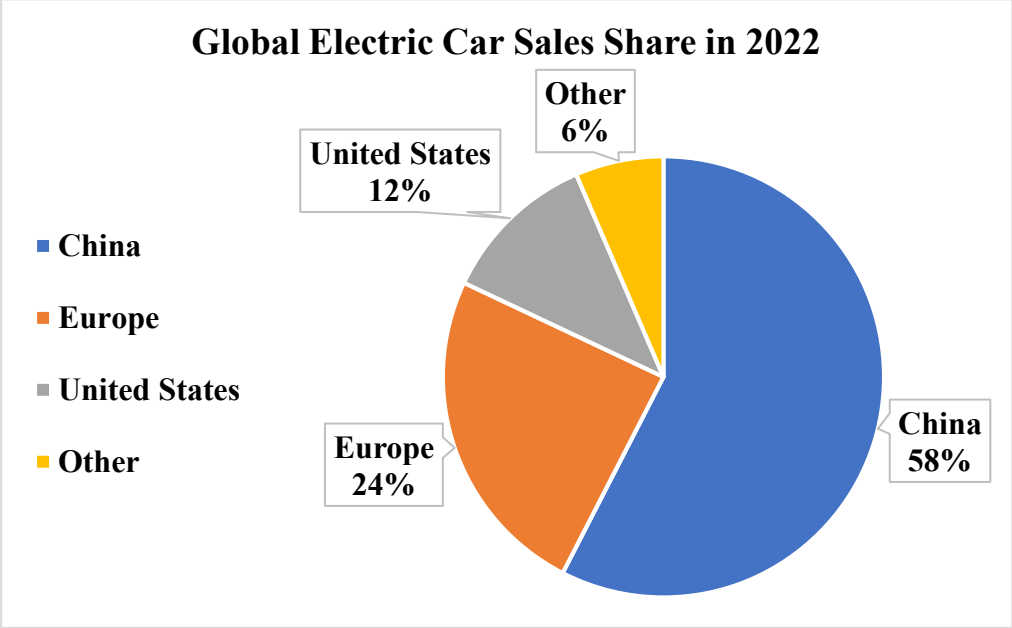

Figure 1.1. Global Electric Car Sales in 2022.

As can be seen in the Figure 1.1, in countries with the highest economic figures, such as China, Europe and the United States, electric vehicle sales are approximately 94 percent [31]. The fact that other countries are so far behind in the number of electric vehicles shows that they should pay more attention to this issue. In particular, large Asian countries such as Japan and India, countries with developing economies such as Türkiye and South Africa, and South American countries have great potential for increasing the number of electric vehicles. On the other hand, the use of electric vehicles has led to significant changes in terms of energy use and this potential is growing. Globally, electric vehicles consumed 110 TWh of electricity in 2022, accounting for almost 0.5 percent of global electricity use. The use of electric vehicles has

reduced the use of fossil fuels by about 1 percent. These data show that there is still much more potential. With investments in innovation and R&D and increased awareness, electric vehicles will increase in number and contribute to sustainable transportation on a global level in the coming years. On a brand basis, China-based BYD company has accounted for 17.5 percent of the electric vehicles sold in 2022. In second place is Tesla with a share of 12.5 percent [32]. In 2022, the best-selling electric vehicle in Canada was the Tesla Model 3. It ranked first with 10922 sales figures. This model was followed by the Chevrolet Bolt model with 5674 sales. The brands of the 10 best-selling vehicles in Canada are Tesla, Chevrolet, Hyundai, Ford, Ford, Volkswagen, Nissan, Kia and Mini Cooper [33].

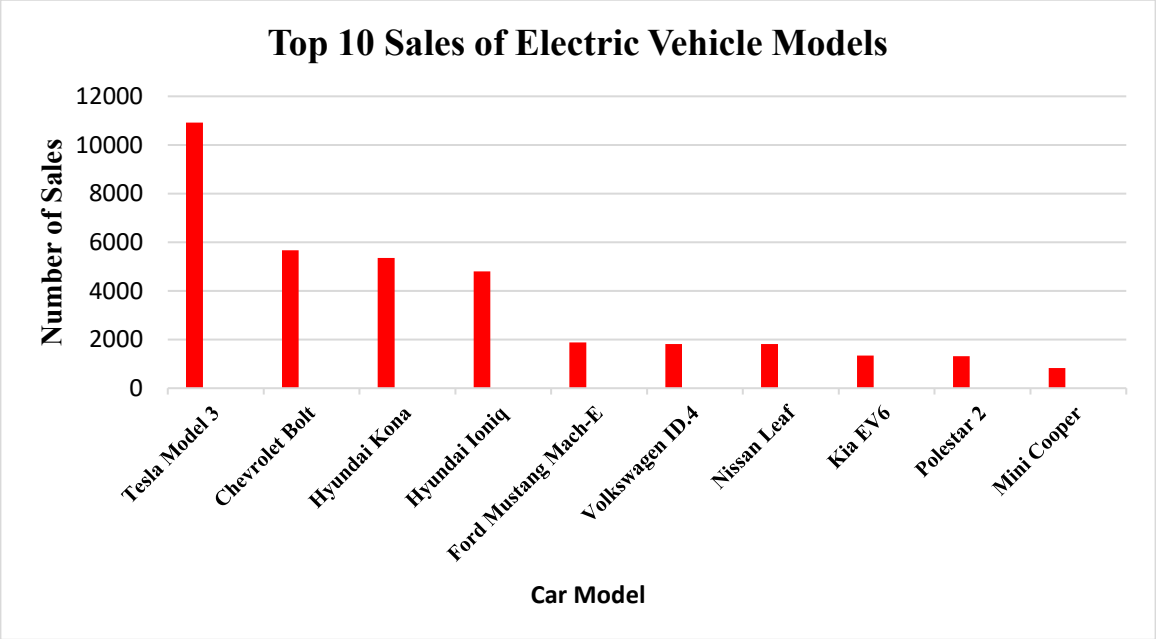

Figure 1.2. Electric Car Sales in Canada in 2022

1.4. Well-To-Wheels Energy Efficiency Comparison Between IC-Powered Vehicles and Electric Vehicles

Well-to-wheel (WTW) is a comprehensive approach used to assess the life cycle and total energy consumption of a primary energy source up to the point of use. For vehicles, WTW refers to the cycle of energy from raw materials until it is transferred to the wheels. Given the high

efficiency of electric vehicles, the use of electrical energy, a tertiary energy source, reduces WTW efficiency. The fuel journey that starts with the primary energy source is converted into electrical energy using renewable and non-renewable energy sources. These energy transformations can be obtained from renewable energy sources such as solar panels, wind turbines, dams, or power plants using natural gas, diesel, gasoline and nuclear fuel. This electrical energy is then transferred to the grid via transmission lines and the electric vehicle is charged. During charging, this electrical energy is transferred to the battery and stored as chemical energy. The chemical energy is then converted into electrical energy and transferred to the motor. Energy losses in the generation, transmission and utilization of energy reduce overall efficiency [34]. In general, the use of various resources during the conversion of fuel into electrical energy results in variable efficiencies between 20 percent and 75 percent. Considering that the average transmission losses worldwide are ten percent, the efficiency drops below 70 percent at best. Considering that battery efficiency is 85 percent on average and motor efficiency is 90 percent, we can say that the WTW efficiency of electric vehicles varies between 13 and 54 percent [35].

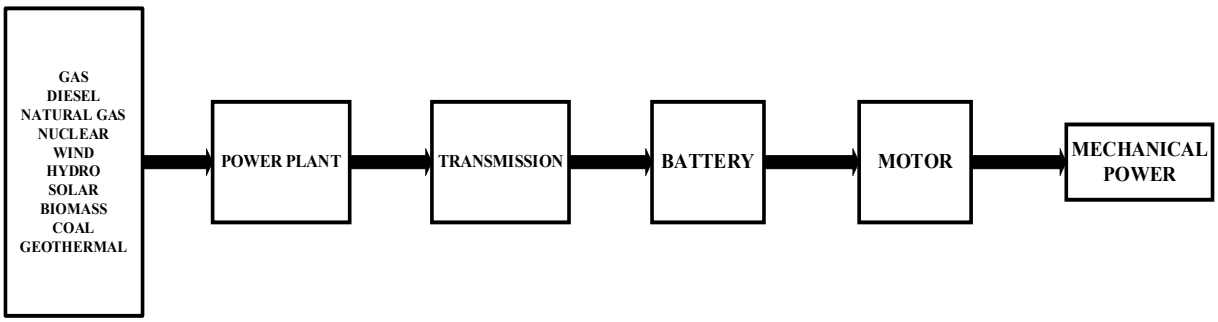

Figure 1.3. Lifecycle of electricity for EV application.

According to a comprehensive study by Argonne National Laboratory, well-to-tank efficiency averages around 80 percent for vehicles using internal combustion engines. The low tank-to-wheel efficiency of these vehicles greatly reduces their overall efficiency. TTW efficiency is between 14 and 35 percent for IC-powered vehicles. Average WTW energy efficiency ranges between 11 and 30 percent [36]. To summarize, vehicles using internal combustion engines have high well-to-tank efficiency but low tank-to-wheel efficiency. Electric vehicles, on the other

hand, show the opposite characteristic. While electric energy is transferred to the wheels at very high rates, the efficiency is very low in the process of generating and reaching the engine. The average efficiencies of biomass, coal, hydroelectric, geothermal, natural gas, natural gas combined cycle, nuclear, photovoltaic and wind power plants are 0.35, 0.40, 0.82, 0.20, 0.36, 0.52, 0.32, 0.20 and 0.28 percent, respectively. Considering that the average transmission efficiency is 94 percent, battery efficiency is 80 percent and average motor efficiency is 88 percent, the WTW efficiency for electric vehicles ranges from 13 to 54 percent. For hydropower, an efficiency of 54 percent was achieved, but overall WTW remained between 13 and 34 percent. Compared to IC-powered vehicles, the efficiencies are close, but there is no factor that makes electric vehicles very efficient in this context. WTW efficiency can be increased in some ways. One of them is to use IC engines and electric motors as a hybrid mode. Hybrid vehicles provide a diversity of performance, reducing fuel consumption and increasing efficiency. As a result of research, hybrid electric vehicles have been shown to have WTW efficiencies up to 50 percent [37]. From another point of view, it can be aimed to prevent transmission losses. For example, solar panels or wind turbines can be used for on-site generation and transmission losses can be avoided. Therefore, if companies and institutions with high vehicle capacity charge their electric vehicles in power generation systems, losses can be reduced and WTW efficiency can be increased by 5 to 10 percent. Another example is charging electric vehicles at home with the smart home model. Charging electric vehicles with individual solar panels can both prevent transmission losses and offer easy solutions with individual plans without the need for large organizations. Therefore, integrating renewable energy sources with electric vehicles is one of the most important factors in increasing efficiency. As a result, electric vehicles with WTW efficiencies ranging from 11 to 34 percent can offer a sustainable solution compared to IC-powered vehicles with WTW efficiencies of 10 to 30 percent. On the other hand, considering that power generation worldwide is still being met from non-renewable sources, the WTW efficiency of electric vehicles needs to be increased to over 30 percent.

1.5. Electric Machines for Traction Applications

Electric motors for traction are an essential part of electric vehicles (EVs) and are in the role of converting electrical energy from the battery of the car to mechanical energy to drive the wheels. Electric vehicles use a variety of electric traction motor types, each having specific characteristics and benefits [38]. Different types of electric machines are used for electric

vehicles according to their size, power, performance, speed and characteristics for different applications. These are DC Series Motors, Brushless DC motor, Induction motors, Switched Reluctance Motors and Permanent Magnet Synchronous Motor [39].

1.5.1. DC Series Motors

Even though their application in modern EVs has its limitations when compared to other motor types like permanent magnet synchronous motors (PMSMs) or induction motors, DC series motors are a type of electric machine with particular characteristics that make them suitable for some electric vehicle (EV) applications. These motors have been identified by their simple construction and minimal component weigh in, which makes them affordable to produce and maintain [40]. The most important advantage of dc series motors is their ability to provide high torque at low speeds. This makes them particularly suitable for applications where the vehicle needs to accelerate from a standstill. Forklifts, industrial carts, and various types of electric locomotives are just a few examples of the electric vehicles that might benefit significantly from this characteristic. Another important advantage is that their speed and torque can be easily controlled by adjusting the voltage applied to the motor [41]. This makes it possible to precisely control the acceleration and deceleration of the vehicle. On the other hand, the drawbacks of DC series motors are their relatively low efficiency, limited speed range, and potential to overheat at high speeds especially while operating under large loads. They require routine maintenance because of their brushes and commutator [42]. In India, Dc Series Motor is used for train applications. For example, Indian Locomotive Class WAM-4 locomotive model uses Dc Series Motor.

1.5.2. Brushless DC Motors

Brushless DC (BLDC) motors are electric motors of that kind, also known as electronically commutated motors (ECMs), that are becoming increasingly common in electric vehicle (EV) applications because of their effectiveness, reliability, and precise control abilities. The traction characteristics of BLDC motors include high starting torque and high efficiency around 95–98%. For EVs, this efficiency leads to improved energy utilization and a wider driving range [43]. BLDC motors are virtually maintenance-free as they do not have brushes that can wear out. This means BLDC motors have a longer operating life and require less maintenance than brushed DC motors. This results in less breakdown time and lower maintenance costs for electric vehicle

owners. BLDC motors are also compact and lightweight, which makes them excellent for integration into the limited area of electric cars. Although the high cost of permanent magnets and the high heat weakens of magnets do not allow for heavy applications, BLDC motors are suitable for use in light-weight operations such as electric scooters and three-wheel automobiles [44]. BLDC machines are mostly used on light duty applications. For example, as you can see in the Figure 1.5, 3 wheels electric cars use this type of machine. These cars are so effective for short distances.

Figure 1.5. Indian locomotive class wam-4 [54].

Figure 1.4. Speego CR 3 wheels car [55].

1.5.3. Switched Reluctance Motors

Variable reluctance motors, also known as switched reluctance motors (SRMs), are an innovative option for electric vehicle (EV) applications. SRMs are not as widely used as other motor types like permanent magnet synchronous motors (PMSMs) or induction motors, but they offer specific characteristics that make them well-suited for particular EV applications. SRMs have no magnets on the rotor unlike permanent magnet motors do. Instead, they operate by using the magnetic reluctance phenomenon. Due to their high torque density, SRMs are ideal for applications demanding a significant amount of torque output, such as off-road or heavy-duty EVs. In terms of design, SRMs have a robust and simple structure, reducing maintenance and production costs, and can operate at high temperatures [45]. Unlike induction motors, SRMs can operate efficiently over a wide speed range, which can provide flexibility in various driving

conditions. In contrast to all this, precise and complex control mechanisms are used to optimize performance and efficiency. This increases their cost and complexity. In addition, one of the most important problems with this motor is its higher noise production compared to other types of motors, which may necessitate some noise reduction measures [46].

1.5.4. Induction Motors

Induction machines, especially three-phase induction motors, have played an important role in electric vehicle applications. Robustness, simplicity and reliability make them advantageous in electric vehicle applications. In addition to dc motors, induction motors also can provide high torque at low speeds [47]. With this feature, it can play an important role in bus and industrial applications. Regenerative braking is possible with induction motors during operations such as deceleration and braking, so it can recover energy, contributing to increased energy efficiency and extended range. Induction motors are more cost-effective than other types of motors because they are more widespread and the production phase is less costly [48]. In electric vehicle applications where cost is an important factor, induction motors may become attractive for low-cost vehicles. Some disadvantages are that it is less efficient than PMSM motors, has a limited speed range for some applications, speed and torque control requires additional sensors and induction motor control is more straightforward than other motor types except for DC motors, and high-speed operations cause additional costs in terms of temperature problems and lubrication. Today, induction motors are used for buses, industrial vehicles and electric vehicle applications [49]. Probably, the most popular electric vehicle application is the Tesla Model S.

1.5.5. Permanent Magnet Synchronous Motors

Among electric motors, it is the most popular motor type for new generation electric vehicles. The most important reasons for this are its high efficiency, precise control and wide speed range, which provide excellent performance for electric vehicles [50]. Thanks to these advantages, it has become a preferred motor type for many modern electric vehicles. For electric vehicles to offer longer driving ranges, they need to make better use of energy. PMSM motors provide excellent energy transfer with efficiencies exceeding 90 percent [51]. Precise control of motor speed and torque helps to adapt to various driving conditions, such as acceleration, deceleration and regenerative braking. One of the most critical advantages is that it has a higher power density than other motor types. That is, they produce more power for their size and weight [52]. PMSM

motors, like some other types of motors, can act as generators during deceleration or braking phases. By converting kinetic energy into electrical energy, it can feed the vehicle's battery, increasing efficiency and vehicle range. Thanks to all these features, they can be used in a wide range of applications, from cars to buses. In addition to all these advantages, they can increase production costs with their expensive magnets and compact structure. Advanced and high-tech systems may also be required for precise control. Most of the electric cars are using PMSM nowadays, for example Nissan Leaf.

Figure 1.7. Tesla Model S [56].

Figure 1.6. Nissan Leaf [57].

Table 1-1. Comparison of Motor Types

Characteristics	**Motor Type**			
	SRM	**PM**	**IM**	**DC**
Power Density	Medium	Very high	Medium	Low
Efficiency	Medium	Very high	Medium	Low
Controllability	Medium	High	Very high	Very high
Reliability	Very high	High	Very high	Medium
Technological Maturity	High	High	Very high	Very high
Cost	Low	High	Very Low	Low

When all motor types are classified according to their efficiency, power density, controllability, reliability, technological maturity and price, we can see that each motor is advantageous over the other in a certain area. Although PMSM is the most expensive model in terms of price, it offers the best performance in terms of power density. The fact that the induction motor and dc motor are among the most technologically advanced models has made them affordable [53]. In the Table 1.1, motor types are compared to each other according to power density, efficiency, cost and other features.

1.6. The Advantages of Electric Motors Over Internal Combustion Engines for Traction Applications

A critical decision in the changing transportation area is whether to use internal combustion engines (ICEs) or electric machines (including electric motors) for vehicle applications. It is crucial to compare these two power technologies as the car industry transitions to cleaner and more sustainable solutions. Electric motors and internal combustion engines have different characteristics in electric vehicle applications in terms of their environmental impact, efficiency, operational costs, refueling and charging infrastructure, performance and driving experience. When implemented in vehicle applications, electric machines, particularly electric motors, provide various benefits over internal combustion engines (ICEs). These benefits contribute to understanding why electric cars (EVs) are becoming more and more popular. Based on environmental impact, when electric motors use electrical energy as their energy source, they have no carbon emissions in terms of their environmental impact. Also known as, compared to ICE vehicles, which rely on fossil fuels, EVs can have a much-reduced carbon footprint when powered on electricity by renewable sources. In order to reduce dependency on fossil fuels and increased energy independence, electric machines can be powered by a number of energy sources, including renewable energy [58]. Unlike fossil fuels, electric machines have the possibility to use sources such as solar energy, wind energy and hydroelectric energy. In terms of noise pollution, electric machines are quieter than internal combustion engines, which reduces noise pollution in communities and improves the quality of life for citizens [59]. For example, in big city centers, people are disturbed by loud noises during rush hours as traffic density is at a high level. Secondly, the most important feature that makes electric vehicles more efficient than conventional vehicles is their electric motors. They consume less energy while operating more efficiently because they convert more electrical energy to mechanical energy. While the

efficiency levels of internal combustion engines are between 20 and 40 percent, the efficiency of electric motors is around 90 percent on average [60]. Also, to increase efficiency and extend the range of an electric vehicle, energy can be recovered during braking and acceleration and converted back into electricity [61]. This is called regenerative braking system. This system allows to generate electricity while braking or going downhill. Thirdly, electric machines reduce the maintenance costs because they have fewer moving parts compared to ICEs. There are no complex gearbox systems, spark plugs or oil changes to be concerned about it [62]. Another important advantage of electric motors is instant torque and smooth acceleration. Quick acceleration and sensitive performance are made possible by the instant torque that electric motors produce at zero rpm [63,64]. Comfort for passengers is increased by the smooth, vibration-free driving experience that is provided by electric machines. Lastly, urban planning may change as a result of the popularity of electric vehicles and shared transport options, making cities more sustainable and cleaner.

1.7. Permanent Magnet Synchronous Motors for Electric Vehicle Applications

The use of permanent magnet synchronous motor has increased considerably in recent years. While in the twentieth century dc motors and induction motors were common with electric vehicle applications, today PMSM motors are found in almost every new model. The PMSM has become indispensable for the new generation of electric vehicles due to its high efficiency, high torque inertia ratio, high torque values for its volume and mass, high power factor and many other physical and electrical features. Compared to PMSM and DC motors, the PMSM produces lower audible noise, offers longer lifetime, can reach high speeds and offers high power density [65]. On the other hand, it offers high efficiency and power factor compared to induction motors. For example, one study showed that the PMSM motor was more than four percent more efficient than the induction motor when tests with the same ratios were carried out [66]. If high-energy magnets are used, the PMSM can reach higher power ratings. This provides the ability to produce different types of motors within the same design. Motors of the same size can be designed for different cost ratios. For example, in a situation where costs need to be reduced, cheaper magnets can be selected or power density can be increased with powerful magnets in the same dimensions. The PMSM can also produce high torque at low speeds and can provide an advantage during acceleration. On the other hand, the PMSM has a complex structure and this requires high technology, and the biggest disadvantage is the high cost. The smaller size makes

the structure of the PMSM motor complex and creates heating problems. A good cooling system is essential for PMSM applications. Although it provides easier cooling than Induction motors because the rotor generates less heat compared to that of induction motor, it is affected by heat transfer due to its small size. With all these advantages, it will be a preferred electric motor model in the coming years.

The PMSM has a three-phase stator, similar to induction motors, and what differentiates these two motors is that the PMSM has a rotor with permanent magnet. Motor characteristics depend on the type and location of the magnet used. The detail that determines PMSM types is how the permanent magnet is placed in the rotor. The magnet can be positioned on the rotor or embedded in the rotor. PMSM can be classified into two main categories: surface mounted and buried or interior PMSM.

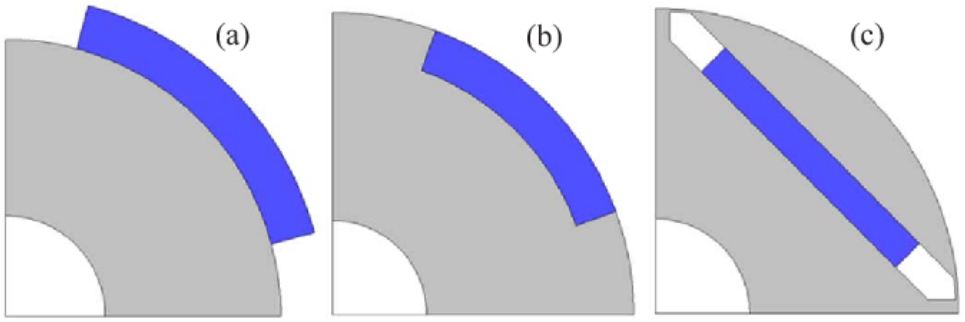

Figure 1.8. Main types of PMSM rotor configurations: (a) surface, (b) inset and (c) interior [68].

There are two variations of surface-mounted PMSMs. The first is the projection type, where the magnet projects from the rotor surface, and the inset type, where the magnet is placed inside the rotor and provides a smooth rotor surface. Placing the magnet on the rotor surface is the simplest and cheapest way of constructing the PMSM. It is simply fixed to the rotor surface with epoxy glue. These structures are less robust than models with magnets built into the rotor and are not suitable for high-speed applications. A second alternative is to embed the magnet into the rotor. The interior magnet design brings the advantages of greater mechanical robustness and it is more suitable for high-speed operations [69].

1.8. Thesis Contribution

In this thesis, the advantages that electric motors can provide for the transportation industry are discussed. As a research topic, thermal management, which is one of the most important problems in electric motors, is addressed. Predicting the temperature parameters for thermal management in advance and completing the design processes will increase efficiency, temperature prediction studies of two different types of motors were investigated.

A thermal circuit is designed using a Lumped Parameter Network Method to estimate the temperature parameters of the motors. This circuit is analyzed and temperature limits are determined. In addition, the results are compared and supported by simulation and experimental studies.

In the introduction part of this thesis, research has been focused on how electric vehicles can be more sustainable. As a literature study, the integration of electric vehicles into the transportation sector, the differences compared to conventional vehicles and the use of electric motors in this sector are investigated.

The organization of the thesis has been done as follows.

1. In the chapter 2, thermally analysis methods are examined and the LPTN method is explained. The importance of thermal management for electric motors is also discussed.
2. In Chapter 3, thermal modeling for two different PMSM motors that can be used in electric vehicle applications are proposed and investigated.
3. In Chapter 4, experimental studies are presented. Temperature measurements were made with real-time experiments. In addition, the results are supported and compared with simulation parameters. With all these results, the applicability of thermal modeling to motors with different types of designs is examined.
4. Chapter 5 presents the conclusion and future work.

2. THERMAL MODELING BACKGROUND

2.1. The Importance of Thermal Limits for Electric Machines

In electric vehicles, traction motors have an important role to perform, as they produce the necessary propulsion. The design of the electric motor is crucial for vehicle performance. Therefore, in order for vehicle performance to be at the desired levels, the motor must meet certain requirements during operation. Torque and speed capability will determine the overall power performance, directly affecting the vehicle's range and operational sustainability. Traction motors must be designed according to performance in order to meet parameters such as high torque at low speeds, high power at high speeds and high efficiency. Additionally, traction motors ought to provide quicker rates of deceleration and acceleration because vehicles need to start and stop frequently [69], [70].

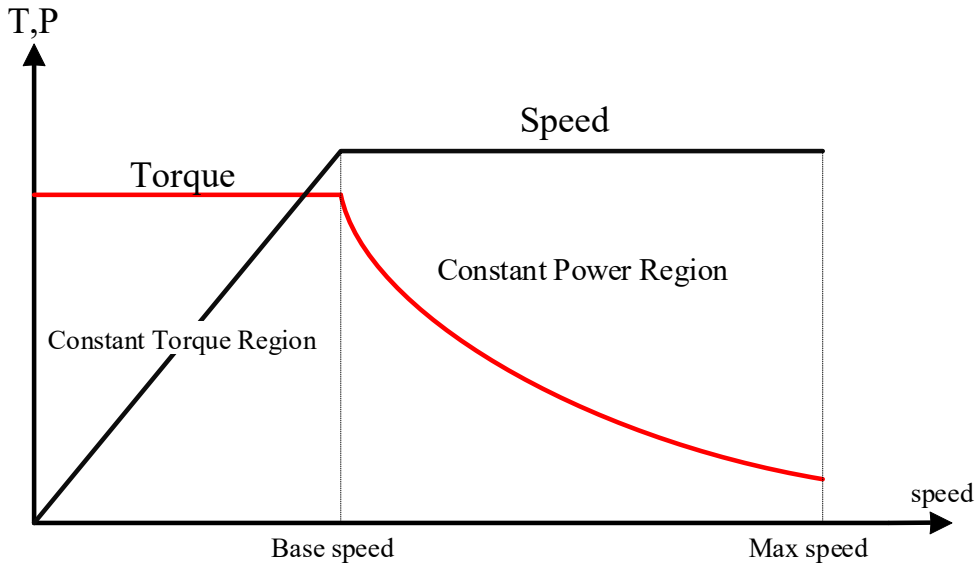

Figure 2.1. Torque-Speed Characteristic of Electric Machine.

All these features bring with them some concerns. First of all, in order to provide all these complex performances, their size and weight must be kept to a minimum. Minimal size and dimensions play an important role in the complexity of the motor. If the motor, which is compact to balance the whole system, is not designed properly to produce high torque and power, it can

cause many electrical and mechanical problems. Secondly, the electric motor, which consists of a compact size that provides all the requirements of high speeds high torque, releases significant amount of heat and increases the temperature of the motor. As is well known, high temperatures can cause motor failure and the motor must be kept within acceptable temperature levels [67].

Electric motors generate heat due to the electrical resistance of the components and the friction of the mechanical parts. This heat generation causes an increase in temperature inside the motor. An electric motor's performance and lifespan can be significantly affected by its operating temperature [71]. Electric machines, such as the electric motors used in electric vehicles (EVs) and other applications, can experience a number of issues as a result of high temperatures.

- **Efficiency**: Electric motors can reach high efficiencies at certain temperatures. Energy consumption and motor performance reduce the efficiency of the motor if the operating temperature rises too high [72]. Research showed that the higher torque can be obtained at 25 °C compared to 150 °C [73].

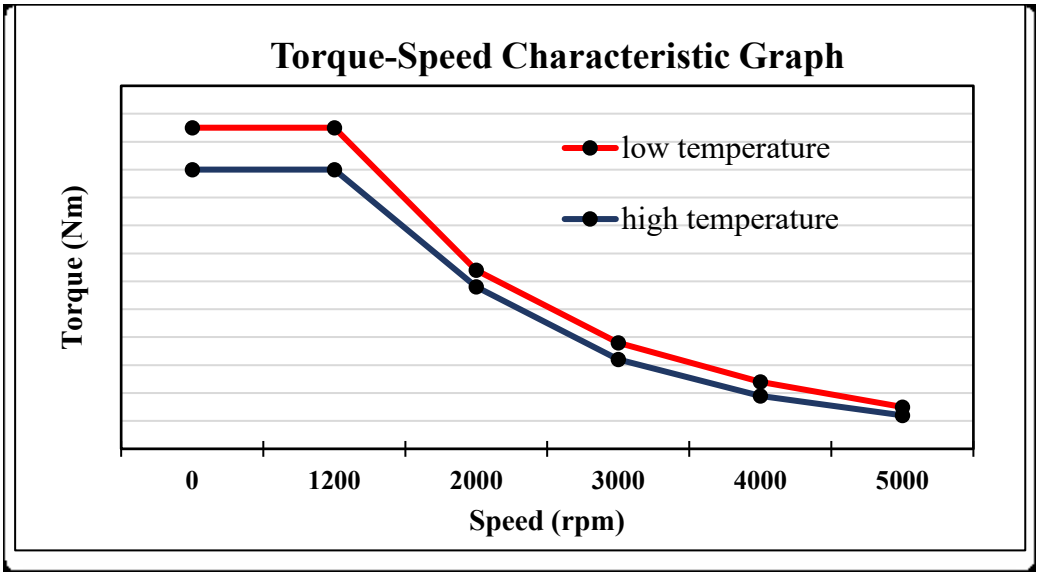

Figure 2.2. Torque-speed characteristic on different temperatures.

- **Heat Dissipation**: Thermal dissipation inside the motor is very important. If thermal dissipation is concentrated in a specific area, it can render cooling systems ineffective and

cause temperature-related problems in that area. Overheating of the motor can affect its ability to distribute heat and lead to potential damage [74].

- **Insulation Breakdown**: The windings in electric motors are insulated with insulation material to prevent short circuits. There is a certain temperature point that affects the insulating materials. At high temperatures, these materials can become degraded, frayed and corroded, leading to potential electrical faults [75].

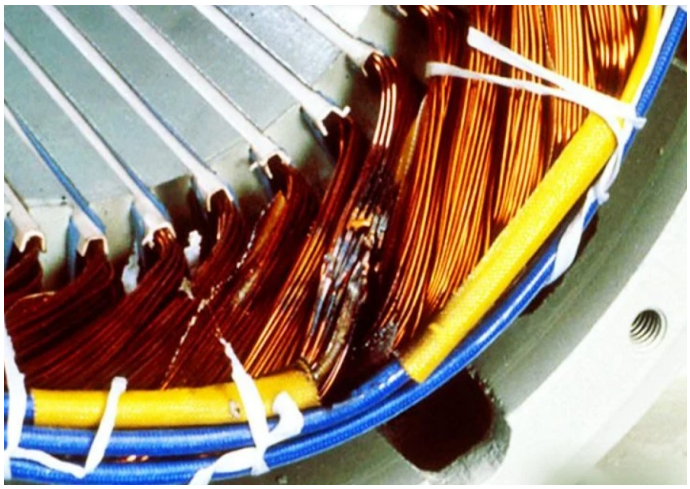

Figure 2.3. Insulation breakdown example [76].

- **Lubrication:** Electric motors have moving parts and bearings. These moving parts use oil for smooth operation and to reduce friction. When these components are exposed to high temperatures, the lubricant can break down, causing friction and corrosion [77]. This can lead to mechanical failure at high speeds and reduced efficiency due to increased friction losses.

- **Thermal Expansion**: Metal parts inside the motor are sensitive to thermal expansion. Components such as the rotor and stator can expand at high temperatures. This expansion affects the tolerances inside the motor and can cause mechanical problems by changing the shape of the mechanical parts.

- **Magnet Strength**: In permanent magnet motors, due to overheating, the magnets demagnetize and reduce the performance and efficiency of the motor [78].

Since high power is obtained in traction motors, high losses are inevitable. Although the efficiency of electric motors is high, their losses are also high due to the high-power density. These losses are converted into heat energy and cause an increase in the operating temperature of the motor. As a result, the motor can exceed its effective operating temperature and cause problems. In the permanent magnet synchronous motor, it is thermally more difficult than other motors due to its compact structure. The small size of the PMSM means that at high power and torque levels it is exposed to heat more quickly and the temperature rise is faster. This is what makes PMSM challenging. An excessive increase in motor temperature can cause permanent damage. Another important part that distinguishes PMSM from other motors is its magnets, which are sensitive to temperature. High temperatures can affect the magnet and reduce efficiency.

Monitoring and controlling the operating temperature are essential to maintain the optimum performance and lifetime of an electric motor. It is important that the motor operates within a certain temperature range and cooling systems are used for this. Regular maintenance and inspection to identify temperature-related problems can prevent such problems.

2.2. Thermal View of Electric Machines

Almost all of the losses in electric motors are converted into heat energy and these losses cause the motor to warm up. Before calculating or estimating the temperature rise, heat sources must be identified. It is important to determine what these heat sources are and where they are located in order to define the heat distribution. Keeping the temperature within the operational limits is one of the most important steps of the design phase. The cooling system to be designed must be designed in parallel with the motor design. Too little or too much cooling load damages the motor and keeps it from operating within the efficient temperature range. The losses in the electric motor are under two main headings as electromagnetic losses and mechanical losses [79]. Electromagnetic losses can be divided into 4 different classes: copper loss, stray load loss, magnet loss and core loss. The reason for copper losses is the electrical resistance of copper wire. While copper resistance can directly affect efficiency, the dissipation of losses through heat

energy causes the temperature of the motor to increase significantly. Core losses occur in the core materials inside the motor and have two different causes [80]. The first of these is hysteresis losses. It is caused by repeated magnetization and demagnetization of the iron core as the magnetic field changes [81]. The other is eddy current loss. With the changing magnetic field, eddy current is induced in the core and this current flows through the core and dissipates its energy through heat. Magnet losses are losses due to hysteresis and eddy current on the magnet and generate heat energy [82]. Mechanical losses are the losses that occur when the mechanical parts of the machine as friction and air resistance. These losses occur due to friction on the bearings and shaft, while the force acting on the airgap is windage losses [83]. When all these losses are taken into consideration and the losses are transferred to the motor with heat energy, it is seen that the temperature increase is inevitable.

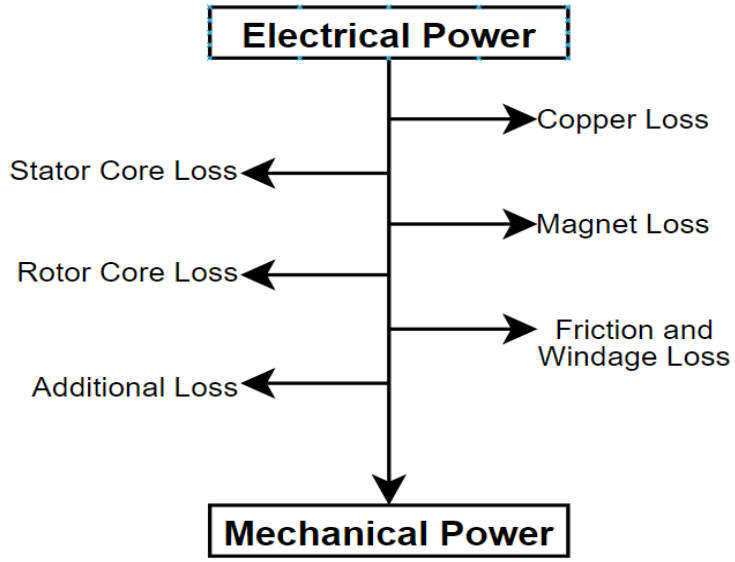

Figure 2.4. Power flow diagram of electric machines.

2.3. Thermal Analysis Options of Electric Machines

The temperature rise needs to be controlled during long-term operation of electric machines. The cooling system design must be suitable to keep the motor temperature within a safe

temperature range and to maintain its high efficiency. These temperature limits need to be determined and estimated at the design stage. In order to avoid any problems during the motor production phase, the maximum temperature it can reach before production should be simulated or estimated using some methods. Depending on the size, characteristics and power ratings of the motor, the temperature distribution can be determined and the cooling type can be selected to provide the optimum level of cooling. Through the simulations developed, it is not only possible to predict the motor temperature but also to calculate it analytically. Considering that the errors may increase depending on the design geometry, the calculations should be made according to a certain reference and applied for all motor components. In addition, new generation motors may have a specific structure with the effect of integration with the developing technology and simulations may not respond to these design templates. At this point, it is necessary to calculate the parameters analytically. Some methods are used to estimate the motor temperature. The two primary categories of thermal analysis techniques for traction motors are analytical and numerical techniques [84].

- **Analytical Thermal Modeling**: This approach involves designing mathematical models that explain how heat is generated and transferred throughout an electric machine. Equations for the transfer of heat by conduction, convection, and radiation could be included in these models. Preparatory design and performance estimation frequently involve the use of analytical models [85]. The analytical technique used in the thermal analysis is referred to as Lumped Parameter Thermal Network (LPTN) modelling that a thermal network is developed employing thermal resistances and capacitances. Using this network, the transfer of heat between components within the machine is analyzed. Each component inside the machine is represented by its thermal resistance and capacitance.

The numerical method is that offers analysis in two different ways. The first one is called Finite Element Analysis (FEA) and the second one is called Computational Fluid Dynamics (CFD) [84].

- **Finite Element Analysis (FEA)**: FEA is a method of numerical simulation that can be used to resolve challenging problems with temperature. The heat transfer equations for each smaller component of the electric machine are solved. FEA enables precise and thorough modelling of the machine's thermal distribution.

- **Computational Fluid Dynamics (CFD)**: The movement of air or other cooling fluids inside and around the electric machine is examined using CFD. This approach helps in understanding how well the cooling system distributes heat from the machine's parts.

Among these three methods, LPTN modeling analysis is simple, easy to understand and the fastest in predicting motor temperature. In addition to these advantages, since it treats the motor parts as a point, it can only observe the temperature rise of a point and cannot produce a thermal interaction map. However, when using the calculation technique, the low number of parameters compared to other models and the fact that it can be obtained with more understandable and easy formulas during the analysis phase are generally used in applications where a quick response can be obtained. On the other hand, since numerical methods show the temperature distribution, it can be used to catch errors in the design phase. Compared to LPTN modeling, it does not stay only at a certain point but show the temperature distribution, which makes these models complex and takes a long time to solve. Although they are suitable methods for detailed studies, they require a very long-time study. If we classify these three methods among themselves, LPTN is the fastest method, but it has the lowest accuracy. It can be used in small applications, but it may not give an error rate below the desired level in applications requiring very high speeds and sensitive measurements. The most reliable and accurate model among these models is CFD [86]. However, its complex structure and the high number of formulas to be solved keep the process time long.

2.4. Lumped Parameter Thermal Network (LPTN) for Electric Machines

Lumped parameter network is a model for modeling and simplifying the thermal behavior of electric motors and other electronic devices. Based on heat transfer theory, a circuit diagram is created to represent the thermal properties of the parameters [87]. The purpose of this modeling is to mathematically explain the thermal behavior of the system. This diagram is used to predict the temperature of specified points of the components within the system. For electric motors, this approach is created by connecting points representing each region or part within the motor. The thermal properties of each element or part are calculated. These thermal properties are thermal resistance and capacitance values. Each material has its own specific thermal properties. For example, two different materials have different specific heat capacities and thermal conductivities, and these values generate different resistance and capacitance values at each stage. Examples of these classifications within the motor can be classified as housing, stator, windings, rotor and shaft.

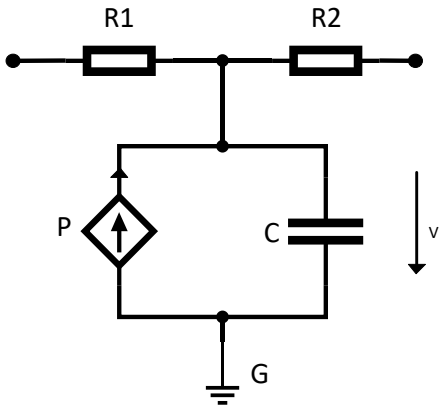

Figure 2.5. Example circuit application.

As shown in the Figure 2.7, an example circuit for a substrate includes resistance, capacitance and heat source [88]. In addition, a heat source is required to complete the circuit, and this heat source is losses for electric motors. Almost all of the losses inside the motor are converted into heat loss. In the simulation, experiment and modeling data used in this thesis, it is assumed that all losses are released as heat. When modeling, a circuit similar to an electrical circuit is used for analysis and the analysis is performed using electrical parameters. The relationship between electrical parameters and thermal parameters is shown in the Table 2.1.

Table 2-1 Electric and thermal parameter relations.

Electrical Parameter	**Unit**	**Thermal Parameter**	**Unit**
Voltage	V	Temperature	°C
Current	A	Heat	W
Conductance	S	Thermal Conductance	W/m°C
Conductivity	S/m	Thermal Conductivity	W/°C
Resistivity	Ω/m	Thermal Resistivity	m°C/W
Resistance	Ω	Thermal Resistance	°C/W
Capacitance	F	Thermal Capacitance	J/°C

As seen in the Table 2.1, each electrical quantity has a thermal quantity equivalent. Voltage represents temperature change while current represents heat. The electrical values of resistance and capacitance are also valid for thermal parameters.

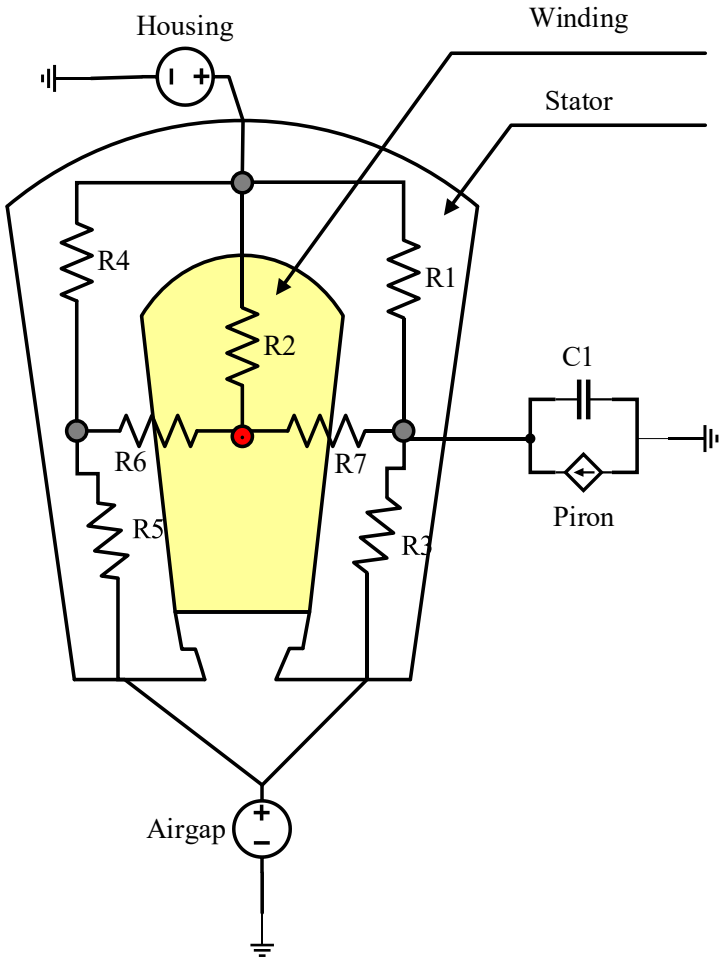

Figure 2.6. An example equivalent circuit of stator.

An example equivalent circuit model is shown in the Figure 2.8. This equivalent circuit model is designed to cover the slots, teeth and yoke region of the stator part. As can be seen, a point is defined in each region and these points are connected to each other. By determining the thermal resistance parameters between the points and calculating the thermal capacitance values in the region where the points are located, thermal effects on the system can be calculated. It is very important at which point the losses that make up the heat source will be located. Each loss

must be classified and applied to the point assigned to that region [89]. Thus, the point of origin of the heat can be determined and the propagation of the heat from this region can be shown and its effects can be measured.

Another important issue when modeling is nodalization. When nodalization is done, it is important which region of which part will be defined. The objects can be represented by a single point or can be separated by more than one point. These points connect the objects and form the circuit. How many parts to divide the specified component into can vary in terms of its geometric properties. If the material is moving in a uniform direction, it can be represented by a single point. However, models with hexahedron geometric properties, such as stator teeth, can be represented by more than one point.

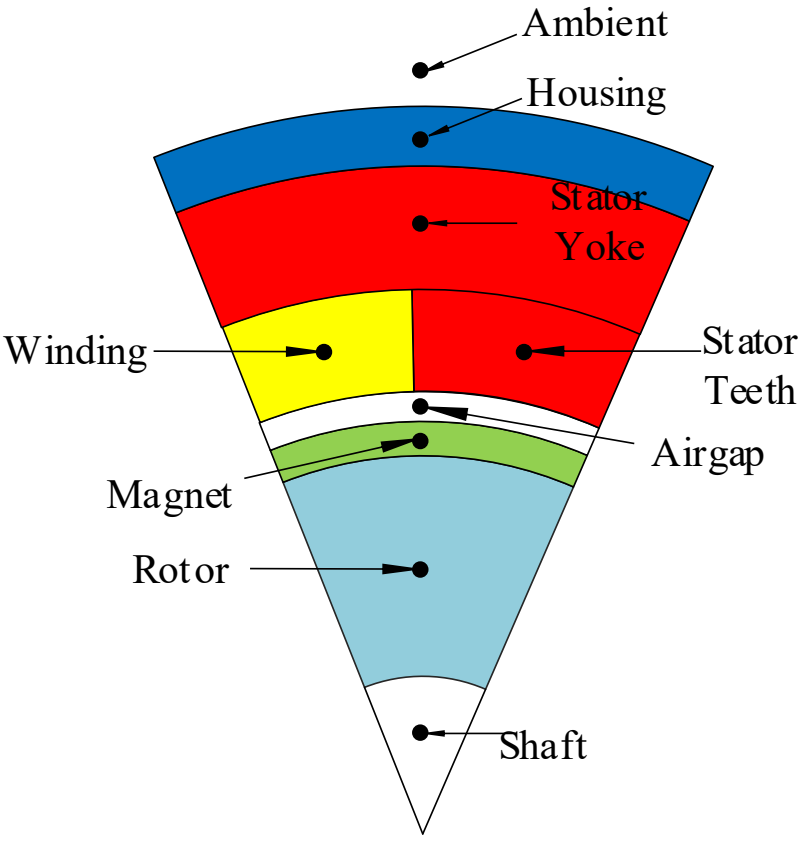

Figure 2.7. Example nodalization of SPMSM.

For example, the Figure 2.7. above shows an example of nodulization of a surface permanent magnet synchronous motor. In this model, some of the regions defined from the ambient point to the shaft region are expressed at a single point, while others are expressed at multiple points. This is due to the geometric structure of the component and the surface areas of the different materials it comes into contact with. Node placement can be proposed with more points to increase accuracy [90]. For example, since the rotor is placed in a radial geometry with the shaft and magnet, it can be connected to each other with a single point. On the other hand, the windings are in direct contact with the stator yoke, teeth and airgap, so they are divided into two points.

In the LPTN method, there is no need for capacitance values to find the steady state temperature as time variation is not taken into account. To find the steady-state temperatures of the model, it is enough to determine the thermal resistivity, heat source and flow [91]. The structure of the material also determines the type of heat transfer. For example, conduction heat transfer occurs between the stator and the frame, while convection heat transfer occurs on the airgap. The steady state temperature increase can be described by the following matrix.

$$[T] = [G]^{-1}[P] \tag{2.1}$$

Where the temperature matrix is [T], the loss matrix is [P] and the thermal conductance matrix is represented as [G]. Thermal conductance is the inverse of the thermal resistance. The difference between steady state and transient analysis is the time variation. For this to occur, thermal capacitances are added to the circuit and the transient circuit is complete. The following matrix equation is used to describe the temperature rise.

$$\frac{d}{dt}[T] = [C]^{-1}[P] - [C]^{-1}[G][T] \tag{2.2}$$

In this equation, [C] is the thermal capacitance matrix.

2.4.1. Thermal Resistance

When thermal analysis of a motor or electronic circuit is carried out, thermal resistances measure how heat will dissipate or be impeded. Thermal resistance is a measure of the ability of a material or component to resist the flow of heat. From another point of view, it can be defined as the ability to resist heat transfer [92]. It is usually represented by the symbol R and in this thesis it

is symbolized by R. Thermal resistance is similar to electrical resistance, the difference is that heat flow is considered instead of electric current. Increasing the thermal resistance value makes it difficult for heat to pass through the material. Conversely, a decrease in thermal resistance raises thermal conductivity. The thermal resistance of a material is determined by parameters such as its surface area, thickness and thermal conductivity.

$$Thermal\ Resistance = R = \frac{Temperature\ Difference\ \Delta T}{Heat\ Flow\ (P)} = \frac{C°}{W} \tag{2.3}$$

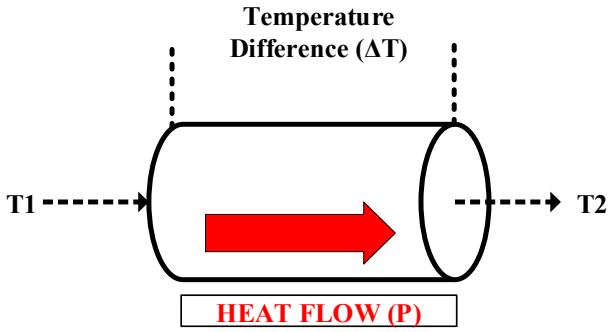

Figure 2.8. Heat flow schematic.

Using Ohm's law, the connection between thermal resistance and electrical resistance can be explained.

$$Electric\ Resistance = R = \frac{Voltage\ Difference\ \Delta V}{Current\ (I)} = \frac{V}{A} \tag{2.4}$$

Heat transfer takes place in three different ways. These are conduction, convection and radiation heat transfer. For conduction heat transfer, the thermal resistance can be calculated;

$$R_{conduction} = \frac{l}{k * A} \tag{2.5}$$

A is the cross section area of the material, l is the length of the material and k is the thermal conductivity of the material. If it is necessary to calculate thermal resistance for liquids and gases, convection thermal resistance should be calculated since heat transfer will be provided by convection. The thermal resistance due to convection formula is;

$$R_{convection} = \frac{1}{h * A} \tag{2.6}$$

Where A is the surface area, h is the convection heat transfer coefficient. For radiation heat transfer, thermal resistance would be able to calculate;

$$R_{radiation} = \frac{1}{\sigma * e * A(T_2^2 + T_1^2) * (T_2 + T_1)} \tag{2.7}$$

Where σ is the Stefan-Boltzmann constant, e is the emissivity of material surface and A is the surface area. It is easy to calculate the thermal resistances of materials with regular shapes. Different formulas are used when the shape and direction of heat flow change. Since the thermal analysis of the electric motor will be performed within the scope of this thesis, thermal resistance calculations are given for the following shapes and situations.

2.4.2. Thermal Resistance for Cylinders

Radial heat transfer occurs in areas with hollow cylinder geometry such as the rotor, shaft, stator yoke and housing [93]. The thermal resistance of a cylindrical structure can be found as;

$$R = \frac{\ln\left(\frac{r_o}{r_i}\right)}{2 * \pi * l * k} \tag{2.8}$$

Where r_o is the outer radius, r_i is the inner radius, l is the length of the material and k is the thermal conductivity of the material. If the component is limited to a certain angle, the formula can be modified as follows.

$$R = \frac{2\pi}{\alpha} \frac{\ln\left(\frac{r_o}{r_i}\right)}{2 * \pi * l * k} \tag{2.9}$$

The angle of the material is important to determine the thermal resistance.

2.4.3. Thermal Resistance Calculations for Airgap

It is difficult to calculate thermal resistance in regions with a certain air flow. In the airgap region inside electric motors, an air flow occurs with the rotation of the rotor. The convection heat transfer coefficient depends on the state of the air flow [94]. The heat transfer coefficient is found as shown below with dimensionless numbers;

$$R_{airgap} = \frac{1}{h_{airgap} * A_{airgap}} \tag{2.10}$$

$$h_{airgap} = \frac{Nu * k_{air}}{l_{airgap}} \tag{2.11}$$

To calculate the heat transfer coefficient Nusselt number should be found. The Taylor number describes how important viscous force is in compared to centrifugal force or inertial force caused by the rotation of a fluid about a vertical axis [91]. Taylor number is written;

$$Ta = \frac{\rho_{air}^2 * \omega^2 * r_{average} * l_{airgap}^3}{\mu^2} \tag{2.12}$$

Where ρ is the density of air, ω is the rotor angular speed, r is the average radius of airgap ((stator radius + rotor radius)/2), l is the airgap length and μ is the air dynamic viscosity. Modified Taylor number should be calculated if it is necessary, but in this thesis the airgap thickness is so small compared to radius. So geometric factor is considered 1. The relationship between Taylor and Nusselt numbers is given in the table.

Table 2-2. Nusselt number colorations with Taylor number.

$\boldsymbol{Nu = 2}$	$\mathbf{Ta_m < 1700}$
$\boldsymbol{Nu = 0.128 Ta_m^{0.367}}$	$\mathbf{1700 < Ta_m < 104}$
$\boldsymbol{Nu = 0.409 Ta_m^{0.241}}$	$\mathbf{10^4 < Ta_m < 107}$

2.4.4. Thermal Resistance Calculations for Windings

Thermal modeling of stator slots is difficult to solve by generalizing for different designs. Insulation systems are used during production and operation to prevent various problems. Firstly, there is an insulation between the copper windings and the stator iron. This insulation causes the thermal resistance to increase. Also, the copper windings are covered with a layer of impregnation. The different conductivity of these materials affects the heat distribution. On the other hand, heat production is spread over all the windings. Finally, winding formats can be different for each application. Different winding types can cause different thermal dissipation.

When all these components come together, the highest error for the modeling is expected to be on the windings. In this thesis, the relationship between the stator slot filling factor and the equivalent thermal conductivity of the slot mixture is used. For a more accurate calculation, the effects of winding insulation and air film on the thermal resistance should also be calculated. First, the equivalent height and width of the slit can be calculated by considering different shapes [95,96].

$$b = \frac{x_2 + x_3}{2} - 2d \tag{2.13}$$

$$h = \frac{2 * A_{slot}}{x_2 + x_3} \tag{2.14}$$

Where b is the equivalent width, h is the equivalent height, d is the equivalent insulation thickness and A is the slot area. The contribution of slot material for thermal resistance;

$$R_{x0} = \frac{b}{(h - t)k_{eq}} \tag{2.15}$$

$$R_{y0} = \frac{h - t}{b * k_{eq}} \tag{2.16}$$

The distance of two layers is mentioned as t and equivalent thermal conductivity cam be written as;

$$k_{eq} = 0.2749\big((1 - Kf) * A_{slot} * l_{core}\big)^{-4471} \tag{2.17}$$

The contribution of air film and insulation;

$$R_{ix} = \frac{d_i}{h * k_i} + \frac{d_a}{h * k_{air}} \tag{2.18}$$

$$R_{iy} = \frac{d_i}{b * k_i} + \frac{d_a}{b * k_{air}} \tag{2.19}$$

Where d_i is the insulation thickness, d_a air film thickness, k_i insulation thermal conductivity and k_{air} air film conductivity. The radial and circumferential conduction will be;

$$R_x = \frac{1}{2}\left(R_{ix} + \frac{R_{x0}}{6}\right) \tag{2.20}$$

$$R_y = \frac{1}{2}\left(R_{iy} + \frac{R_{y0}}{6}\right) \tag{2.21}$$

Since these expressions the resistance for per unit length. The total amount of resistance on slots is equal to;

$$R_w = \frac{R_x * R_y}{N_s * l * (R_x + R_{y)}} * \left(1 - \frac{R_{x0} * R_{c0}}{720 R_x * R_y}\right) \tag{2.22}$$

Where Ns is the slot number and l are the length of the slots. Also, axial resistances for different geometers can be calculated with the formula below;

$$R_{waxial} = \frac{l}{N_s * A_{cu} * k_{cu}} \tag{2.23}$$

Where A_{cu} is the copper area and k_{cu} is the thermal conductivity of the copper.

2.4.5. Thermal Capacitance

Capacitance is not required for steady state temperature. When transient analysis is required for the LPTN model, capacitance values need to be calculated. Thermal capacitance is the capacity of an object to retain and store heat. It is similar to the capacitance used in electrical circuits [97]. The thermal capacitance of a material is determined by the specific heat capacity of the material. The formula to calculate the thermal capacitance is;

$$C = mC_p = \rho V C_p \tag{2.24}$$

Where m is the mass of, Cp is the specific heat capacity and V is the volume of the material.

2.5. Summary

In this chapter, the effects of the temperature limit on electric machines, the thermal behavior of the electric motor and the analysis methods of calculating this temperature distribution are discussed. The Lumped Parameter Network Thermal Method, which will be used for modeling in this thesis, is explained in the literature. The equivalent circuit diagram for the thermal model and how to calculate the parameters are explained. The nodalization required for thermal modeling is shown on an example diagram. In the next section, the thermal modeling of two different PMSM motors is investigated and the prediction of temperature parameters is analyzed.

3. PROPOSED LUMPED PARAMETER NETWORK METHOD OF SURFACE PERMANENT MAGNET SYNCHORONOUS MOTOR AND SOFT MAGNETİC COMPOSİTE PERMANENT MAGNET SYNCHORONOUS MOTOR

In this thesis, the thermal analysis of two different types of PMSMs designed in the PEER GROUP laboratory by the Power Electronics and Energy Research group at Concordia University has been analyzed. The first one is Surface mounted PMSM and the other one is Spoke type PMSM which used Soft Magnetic Composite. The reason for choosing two different motors is to address the thermal performance of two motors with different conditions and geometry. SPMSM is a simple and geometrically unchallenging model in design. The SMC PMSM model was used to learn and compare how it performs under thermal analysis due to its innovative magnet and stator design. The aim of all these comparisons is to determine the suitability of the models, which have been introduced in specific forms with the development of new technologies in terms of design, for thermal analysis.

3.1. Machine Design of Surface PMSM

In this motor, the magnet is placed on the rotor. It consists of thirty-six slots and produces 32 Nm of torque at 1300 rpm. It has a power of six kW. It gives higher torque value at lower speed than the other selected model. Fan cooling type is selected for the cooling system.

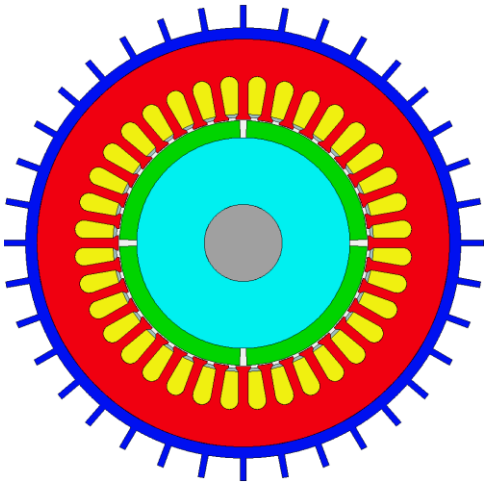

Figure 3.1. Radial view of SPMSM on MOTOR-CAD.

Figure 3.2. SPMSM view on the bench.

3.2. Machine Design of SMC PMSM

In this type of motor, the magnet is placed vertically in the rotor which is called spoke type PMSM. Since it has a specific design, it has a geometrically complex structure. This motor, which can reach high speeds, has a base speed of 3400 rpm and can reach 10000 rpm. It can produce a maximum torque of 20 Nm. SMC material, an innovative model, is used for stator lamination.

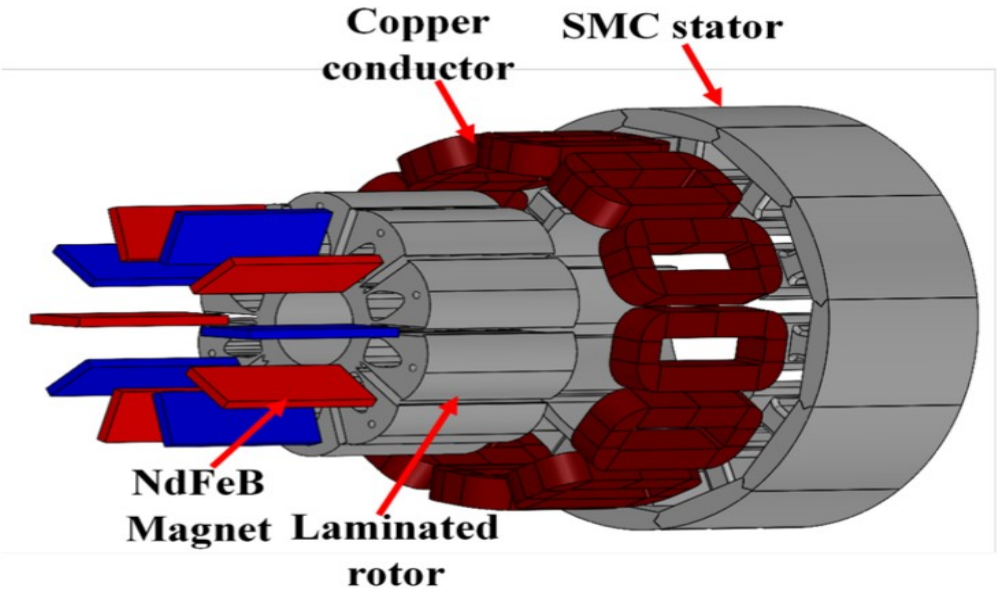

Figure 3.3. SMC PMSM design view [98].

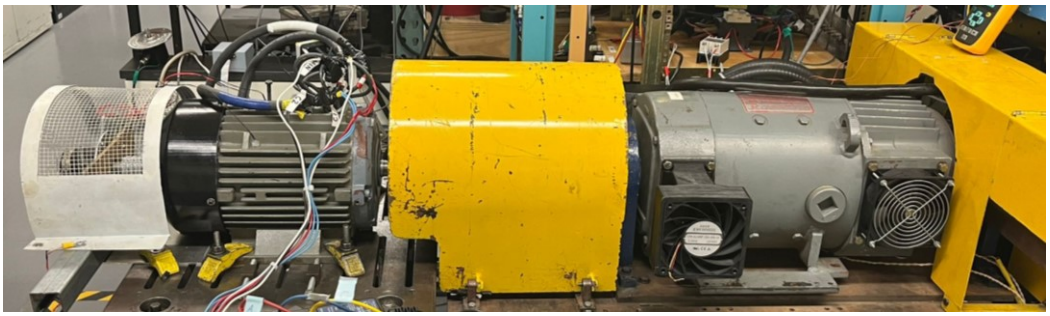

Figure 3.4. SMC PMSM view on the bench.

3.3. Design Differences Between Two Motors

Some criteria were taken into consideration when selecting two different types of motors for thermal analysis. First of all, models operating at the same power but giving different outputs were discussed. In addition, different models were preferred in terms of design. One of the motors has a simple design that can be considered old, while the other motor has a new design and a complex structure. When the speeds of the two motors are compared, the base speed of the SMC PMSM model reaches 3400 rpm, while the base speed of the SPMSM is 1300 rpm. On the other hand, SPMSM provides 32 Nm of mechanical torque at full load, while SMC PMSM provides a maximum torque output of 20 Nm. Also considering the rated current values, one model has a rated current of 20 A while the other model has 170 A. These different parameters will affect the motor operating temperature in different directions. Different temperature spread may create the need for different cooling systems. For example, the heat loss of 170 A current on the windings may cause overheating and may require a cooling system design that can directly affect the stator. Finally, when thermal analysis is performed, different designs may create differences on the models. When the modeling is done for a complex design, the margin of error may increase according to the assumptions to be made by analytical procedures. In addition, in this thesis, these two different types of motors were selected to analyze whether analytical thermal modeling can give accurate results for new and complex designs and to gain an innovative understanding.

Table 3-1. SPMSM and SMC PMSM specifications.

SPMSM		**SMC PMSM**	
Phase	3	**Phase**	3
Power(hp)	8	**Power(hp)**	7.1
Rated current (A)	16	**Rated current (A)**	170
Dc bus (V)	300	**Dc bus (V)**	100
Base speed (rpm)	1300	**Base speed (rpm)**	3400
Pole	4	**Pole**	10
Number of slots	36	**Number of slots**	12
Stator outer diameter (mm)	180	**Stator outer (mm)**	180
Stator stack length (mm)	125	**Stator stack length (mm)**	80
Rotor Outer Diameter (mm)	107	**Rotor Outer Diameter (mm)**	113
Magnet Thickness (mm)	7.5	**Magnet Thickness (mm)**	4
Shaft Diameter (mm)	35	**Shaft Diameter (mm)**	33

3.4. Thermal Model for Surface PMSM

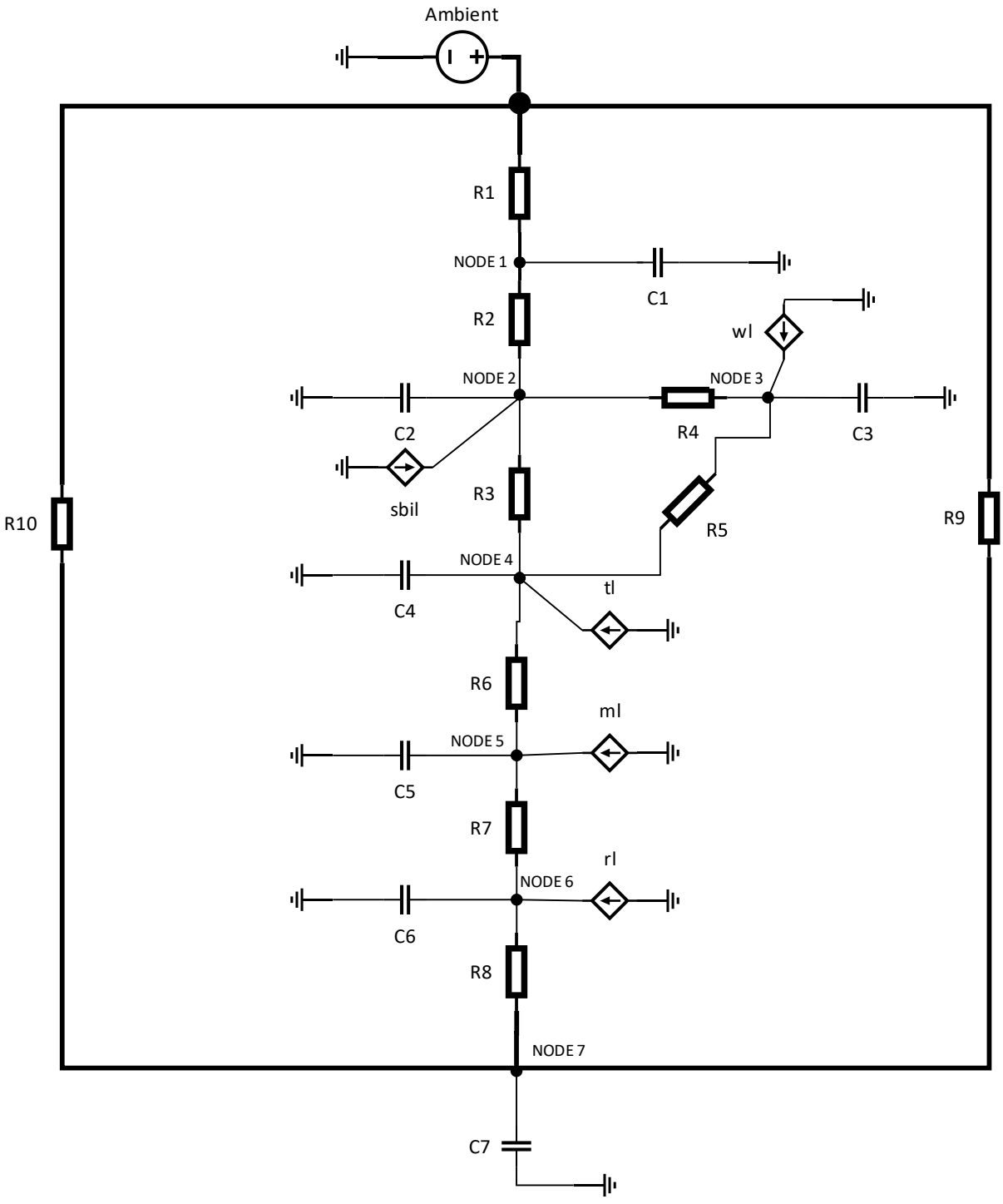

Figure 3.5. Simplified Model of SPMSM.

Table 3-2. Thermal Network Descriptions.

RESISTANCES	LOCATIONS OF THERMAL RESISTANCES
R1	Between Housing Frame And Ambient
R2	Between Housing Frame And Stator Yoke
R3	Between Stator Yoke And Stator Teeth
R4	Between Stator Yoke And Slot
R5	Between Teeth And Slot
R6	Airgap Resistance
R7	Between Magnet And Rotor
R8	Between Rotor And Shaft
R9	Between Shaft (Front Side) And Ambient
R10	Between Shaft (Rear Side) And Ambient
CAPACITANCES	**DESCRIPTIONS OF THERMAL CAPACITANCES**
C1	Housing Frame
C2	Stator Lamination (Back Iron)
C3	Stator Lamination (Tooth)
C4	Winding
C5	Magnet
C6	Rotor Lamination
C7	Shaft
LOSSES	**DESCRIPTION OF LOSSES**
wl	Winding Losses
sbil	Stator Back Iron Losses
tl	Stator Tooth Losses
ml	Magnet Losses
rl	Rotor Back Iron Losses

Table 3-3. Thermal Properties of SPMSM for resistance calculations.

Motor Part	**Material**	**Thermal Conductivity (W/M°C)**
Housing	Iron (Cast)	52
Stator Lamination (Back Iron)	M330-35A	25
Stator Lamination (Tooth)	M330-35A	25
Winding	Copper (Pure)	401
Rotor Lamination	M330-35A	25
Magnet	Recome 28	10
Shaft	Steel	80

3.4.1. Thermal Resistance Calculations of SPMSM

R1 is the thermal resistance between housing frame and ambient. There is a convection heat transfer in this region. The formula of the resistance is;

$$R_{convection} = \frac{1}{hA} \tag{3.1}$$

In this formula, h is the convection heat transfer coefficient, A is the area of the frame. h of the air determined as a 15 W/m^2C^o. The area of the housing is 0.3125 m^2. So;

$$R_1 = R_{convection} = \frac{1}{15 * 0.3152} = 0.213 \frac{W}{C°} \tag{3.2}$$

R2 is the resistance between housing and stator yoke outer which upper part of back iron. This resistance can calculate in this formula;

$$R2 = R_{housing} + R_{contact} + R_{yokeouter} \tag{3.3}$$

$R_{housing}$ is the radial thermal resistance of the frame and it can be calculated;

$$R_{housing} = \frac{ln\frac{r_{oh}}{r_{ih}}}{2 * \pi * l * k} \tag{3.4}$$

Where is k is the thermal conductivity of the material, l is the length, r_{oh} is the outer Radius of the frame, r_{ih} is the inner Radius of the frame.

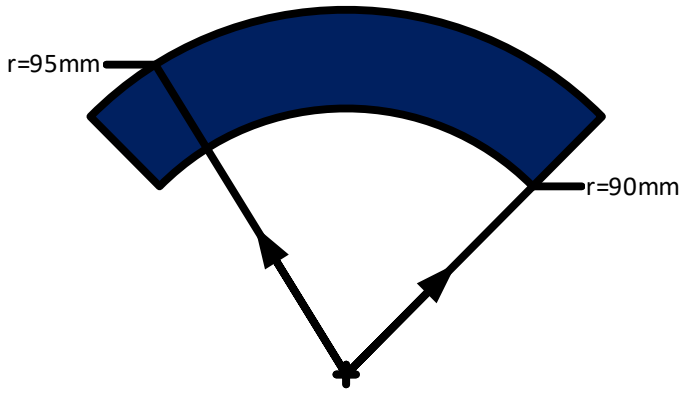

Figure 3.6. SPMSM housing schematic view.

$R_{housing}$ is;

$$R_{housing} = \frac{ln\frac{95}{90}}{2 * \pi * 0.13 * 52} = 0.00127\ \frac{W}{C°} \tag{3.5}$$

$R_{yokeouter}$ is the radial resistance of the stator yoke upper part. It can be calculated with the same formula.

$$R_{yokeouter} = \frac{ln\frac{90}{82.5}}{2 * \pi * 0.13 * 25} = 0.0043\ \frac{W}{C°} \tag{3.6}$$

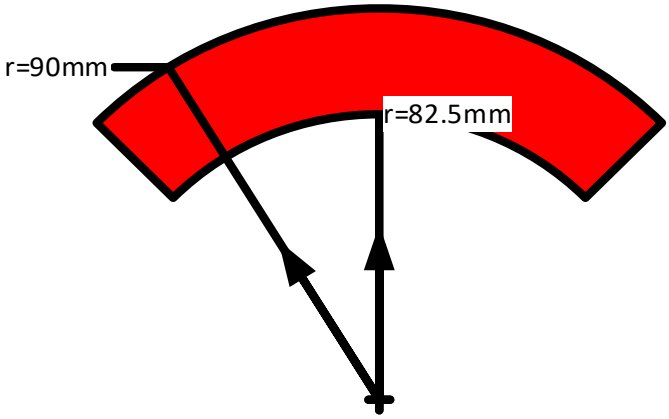

Figure 3.7. SPMSM stator yoke upper side schematic view.

$R_{contact}$ is the contact resistance between housing and stator yoke. To calculate the contact resistance, for the gap between two materials, Motor-Cad interface material is used for calculations. The gap between lamination and metal is taken 0.03mm which is average surface contact number of the model. The thermal conductivity of the material is 0.03171 W/m°C. $R_{contact}$ is;

$$R_{housing} = \frac{ln\frac{90.03}{90}}{2 * \pi * 0.13 * 0.03171} = 0.0128\ \frac{W}{C°} \tag{3.7}$$

So;

$$R2 = R_{housing} + R_{contact} + R_{yokeouter} = 0.0184\ \frac{W}{C°} \tag{3.8}$$

R3 is the resistance between stator yoke inner tooth side and tooth outer. For the stator yoke inner resistance is considered that half of the effective area is slot side, the other half is tooth side.

$$R3 = R_{yokeinnertooth} + R_{toothouter} \tag{3.9}$$

$R_{yokeinnertooth}$ is the resistance of the yoke tooth side. To calculate the resistance, we should consider of the effective area with the angle of the slot and tooth side. Since we have 36 slots in this motor, 1 slot and tooth covers 10°. In this machine it is considered for both sides are 5°.

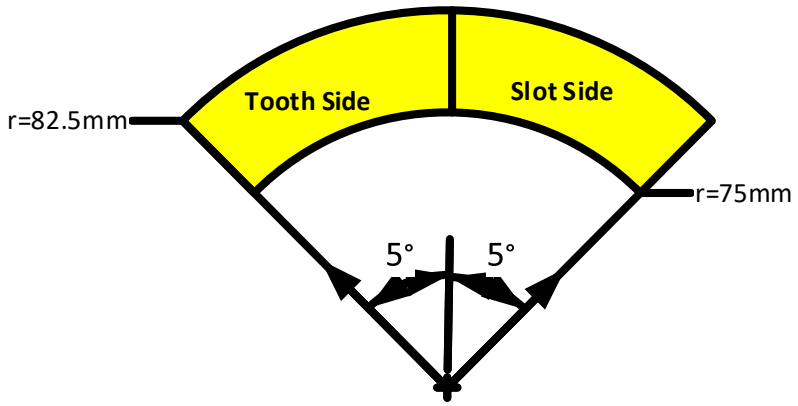

Figure 3.8. Stator yoke inner side schematic view.

$$R_{yokeinner} = \frac{ln\frac{82.5}{75}}{2 * \pi * 0.13 * 25} = 0.00467 \ \frac{W}{C°} \tag{3.10}$$

For tooth side:

$$R_{yokeineertooth} = R_{yokeinner} * \frac{10°}{5°} = 0.0093 \ \frac{W}{C°} \tag{3.11}$$

To find the tooth resistance it is important ot define geometry includes angle and dimension information.

To find the total tooth resistance, as can be seen in the figure 3.9, the tooth is divided 3 pieces in this example. The tooth resistance is;

$$R_{tooth} = R_{A1} + R_{A2} + R_{A3}$$

All three resistances are radial thermal resistance. Appling the radial thermal resistance formula;

$$R_{A1} = \frac{10}{7}\frac{ln\frac{56.5}{54.5}}{2 * \pi * 0.13 * 25} = 0.0035 \ \frac{W}{C°} \tag{3.12}$$

$$R_{A2} = \frac{10}{5}\frac{ln\frac{75}{57.5}}{2 * \pi * 0.13 * 25} = 0.00171\ \frac{W}{C°} \tag{3.13}$$

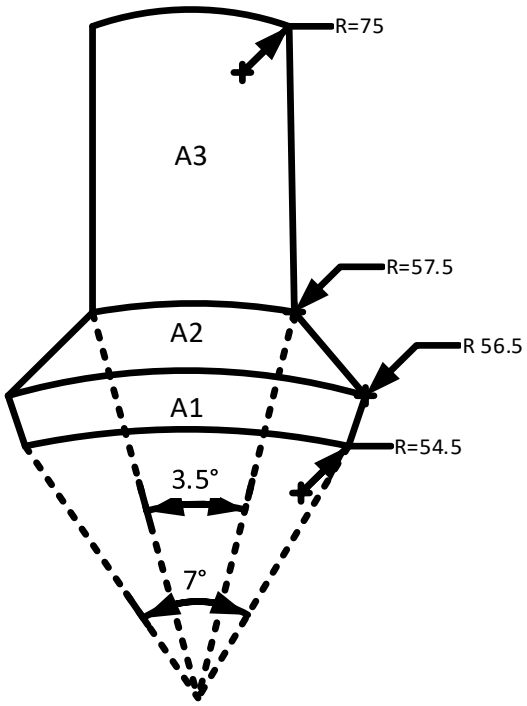

Figure 3.9. Stator tooth schematic view.

$$R_{A3} = \frac{10}{3.5}\frac{ln\frac{56.5}{54.5}}{2 * \pi * 0.13 * 25} = 0.037\ \frac{W}{C°} \tag{3.14}$$

$$R_{tooth} = 0.422\ \frac{W}{C°}$$

$$R_{toothouter} = \frac{R_{tooth}}{2} = 0.0211\frac{W}{C°} \tag{3.15}$$

So;

$$R3 = R_{yokeinnertooth} + R_{toothouter} = 0.0304\ \frac{W}{C°} \tag{3.16}$$

Winding resistance can be calculated;

$$R_w = \frac{R_x * R_y}{N_s * l * (R_x + R_{y)}} * \left(1 - \frac{R_{x0} * R_{c0}}{720 R_x * R_y}\right) \quad (3.17)$$

To determine the R_x and R_y, the contrubition of slot material in thermal resistance; x_2 is 5.73 mm, x_3 is 8 mm, insulation thickness is 0.06 mm, air film insulation is 0.25 mm equivalent thickness of insulation is d = 0.31 mm, the area of the slot is 120 mm^2, Kf is the 0.45, distance between two layer is t = 0.1 mm, k_{eq} is 40.01 W/m°C, k_i is 0.21 W/m°C and k_{air} is 0.03171 W/m°C.

$$b = \frac{x_2 + x_3}{2} - 2d = \frac{0.00573 + 0.008}{2} - 2 * 0.00031 = 0.006245\, m \quad (3.18)$$

$$h = \frac{2 * A_{slot}}{x_2 + x_3} - 2d = \frac{2 * 0.00012}{0.00573 + 0.008} - 2 * 0.00031 = 0.01686\, m \quad (3.19)$$

$$R_{x0} = \frac{b}{(h - t)k_{eq}} = \frac{0.006245}{(0.01686 - 0.0001) * 40.01} = 0.009313\ \frac{m°C}{W} \quad (3.20)$$

$$R_{c0} = \frac{h - t}{b * k_{eq}} = \frac{0.01686 - 0.0001}{0.006245 * 40.01} = 0.067\ \frac{m°C}{W} \quad (3.21)$$

$$R_{ix} = \frac{d_i}{h * k_i} + \frac{d_a}{h * k_{air}} = \frac{0.00006}{0.01686 * 0.21} + \frac{0.00025}{0.01686 * 0.03171} = 0.485\ \frac{m°C}{W} \quad (3.22)$$

$$R_{iy} = \frac{d_i}{b * k_i} + \frac{d_a}{b * k_{air}} = \frac{0.00006}{0.006245 * 0.21} + \frac{0.00025}{0.006245 * 0.03171} = 1.30\ \frac{m°C}{W} \quad (3.23)$$

$$R_x = \frac{1}{2}\left(R_{ix} + \frac{R_{x0}}{6}\right) = 0.243\ \frac{m°C}{W} \quad (3.24)$$

$$R_y = \frac{1}{2}\left(R_{iy} + \frac{R_{y0}}{6}\right) = 0.66\ \frac{m°C}{W} \quad (3.25)$$

The motor has 36 slots and the length of the coil is 0.22 m. The total resistance of winding is equal to;

$$R_w = \frac{0.243*0.66}{36*0.22*(0.243+0.66)} * \left(1 - \frac{0.0093*0.067}{720*0.243*0.66}\right) = 0.022\ \frac{W}{C°} \quad (3.26)$$

Since winding node has two connections with stator yoke and tooth. If we apply circumference formula on winding, the resistance through stator slot and tooth will be 0.033 W/°C and 0.033 W/°C.

In this model the contact areas are considered same since slot side and tooth side have same angular relationship with stator yoke.

R4 is the resistance between inner yoke slot side and winding yoke side. As we find that;

$$R_{yokeineerslot} = R_{yokeinner} * \frac{10°}{5°} = 0.0093 \ \frac{W}{C°} \tag{3.27}$$

And,

$$R4 = R_{yokeineerslot} + R_{windingyoke} = 0.0423 \ \frac{W}{C°} \tag{3.28}$$

R5 is the resistance between inner tooth and winding tooth side. Inner tooth resistance can be calculated;

$$R_{toothinner.} = \frac{R_{tooth}}{2} = 0.0211 \frac{W}{C°} \tag{3.29}$$

$$R5 = R_{windingslot} + R_{toothinner} = 0.0531 \ \frac{W}{C°} \tag{3.30}$$

R6 is the airgap thermal resistance. There is a convection heat transfer through air gap so thermal resistance formula is;

$$R6 = R_{airgap} = \frac{1}{h_{airgap} * A_{airgap}} \tag{3.31}$$

The convection heat transfer coefficient can be found;

$$h_{airgap} = \frac{Nu * k_{air}}{l_{airgap}} \tag{3.32}$$

To determine the Nusselt number, Taylor number should be found;

$$Ta = \frac{\rho_{air}^2 * \omega^2 * r_{average} * l_{airgap}^3}{\mu^2} \tag{3.33}$$

Density of air is 1.293 kg/m^3, dynamic viscosity of air is 1.849*10^{-5} kg/ms, thermal conductivity of air is 26.24*$^{10-}$3 W/m°C at 25 °C, average airgap Radius is 0.05425 m, the airgap thickness is 0.0005 and angular speed is 104.72 rad/s. So, Taylor number is;

$$Ta = \frac{1.293^2 * 104.72^2 * 0.05425 * 0.0005^3}{1.849 * 10^{-5^2}} = 364 \quad (3.34)$$

The airgap thickness is too small so geometrical factor is considered 1. Since Taylor number is smaller than 1700, the Nusselt number is 2. Heat transfer coefficient of airgap is;

$$h_{airgap} = \frac{2 * 26.24 * 10^{-3}}{0.0005} = 104.96 \ \frac{W}{m^2 C°} \quad (3.35)$$

The contact area between magnet and airgap is 0.044 m^2. So thermal resistance of air gap is;

$$R6 = R_{airgap} = \frac{1}{104.96 * 0.044} = 0.22 \ \frac{W}{C°} \quad (3.36)$$

R7 is the resistance between magnet and rotor upper side. In this machine, surface magnet is used and the magnet is not covering the rotor 100%. So, it is important to define the angle of the magnet. The magnet shape is:

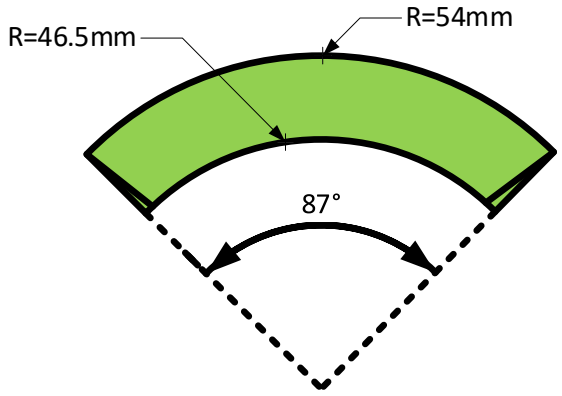

Figure 3.10. Magnet schematic view.

To calculate the magnet resistance, radial thermal resistance formula can be used;

$$R_{magnet} = \frac{90}{87} \frac{ln \frac{54}{46.5}}{2 * \pi * 0.125 * 10} = 0.0197 \ \frac{W}{C°} \quad (3.37)$$

The rotor resistance is;

$$R_{rotor} = \frac{ln\frac{54}{46.5}}{2 * \pi * 0.125 * 25} = 0.0512\ \frac{W}{C°} \tag{3.38}$$

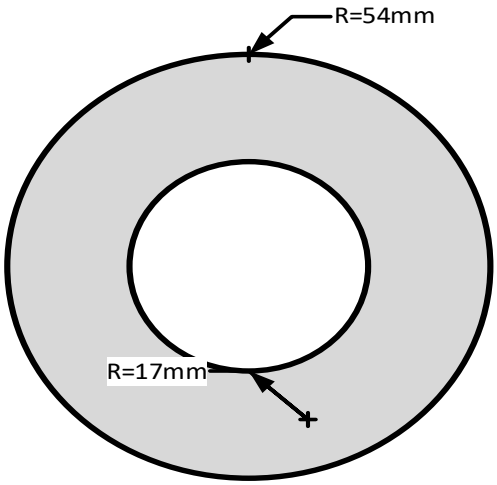

Figure 3.11. Rotor schematic view.

$$R_{rotorouter} = \frac{R_{rotor}}{2} = 0.0256\ \frac{W}{C°} \tag{3.39}$$

So;

$$R7 = R_{rotorouter} + R_{magnet} = 0.0453\ \frac{W}{C°} \tag{3.40}$$

R8 is the resistance between rotor and shaft. The shaft is considered three pieces in this application. For R8, active shaft resistance which has contact with rotor and diameter is 34mm is calculated.

$$R8 = R_{rotorinner} + R_{shaftactive} \tag{3.40}$$

Inner rotor radial resistance is;

$$R_{rotorinner} = \frac{R_{rotor}}{2} = 0.0256\ \frac{W}{C°} \tag{3.41}$$

To calculate the shaft resistance, the formula is;

$$R_{shaftactive} = \frac{l}{kA} = \frac{l}{\pi r^2 k} \tag{3.42}$$

Where l is the length of the shaft which contact length with rotor. L is 125mm for active shaft resistance.

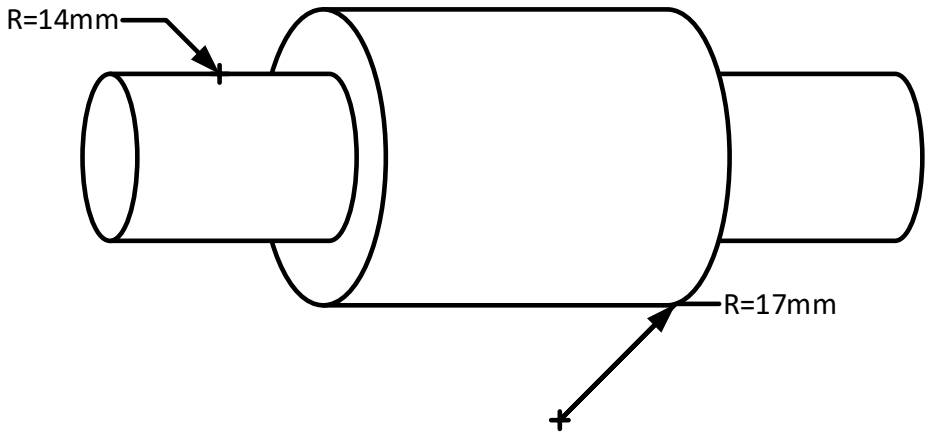

Figure 3.12. Shaft schematic view.

Active shaft resistance;

$$R_{shaftactive} = \frac{l}{kA} = \frac{0.125}{\pi * 0.017^2 * 80} = 1.72 \frac{W}{C°} \tag{3.43}$$

So;

$$R8 = R_{rotorinner} + R_{shaftactive} = 1.745 \frac{W}{C°} \tag{3.44}$$

R9 is the axial resistance of the front and rear side between shaft and housing. The shaft is located symmetrical in the motor so front and rear side have same length which is 62.5mm. The resistance for shaft front and rear side is;

$$R_{shaftactive} = \frac{l}{kA} = \frac{0.0625}{\pi * 0.014^2 * 80} = 1.26 \frac{W}{C°} \quad (3.45)$$

3.4.2. Thermal Capacitance Calculations of SPMSM

Table 3-4. Thermal Properties of SPMSM for Capacitance Calculations.

Motor Part	**Material**	**Mass (Kg)**	**Specific Heat Capacity (J/Kg°C)**
Housing	Iron (Cast)	6.486	420
Stator Lamination (Back Iron)	M330-35A	8.139	490
Stator Lamination (Tooth)	M330-35A	3.235	490
Winding	Copper (Pure)	3.308	358
Rotor Lamination	M330-35A	5.494	490
Magnet	Recome 28	2.375	350
Shaft	Steel	2.019	447

The thermal capacitance of the material depends on the specific heat and mass. Material density and volume could be useful to find the mass information. Material specifications related to the capacitances is given in the table below. Thermal Capacitance can be calculated;

$$C = m * c_p \tag{3.46}$$

Where C is thermal capacitance, c_p is the specific heat capacity and m is the mass of the material in kg. So thermal capacitance of the housing is;

$$C = 6.486 * 420 = 2724 \frac{J}{C°} \tag{3.47}$$

Stator lamination (back iron);

$$C = 8.139 * 490 = 3988 \frac{J}{C°} \tag{3.48}$$

Stator lamination (tooth);

$$C = 3.235 * 490 = 1585 \frac{J}{C°} \tag{3.48}$$

Winding;

$$C = 3.308 * 358 = 1184 \frac{J}{C°} \tag{3.49}$$

Rotor lamination;

$$C = 5.494 * 490 = 2692 \frac{J}{C°} \tag{3.50}$$

Magnet;

$$C = 2.375 * 350 = 831 \frac{J}{C°} \tag{3.51}$$

Shaft;

$$C = 2.019 * 447 = 902 \frac{J}{C°} \tag{3.52}$$

3.4.3. Losses of the SPMSM

As we know, losses in the motor are converted into thermal energy and dissipated in different parts of the motor. To complete the model and analyze the system, heat generated by the motor

need to be determined. This thesis focuses on five different losses. These are stator back iron, stator tooth, armature copper, magnet and rotor iron losses. Mechanical losses were ignored during the model analysis. Since high speeds are not reached and the temperature values of the internal dynamics of the system are measured, the effects of these losses on the system are assumed to be zero. As a result of FEA analysis, motor losses are observed as follows.

Table 3-5. Loss input data of SPMSM.

SPMSM	
LOSS	**QUANTITY (Watts)**
Stator Back Iron	119.1
Stator Tooth	82.04
Magnet	0.70
Rotor Back Iron	0.014
Armature Copper	200.2

3.4.4. LPTN Model Simulation of Surface PMSM on PSIM and Temperature Prediction Results

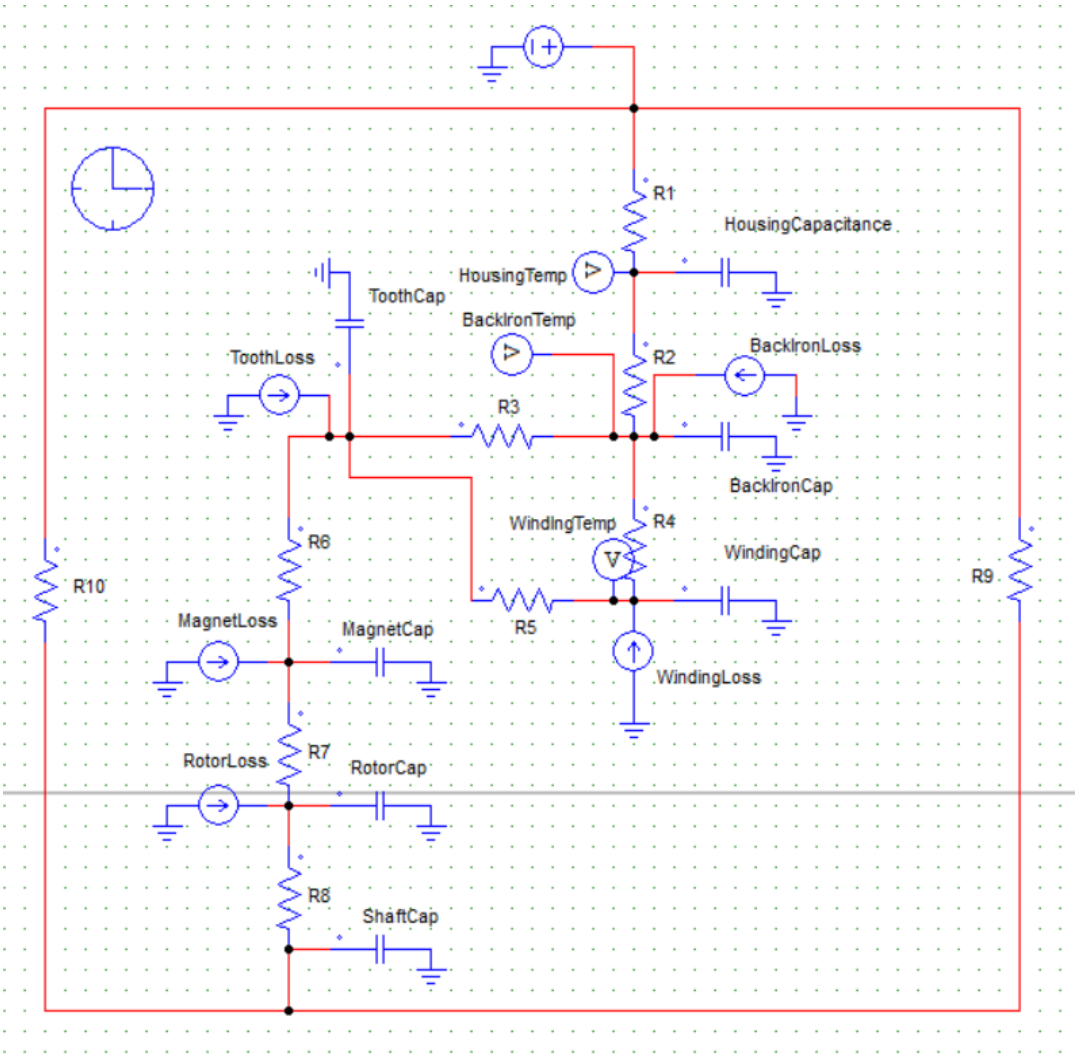

Figure 3.13. Simplified LPTN model view of SPMSM on PSIM software.

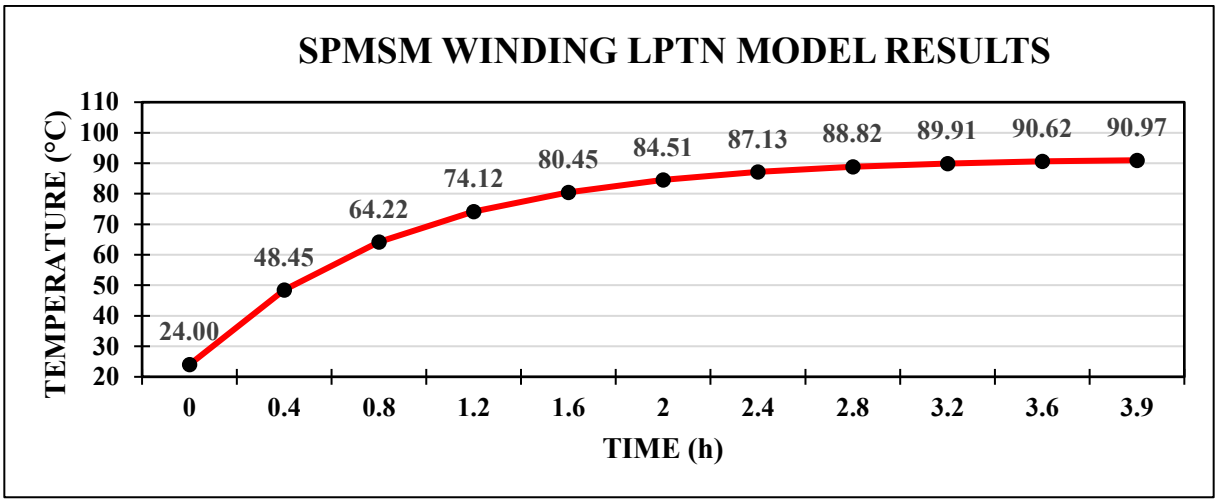

Figure 3.14. Winding model temperature prediction results.

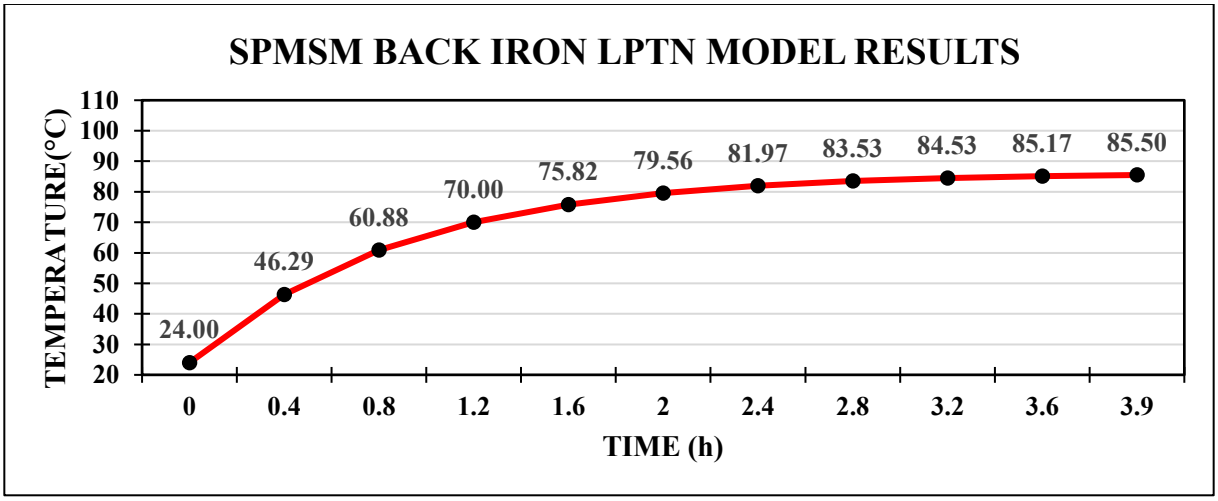

Figure 3.15. Back Iron temperature prediction results.

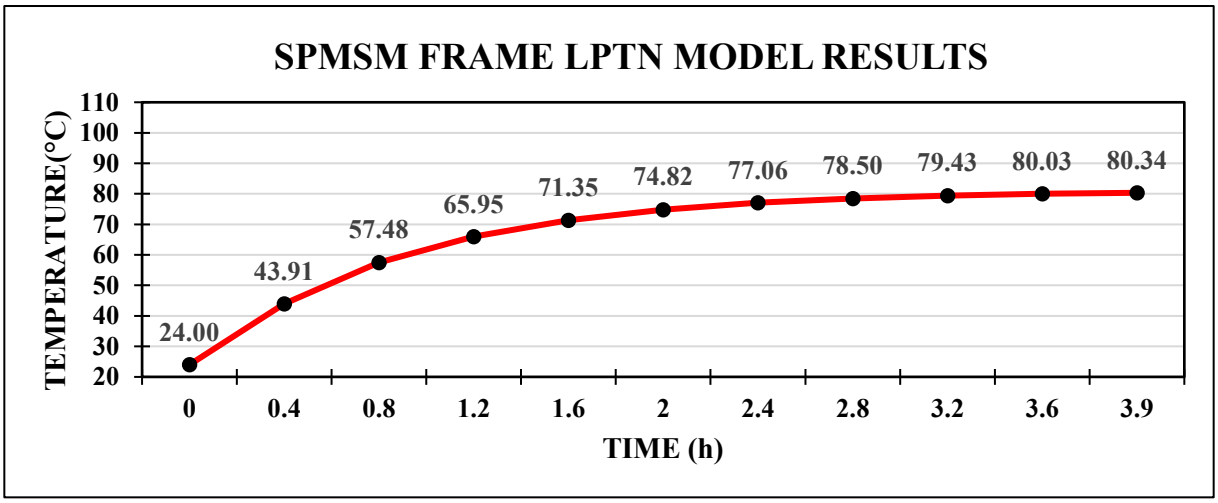

Figure 3.16. Housing frame model temperature prediction results.

3.5. Thermal Model for Soft Magnetic Composite PMSM

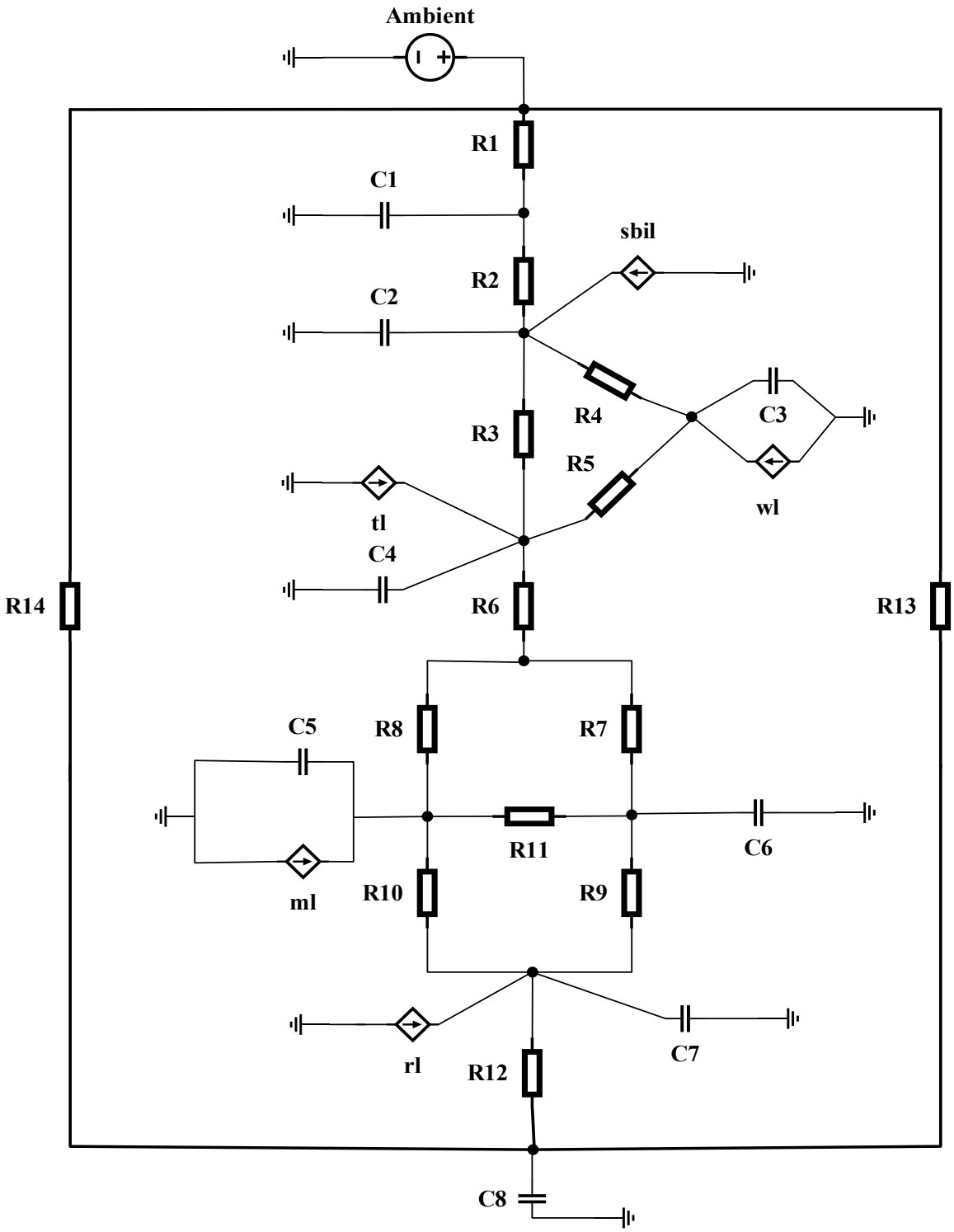

Figure 3.17. Simplified model of SMC PMSM.

Table 3-6. Thermal Network Descriptions.

RESISTANCE	DESCRIPTION OF THERMAL RESISTANCES
R1	Between Housing Frame And Ambient
R2	Between Housing Frame And Stator Yoke
R3	Between Stator Yoke And Stator Teeth
R4	Between Stator Yoke And Slot
R5	Between Teeth And Slot
R6	Airgap Resistance
R7	Between Rotor Upper Part And Inset Airgap
R8	Between Magnet And Airgap
R9	Between Inner Airgap And Rotor Inner Part
R10	Between Magnet And Rotor Inner Part
R11	Between Magnet And Rotor Upper Part
R12	Between Rotor Inner Part And Shaft
R13	Between Shaft (Front Side) And Ambient
R14	Between Shaft (Rear Side) And Ambient
CAPACITANCE	**DESCRIPTION OF THERMAL CAPACITANCES**
C1	Housing Frame
C2	Stator Lamination (Back Iron)
C3	Stator Lamination (Tooth)
C4	Winding
C5	Magnet
C6	Rotor Lamination (Upper)
C7	Rotor Lamination (Inner)
C8	Shaft
LOSSES	**DESCRIPTION OF LOSSES**
wl	Winding Losses
sbil	Stator Back Iron Losses
tl	Stator Tooth Losses
ml	Magnet Losses
rl	Rotor Back Iron Losses

Table 3-7. Thermal properties for resistance calculations.

Motor Part	Material	Thermal Conductivity (W/M°C)
Housing	Iron (Cast)	52
Stator Lamination (Back Iron)	Hoganas 700HR 1P	30
Stator Lamination (Tooth)	Hoganas 700HR 1P	30
Winding	Copper (Pure)	401
Rotor Lamination	Ak Steel M-36	73
Magnet	N30UH	7.6
Shaft	Steel	52

3.5.1. Thermal Resistance Calculations for SMC PMSM

R1 is the thermal resistance between ambient and housing frame. Since the convection heat transfer occurs on that region, the formula of the thermal resistance is;

$$R_{convection} = \frac{1}{hA} \tag{3.53}$$

where h is the convection heat transfer coefficient, A is the contact area between housing and the ambient. The contact area is 0.4437 m^2 of the frame, and convection heat transfer coefficient of the air is 10 W/m^2C^o. So R1 is calculated;

$$R_1 = R_{convection} = \frac{1}{10 * 0.4437} = 0.2254 \ \frac{W}{C°} \tag{3.54}$$

There is a resistance between housing frame and stator yoke. Stator yoke is separated 2 parts. First part is called stator yoke upper which has contact with housing frame. The other part is stator yoke inner part which has contact with slots and tooth. R2 is the thermal resistance between frame and stator yoke upper parts. In that region there are three different resistances. These are housing radial thermal resistance, stator yoke radial thermal resistance and contact resistance between housing and stator yoke.

$$R2 = R_{housing} + R_{contact} + R_{yokeouter} \tag{3.55}$$

$R_{housing}$ is the radial thermal resistance of the frame and it can be calculated;

$$R_{housing} = \frac{ln\frac{r_{oh}}{r_{ih}}}{2 * \pi * l * k}$$

Where is k is the thermal conductivity of the material, l is the length, r_{oh} is the outer Radius of the frame, r_{ih} is the inner Radius of the frame.

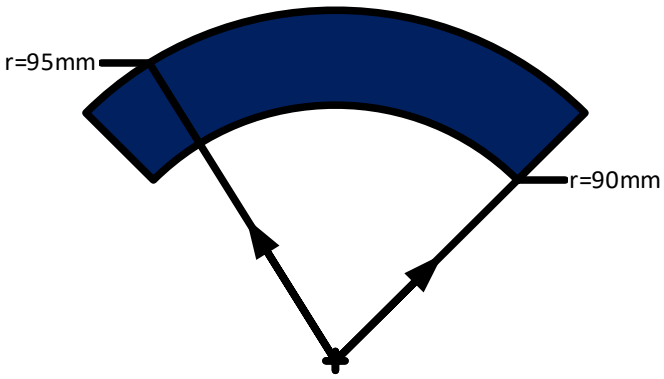

Figure 3.18. Housing frame schematic view.

$R_{housing}$ is;

$$R_{housing} = \frac{ln\frac{95}{90}}{2 * \pi * 0.08\,m * 52} = 0.002068\ \frac{W}{C°} \tag{3.56}$$

$R_{yokeouter}$ is;

$$R_{yokeouter} = \frac{ln\frac{90}{85}}{2 * \pi * 0.08m * 30} = 0.0038\ \frac{W}{C°} \tag{3.57}$$

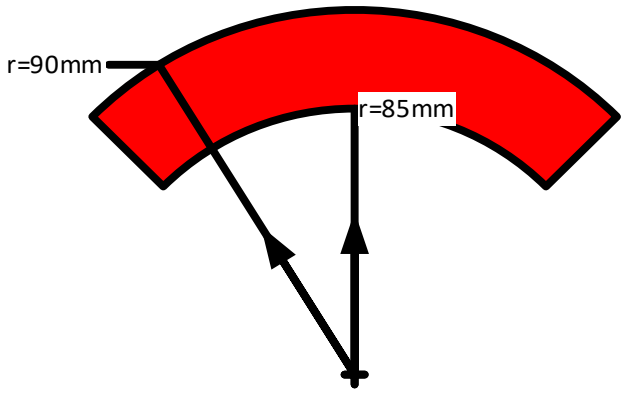

Figure 3.19. Stator yoke upper side schematic view.

$R_{contact}$ is the contact resistance between housing and stator yoke. To calculate the contact resistance, for the gap between two materials, Motor-Cad interface material is used for calculations. The gap between lamination and metal is taken 0.03mm which is average surface contact number of the model. The thermal conductivity of the material is 0.03171 W/m°C. $R_{contact}$ is;

$$R_{contact} = \frac{ln\frac{90.03}{90}}{2 * \pi * 0.08 * 0.03171} = 0.0209\ \frac{W}{C°} \tag{3.58}$$

So;

$$R2 = R_{housing} + R_{contact} + R_{yokeouter} = 0.0268\ \frac{W}{C°} \tag{3.59}$$

The thermal resistances between stator yoke inner slots side and slot and from stator yoke inner tooth side to tooth is called R4 and R3 respectively. The stator yoke inner thermal resistance depends on the angle relations of the tooth and slots. In this model the angle of the stator teeth is

10° and the angle of the slot is 20°. Since there are 12 slots on the stator, each part is 30° mechanical.

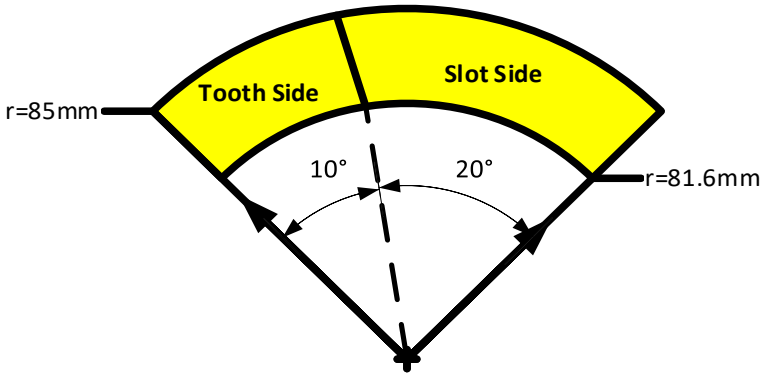

Figure 3.20. Stator yoke inner side schematic view.

The resistance of stator yoke inner side;

$$R_{yokeinner} = \frac{ln\frac{85}{81.6}}{2 * \pi * 0.08 * 30} = 0.0027 \frac{W}{C°} \tag{3.60}$$

For tooth side:

$$R_{yokeineertooth} = R_{yokeinner} * \frac{30°}{10°} = 0.00972 \frac{W}{C°} \tag{3.61}$$

For slot side:

$$R_{yokeineerslot} = R_{yokeinner} * \frac{30°}{20°} = 0.0037 \frac{W}{C°} \tag{3.62}$$

To find the R3 and R4, the thermal resistance of winding and tooth should be calculated. The tooth is separated three different parts to find the total resistance of the tooth. The angle of inner tooth which has contact with airgap is 24° and upper side of tooth has 10° mechanical angle. As you can see in the figure 3.21, there are 3 different areas to determine the total resistance.

Tooth resistance is;

$$R_{tooth} = R_{A1} + R_{A2} + R_{A3} \tag{3.63}$$

In this case all resistances are radial, so it is important to determine the angle and Radius information of the parts. Thermal resistances of A1, A2 and A3 are;

$$R_{A1} = \frac{30°}{24°}\frac{ln\frac{61.5}{57.5}}{2 * \pi * 0.08 * 30} = 0.0056\ \frac{W}{C°} \tag{3.64}$$

$$R_{A2} = \frac{30}{17}\frac{ln\frac{65.75}{61.5}}{2 * \pi * 0.08 * 30} = 0.0078\ \frac{W}{C°} \tag{3.65}$$

$$R_{A3} = \frac{30}{10}\frac{ln\frac{56.5}{54.5}}{2 * \pi * 0.08 * 30} = 0.043\ \frac{W}{C°} \tag{3.66}$$

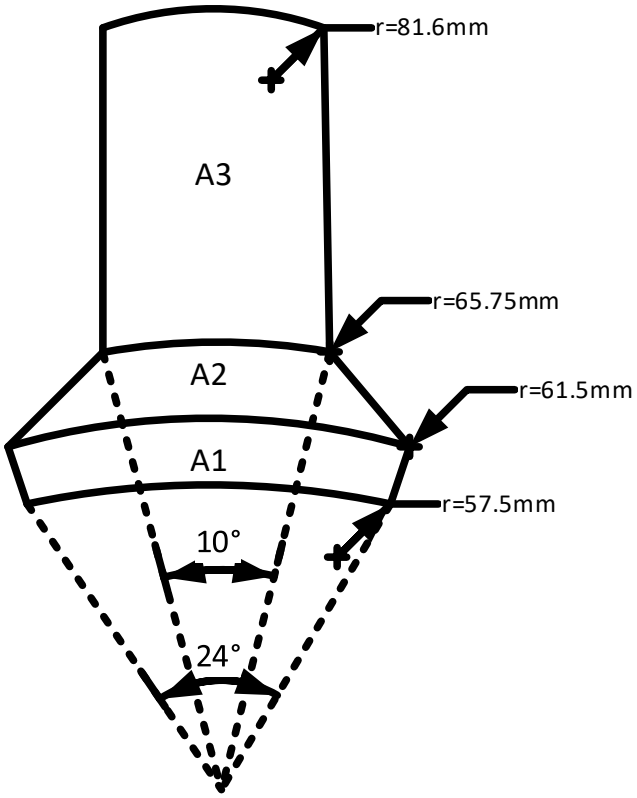

Figure 3.21. Stator tooth schematic view.

$$R_{tooth} = 0.0564\ \frac{W}{C°} \tag{3.67}$$

$$R_{toothouter} = \frac{R_{tooth}}{2} = 0.0282\frac{W}{C°} \tag{3.68}$$

$$R_{toothinner.} = \frac{R_{tooth}}{2} = 0.0282 \frac{W}{C°} \tag{3.69}$$

Stator tooth has 2 contacts. These are slots and stator yoke. Inner tooth is considered for contact of slots and upper side is considered for contact of yoke. So R3 and R4 are;

$$R3 = R_{yokeinnertooth} + R_{toothouter} = 0.0379 \ \frac{W}{C°} \tag{3.70}$$

To calculate the R4 and R5, the winding resistance should be found to contribution of the resistances. Winding resistance can be calculated;

$$R_w = \frac{R_x * R_y}{N_s * l * (R_x + R_{y)}} * \left(1 - \frac{R_{x0} * R_{c0}}{720 R_x * R_y}\right) \tag{3.71}$$

To determine the R_x and R_y, the contrubition of slot material in thermal resistance; x_2 is 18 mm, x_3 is 30 mm, insulation thickness is 0.1 mm, airfilm insulation is 0.2 mm, equivalent thickness of insulaiton is d = 0.3 mm, the area of the slot is 501 mm^2, Kf is the 0.35, distance between two layer is t = 0.05 mm, k_{eq} is 30.8 W/m°C, k_i is 0.21 W/m°C and k_{air} is 0.03171 W/m°C.

$$b = \frac{x_2 + x_3}{2} - 2d = \frac{0.0018 + 0.003}{2} - 2 * 0.0003 = 0.0234 \, m \tag{3.72}$$

$$h = \frac{2 * A_{slot}}{x_2 + x_3} - 2d = \frac{2 * 0.000501}{0.0018 + 0.003} - 2 * 0.0003 = 0.02027 \, m \tag{3.73}$$

$$R_{x0} = \frac{b}{(h - t)k_{eq}} = \frac{0.0234}{(0.02027 - 0.00005) * 30.8} = 0.0374 \ \frac{mC°}{W} \tag{3.74}$$

$$R_{c0} = \frac{h - t}{b * k_{eq}} = \frac{0.02027 - 0.00005}{0.0234 * 30.8} = 0.0282 \ \frac{mC°}{W} \tag{3.75}$$

$$R_{ix} = \frac{d_i}{h * k_i} + \frac{d_a}{h * k_{air}} = \frac{0.0001}{0.02027 * 0.21} + \frac{0.0002}{0.02027 * 0.03171} = 0.3346 \ \frac{mC°}{W} \tag{3.76}$$

$$R_{iy} = \frac{d_i}{b * k_i} + \frac{d_a}{b * k_{air}} = \frac{0.0001}{0.0234 * 0.21} + \frac{0.0002}{0.0234 * 0.03171} = 0.2899 \ \frac{mC°}{W} \tag{3.77}$$

$$R_x = \frac{1}{2}\left(R_{ix} + \frac{R_{x0}}{6}\right) = 0.1704 \ \frac{mC°}{W} \tag{3.78}$$

$$R_y = \frac{1}{2}\left(R_{iy} + \frac{R_{y0}}{6}\right) = 0.1472\ \frac{mC°}{W} \tag{3.79}$$

The motor has 12 slots and the length of the coil is 0.08 m. The total resistance of winding is equal to;

$$R_w = \frac{0.1704 * 0.1472}{12 * 0.08 * (0.1704 + 0.1472)} * \left(1 - \frac{0.0374 * 0.0282}{720 * 0.1704 * 0.1472}\right) = 0.009975 \tag{3.80}$$

Since the rectangular copper is used for this application, the resistance between winding and stator yoke is equal to;

$$R_{windingyoke} = \frac{l}{N_s * A_{cu} * k_{cu}} = \frac{0.08}{12 * 0.00017535 * 401} = 0.095\ \frac{W}{C°} \tag{3.81}$$

$$R4 = R_{yokeineerslot} + R_{windingyoke} = 0.1156\ \frac{W}{C°} \tag{3.82}$$

R5 is the thermal resistance between winding and tooth. So R5 is;

$$R5 = R_{windingtooth} + R_{toothinner} = 0.522\ \frac{W}{C°} \tag{3.83}$$

R6 is the airgap thermal resistance. Since convection heat transfer occurs on airgap, the airgap thermal resistance can be calculated;

$$R6 = R_{airgap} = \frac{1}{h_{airgap} * A_{airgap}} \tag{3.84}$$

The convection heat transfer coefficient can be found;

$$h_{airgap} = \frac{Nu * k_{air}}{l_{airgap}} \tag{3.85}$$

To determine the Nusselt number, Taylor number should be found;

$$Ta = \frac{\rho_{air}^2 * \omega^2 * r_{average} * l_{airgap}^3}{\mu^2} \tag{3.86}$$

Density of air is 1.293 kg/m^3, dynamic viscosity of air is 1.849*10^{-5} kg/ms, thermal conductivity of air is 26.24*$^{10-}$3 W/m°C at 25°C, average airgap Radius is 0.0.056 m, the average airgap thickness is 0.003 and angular speed is 356 rad/s. So, Taylor number is

$$Ta = \frac{1.293^2 * 356^2 * 0.056 * 0.003^3}{1.849 * 10^{-5^2}} = 937076 \quad (3.87)$$

The airgap thickness is too small so geometrical factor is considered 1. The Taylor number is between 10^4 and 10^7, so Nusselt number can be calculated;

$$Nu = 0.409Ta^{0.241} = 11.25 \quad (3.88)$$

Heat transfer coefficient of airgap is;

$$h_{airgap} = \frac{11.25 * 26.24 * 10^{-3}}{0.003} = 98.4 \ \frac{W}{m^2 C°} \quad (3.89)$$

The contact area between rotor and airgap is 0.028 m^2. So thermal resistance of air gap is;

$$R6 = R_{airgap} = \frac{1}{98.4 * 0.028} = 0.38 \ \frac{W}{C°} \quad (3.90)$$

Also, there is an inner airgap inside the rotor. Since the Radius of inset airgap is half, the resistance of inset airgap is assumed 0.19 W/°C. In the rotor side, magnet is located rectangular shape so there are to different resistance are calculated for magnet. One of them is radial direction from rotor to airgap, another one is axial resistance between magnet and rotor. Rotor also has two parts. Rotor inner part is between shaft to magnet, and rotor outer part is between rotor magnet and airgap. In the model, R7 is the thermal resistance between rotor upper part and inset airgap. As you can see on the design, there is a hole near the magnet and this hole is named as a inset airgap. R7 is;

$$R7 = R_{rotorupper} + \frac{R_{insetairgap}}{2} \quad (3.91)$$

Also, the rotor outer Radius is not same for all position. The highest radius is 56.5mm and the lowest radius is 52.5 mm. So, for the formula the outer Radius of the rotor is considered the average value which is 54.5mm. To find the rotor upper part resistance;

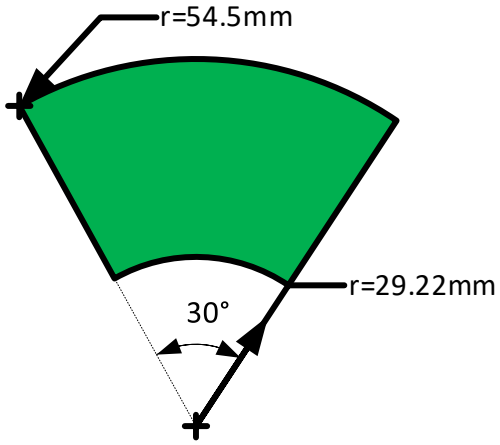

Figure 3.22. Rotor upper side schematic view.

$$R_{rotorupper} = \frac{ln\frac{54.5}{29.22}}{2 * \pi * 0.08 * 73} = 0.0203\ \frac{W}{C°} \tag{3.91}$$

The inset airgap resistance is determined 0.18 W/°C. So R7 is;

$$R7 = R_{rotorupper} + \frac{R_{insetairgap}}{2} = 0.1\frac{W}{C°} \tag{3.92}$$

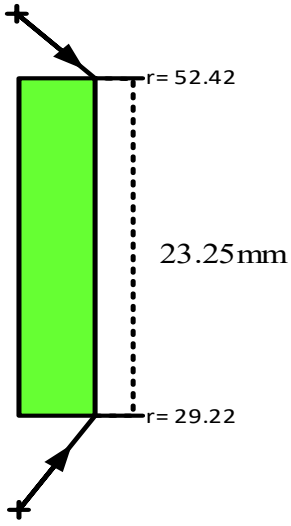

Figure 3.23. Magnet schematic view.

R8 is the radial thermal resistance of the upper side of the magnet. The angle of the magnet is not same for all positions because of the shape of the magnet. The highest angle is 8° and the lowest angle is 4°. So, the average angle which is 4° is used for the formula. The radial resistance of the magnet is;

$$R_{magnetradial} = \frac{36°}{6°} \frac{ln\frac{52.42}{29.22}}{2 * \pi * 0.08 * 7.6} = 0.0256 \frac{W}{C°} \tag{3.93}$$

So R8 can be calculated;

$$R8 = \frac{R_{magnetradial}}{2} = 0.0128 \frac{W}{C°} \tag{3.94}$$

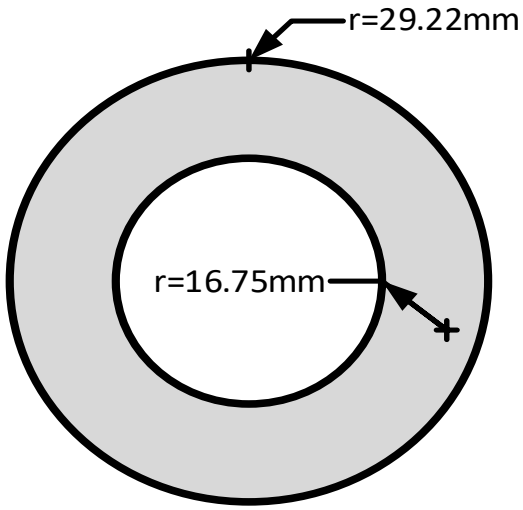

Figure 3.24. Rotor inner side schematic view.

R9 is the resistance between inner airgap and rotor inner part. So R9 is;

$$R9 = R_{rotorinner} + \frac{R_{insetairgap}}{2} \tag{3.95}$$

To find the rotor inner part, the radial thermal resistance formula is applied;

$$R_{rotorinner} = \frac{ln\frac{29.22}{16.75}}{2 * \pi * 0.08 * 73} = 0.0152 \frac{W}{C°} \tag{3.96}$$

$$R9 = R_{rotorinner} + \frac{R_{insetairgap}}{2} = 0.976\ \frac{W}{C°} \tag{3.97}$$

R10 is the resistance between magnet and rotor inner part on radial way;

$$R10 = \frac{R_{magnetradial}}{2} + R_{rotorinner} = 0.204\ \frac{W}{C°} \tag{3.98}$$

Also, there is a thermal resistance between magnet and rotor upper part is called R11. In this region there is an axial heat flow from magnet to rotor upper part. The axial magnet resistance is;

$$R_{magnetaxial} = \frac{l}{kA} = \frac{0.002\ m}{0.02325\ m * 0.08\ m * 7.6} = 0.1415\ \frac{W}{C°} \tag{3.99}$$

So R11;

$$R11 = \frac{R_{rotorupper}}{2} + R_{magnetaxial} = 0.15\frac{W}{C°} \tag{3.100}$$

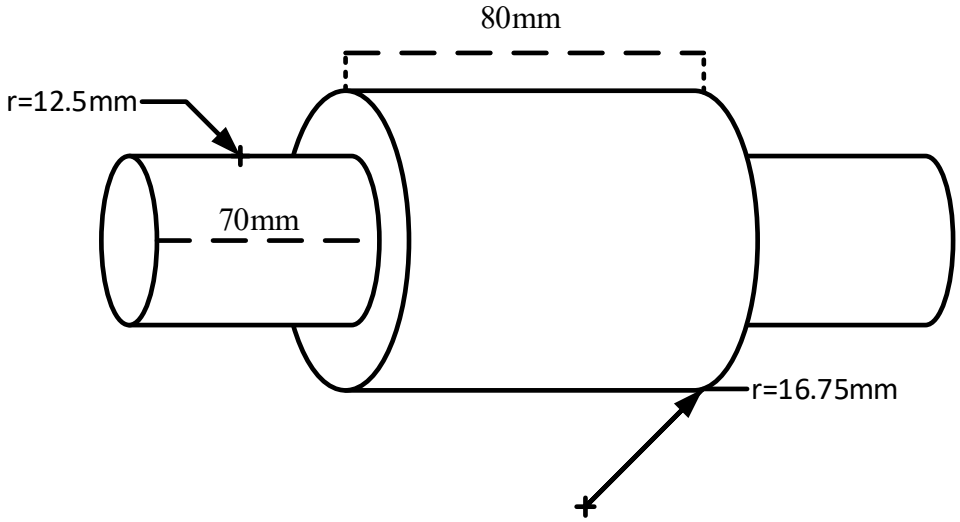

Figure 3.25. Rotor schematic view.

R12 is the resistance between shaft and rotor inner part. The shaft is considered three pieces. For R12, active shaft resistance which has contact with rotor and radius is 16.75 mm is calculated. Active shaft resistance is;

$$R_{shaftactive} = \frac{l}{kA} = \frac{0.08}{\pi * 0.01675^2 * 52} = 1.745 \frac{W}{C°} \quad (3.101)$$

So R12;

$$R12 = R_{rotorinner} + R_{shaftactive} = 1.753 \frac{W}{C°} \quad (3.102)$$

R13 and R14 are the axial resistances of the front and rear side between shaft and housing. The shaft is located symmetrical in the motor so front and rear side have same length which is 70 mm. The resistances for shaft front and rear side are;

$$R_{13} = R_{14} = R_{front-rear} = \frac{l}{kA} = \frac{0.07}{\pi * 0.0125^2 * 80} = 2.74 \frac{W}{C°} \quad (3.103)$$

3.5.2. Thermal Capacitance Calculations of SMC PMSM

Table 3-8. Thermal specifications for capacitance calculations.

Motor Part	Material	Mass (Kg)	Specific Heat Capacity (J/Kg°C)
Housing	Iron (Cast)	5.64	420
Stator Lamination (Back Iron)	Hoganas 700HR 1P	2.902	550
Stator Lamination (Tooth)	Hoganas 700HR 1P	2.094	550
Winding	Copper (Pure)	1.6	385
Rotor Lamination (Inner)	Ak Steel M-36	1.089	420
Rotor Lamination (Outer)	Ak Steel M-36	2	420
Magnet	Recome 28	2.375	350
Shaft	Steel	2.019	447

Thermal capacitance of the material can be calculated;

$$C = m * c_p$$

Thermal capacitance of housing frame;

$$C = 5.64\ kg * 420\ \frac{J}{kgC°} = 2369\ \frac{J}{C°}$$

Stator lamination (back iron);

$$C = 2.902\ kg * 550\ \frac{J}{kgC°} = 1596\ \frac{J}{C°}$$

Stator lamination (tooth);

$$C = 2.094\ kg * 550\ \frac{J}{kgC°} = 1151\ \frac{J}{C°}$$

Winding;

$$C = 1.6\ kg * 385\ \frac{J}{kgC°} = 616\ \frac{J}{C°}$$

Rotor (inner);

$$C = 1.089\ kg * 420\ \frac{J}{kgC°} = 458\ \frac{J}{C°}$$

Rotor (outer);

$$C = 2\ kg * 420\ \frac{J}{kgC°} = 840\ \frac{J}{C°}$$

Magnet;

$$C = 0.433\ kg * 460\ \frac{J}{kgC°} = 616\ \frac{J}{C°}$$

3.5.3. Losses of the SMC PMSM

The assumptions made for SPMSM are also considered for SMC PMSM. Losses in the system;

Table 3-9. Loss inputs of SMC PMSM.

SMC PMSM	
LOSS	**QUANTITY (Watts)**
Stator Back Iron	89
Stator Tooth	131
Magnet	3.362
Rotor Back Iron	1.49
Armature Copper	89.6

3.5.4. LPTN Model Simulation in PSIM and Temperature Prediction Results of SMC PMSM

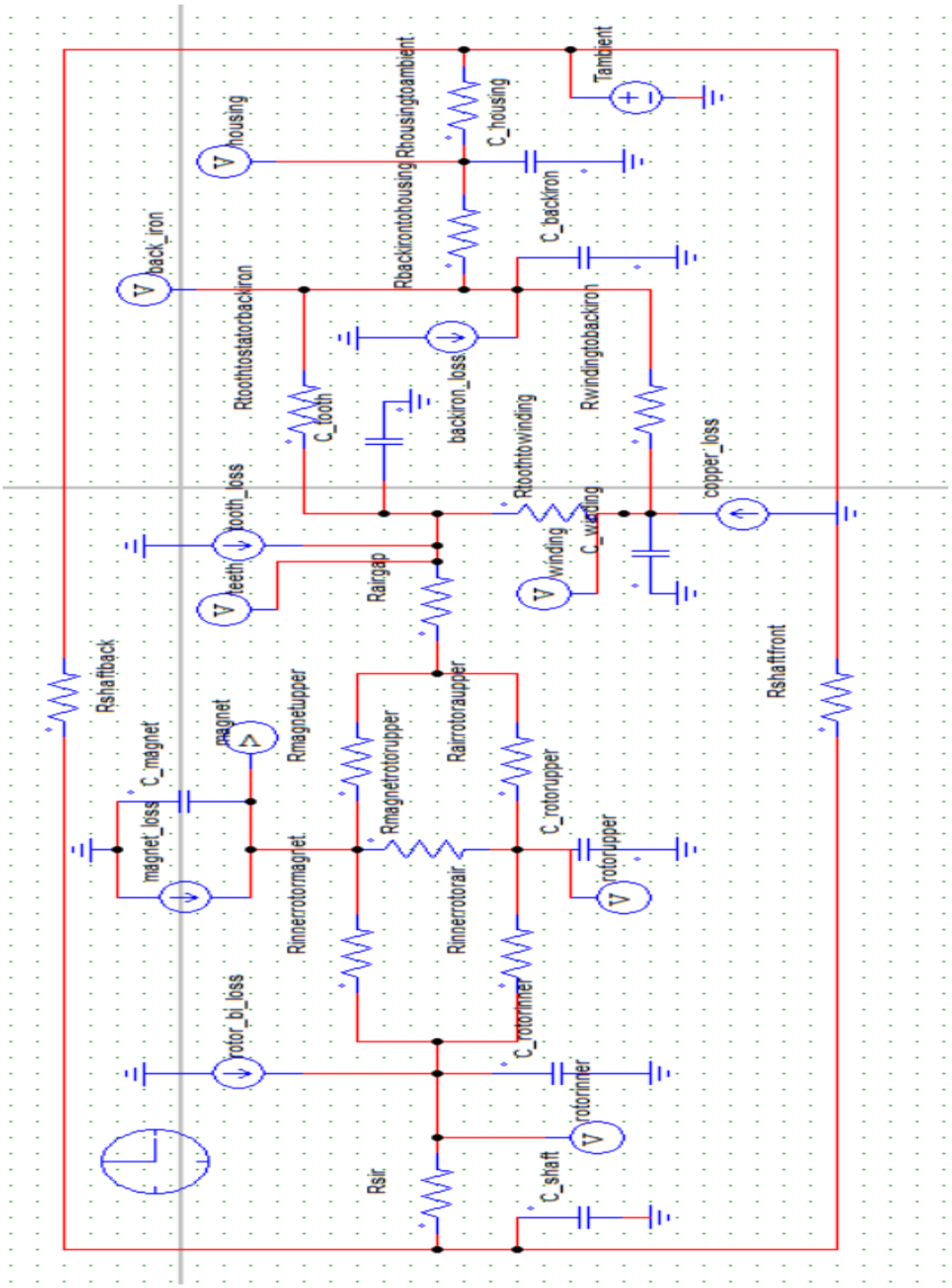

Figure 3.26. Simplified model of SMC PMSM on PSIM software.

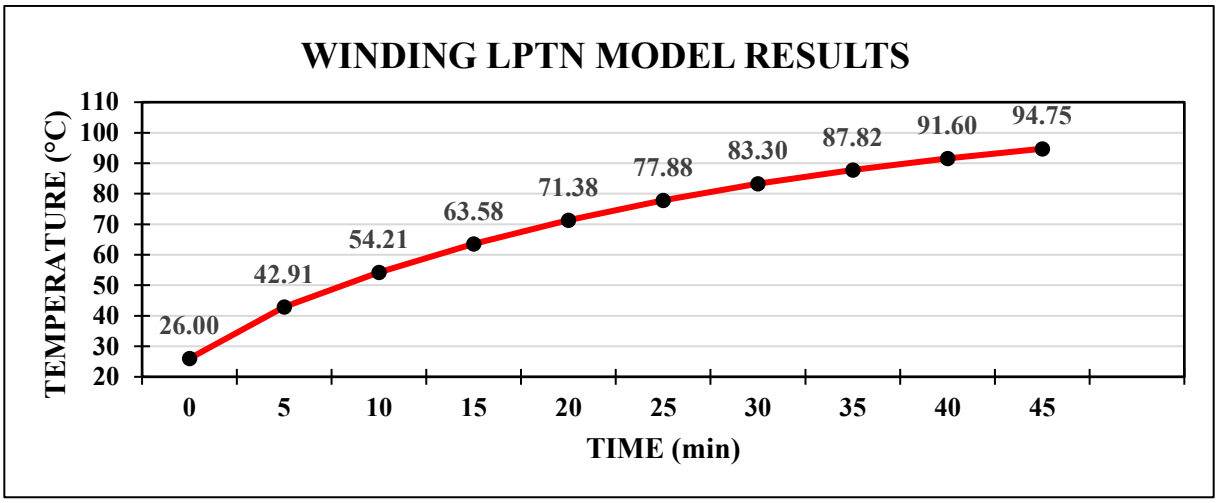

Figure 3.27. Winding model temperature prediction results.

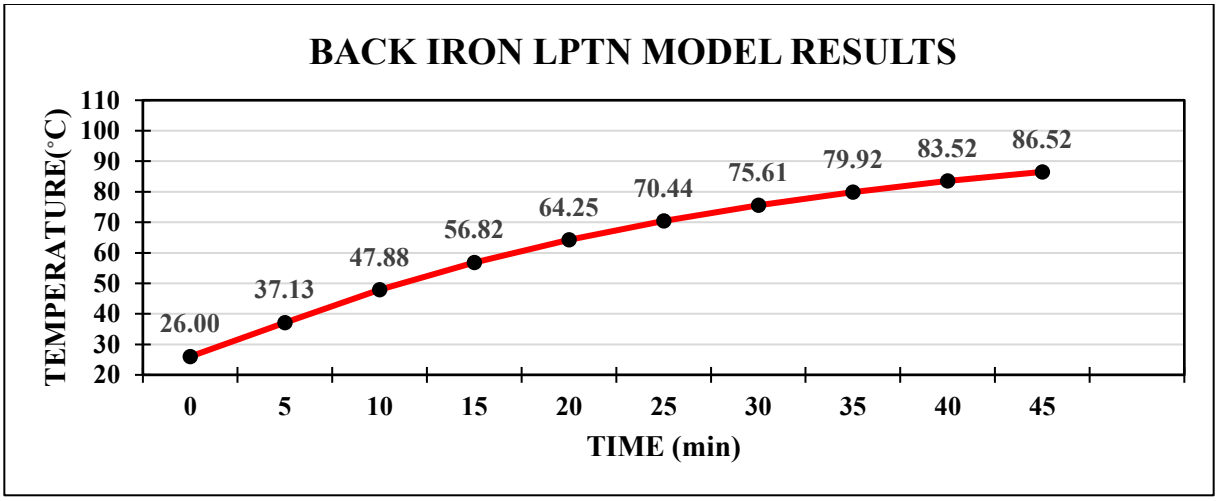

Figure 3.28. Back Iron model temperature prediction results.

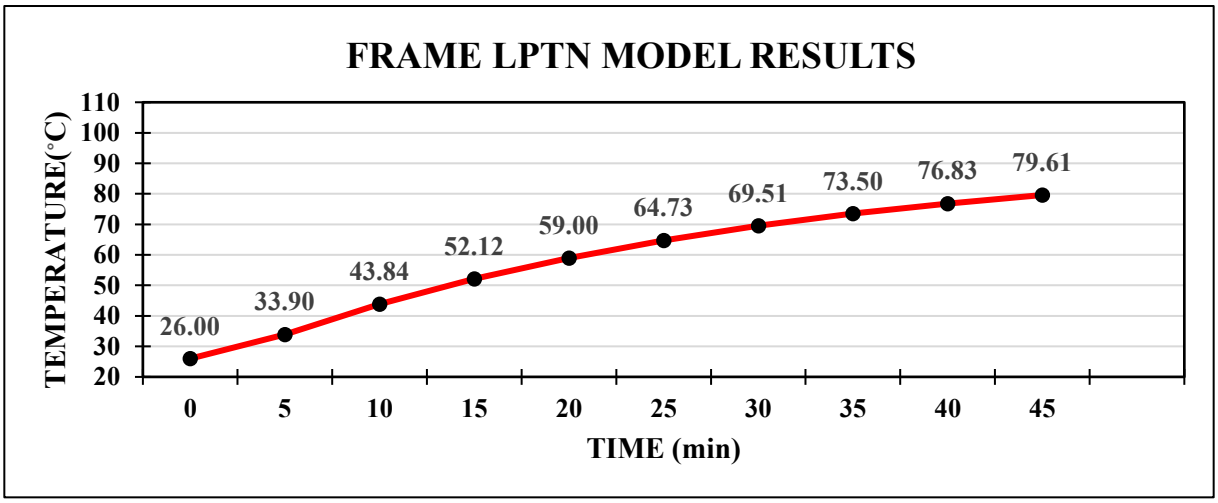

Figure 3.29. Housing Frame Temperature Prediction results.

3.6. Summary

In this section, thermal modeling analyses of two different designs of PMSMs with approximately the same power are presented. Two thermal circuits with two different geometrical structures are designed. Resistance and capacitance calculations are made for these thermal circuits. In order to calculate these parameters, the thermal conductivity, specific heat capacity and physical dimensions of the components inside the motor were determined. A network structure connecting each component is analyzed and temperature parameters are estimated. For resistance calculations, the geometrical structure was analyzed and each unit was calculated with numerical data. As a result of the calculations, the circuit was completed and analyzed with electrical circuit analysis on PSIM software and the temperature rise was monitored. Temperature increases are shown by transient plots for both motors. As expected, the temperature rise of the motor with higher speed and current value was approximately twice as fast. According to the results of the modeling, the winding is the hottest region for both motors, while the housing region, which has direct contact with the environment, is the coldest region. In the next chapter, thermal experiments and simulations are made for both motors to compare the results between the thermal model, simulation and experiment.

4. THERMAL EXPERIMENT OF SPMSM AND SMC PMSM

To run thermal experiments for the SPMSM and SMC PMSM electric motors, temperature sensors were placed at various points inside the motor. Six of them were placed in the end winding area, four in the stator back iron area, one on the stator back iron surface and the last one on the housing frame for SPMSM. The ambient temperature is 24 °C for SPMSM experiment and 26 °C for the SMC PMSM experiment.

Sensors 1, 3 and 5 are placed on the end winding facing the front of the motor. Sensors 6, 8 and 10 are placed on the rear end winding of the motor. Sensors 2 and 4 are placed in the stator back iron facing the front side and sensors 7 and 9 are placed in the rear facing part. Sensor 12 is placed on the stator back iron surface, while sensor 11 is positioned on the housing frame surface. The reason for using more than one sensor for areas inside the motor is that some areas inside the motor heat up more than others. So, there may be irregular heat transfer inside the motor. To prevent this, more reliable results can be obtained by averaging the values recorded by the sensors placed in different regions. The data from these sensors were collected and then averaged and compared with the simulation and thermal model.

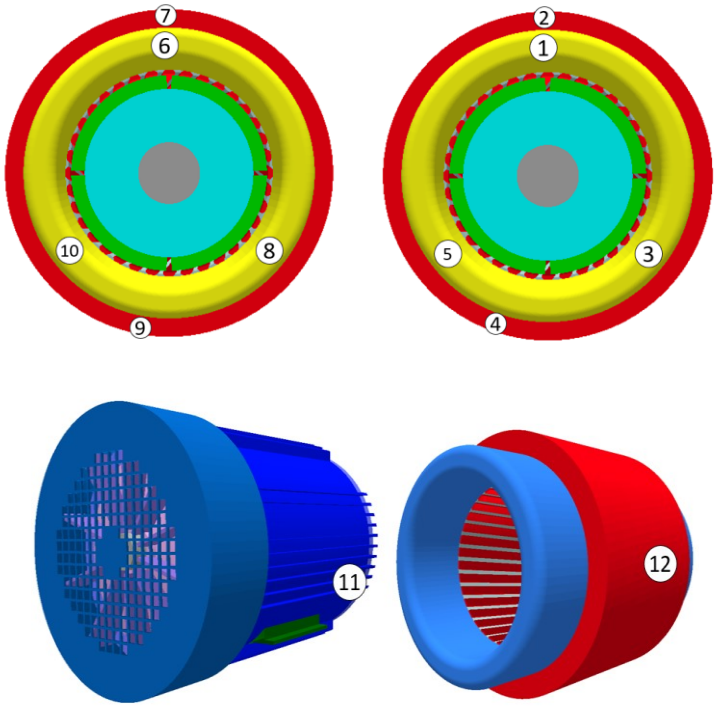

Figure 4.1. Sensor locations on the electric motor.

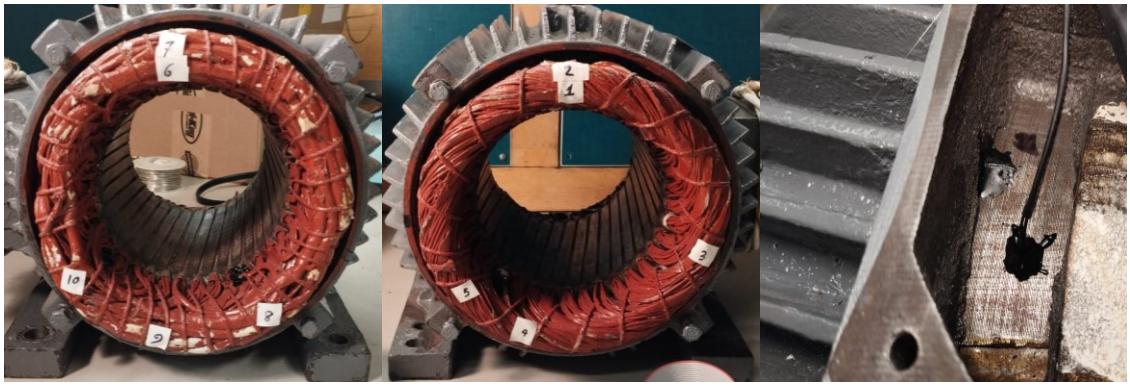

Figure 4.2. Sensor placement on electric motor.

For the SMC PMSM we could not have chance to open the motor so 5 sensors are placed. One sensor placed on active windings. Since the temperature of windings are different on each point, the sensor temperature is considered average temperature of windings. On the other hand, two sensors are placed on stator back iron so we have option to take the average. Also, other two sensors are located on the different parts of frame to estimate the average temperature. Since we have more option to put the thermistors on SPMSM, we would be able to have better results.

4.1. Experiment Setup

A dyno system was used to run the electric motor. SPMSM was operated at 1000 rpm and at full load and SMC PMSM was operated 3400 rpm at half load. When running thermal tests, the time required for the thermal steady state to reach can vary and take a long time depending on the motor type, applied current intensity, motor load and cooling systems. In this experiment, for SPMSM the peak current at full load was set to 16 A and the test continued until the steady state temperature of the motor was reached. After about four hours, the system has stabilized and the motor has reached steady state temperature. For SMC PMSM there were some limitations to reach steady state and full load. Firstly, applying 170 A current to the motor takes some time which is not good for the thermal measurement. If we cannot apply 170 A current in 1 minute, the transient graph of the temperature will change. The reason of this the motor temperature will rise until reach to full load conditions, so it will give wrong results for the experiment aim. On the other hand, the system cannot reach steady state temperature because of the temperature limits of the motor insulations. The operation temperature is determined maximum 120 °C to protect the insulation. According to simulation and model predictions, the temperature will

increase to 150 °C, which is higher than limitations. Therefore, the experiment should stop when the temperature reaches 100 °C to protect the motor. After these limitations, the experiment could run around one hour and in one hour the hottest point of the motor increased 100 °C. The experimental system is based on different components as shown in the figure. First, the electric motor was placed on the bench and its alignment with the dyno was adjusted. Alignment is very critical for the motor to remain stable during the experiment and for the system to operate robustly at a certain level. If the alignment is not done, the motor can be mechanically damaged and cause breakdowns. The experimental set-up contains has a dyno system with 13 kW capacity. It allows the motor to be tested against a real-time load value. In addition, the system can be controlled by computer thanks to the Opal-Rt real-time simulation equipment used in the system. DAQ circuit is used to collect the temperature data from the sensors and obtain numerical values. Inverter is also included in the system to adjust the voltage and current. Variac is used to control the voltage received from the supply. You can see the positions of all components in the figure. SPMSM and SMC PMSM motors are tested on some bench and same conditions.

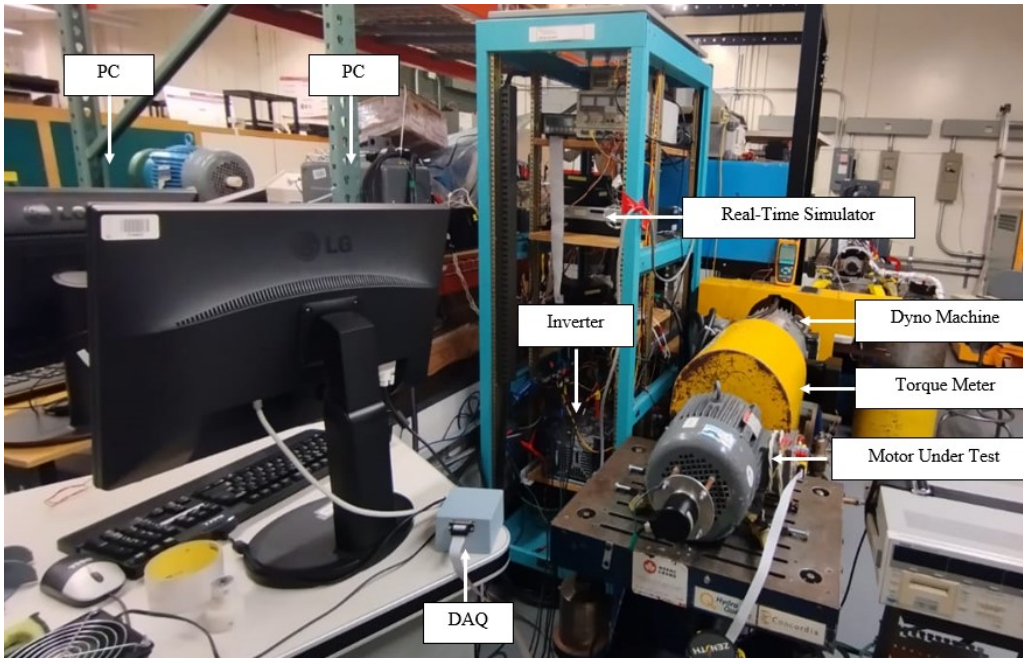

Figure 4.3. Experiment Setup.

4.2. Temperature Results of the Experiment

4.2.1. SPMSM Experiment Temperature Results

As a result of the 4-hours experiment, the temperature values were obtained without any problems. When all the temperature data were collected and the average data at the relevant points were calculated, as predicted, the hottest area was the windings. The winding temperature reached 70 degrees Celsius within one hour. The temperature increase was then seen to reach 80 degrees within 2 hours and 90 degrees at the end of about four hours with the slowing down of the heat transfer. In the stator back iron section with different sensors, the temperature reached an average of 85 degrees at the end of the experiment. Unlike the windings, this area heated up later and reached 75 degrees at the end of 2 hours. As expected, the housing region, which has direct contact with the ambient and transfers heat to the ambient through natural convection, was the region that heated up the latest and reached the lowest temperature. Reaching 80 degrees in about 2.5 hours, the housing reached 83 degrees according to the data obtained at the end of the experiment.

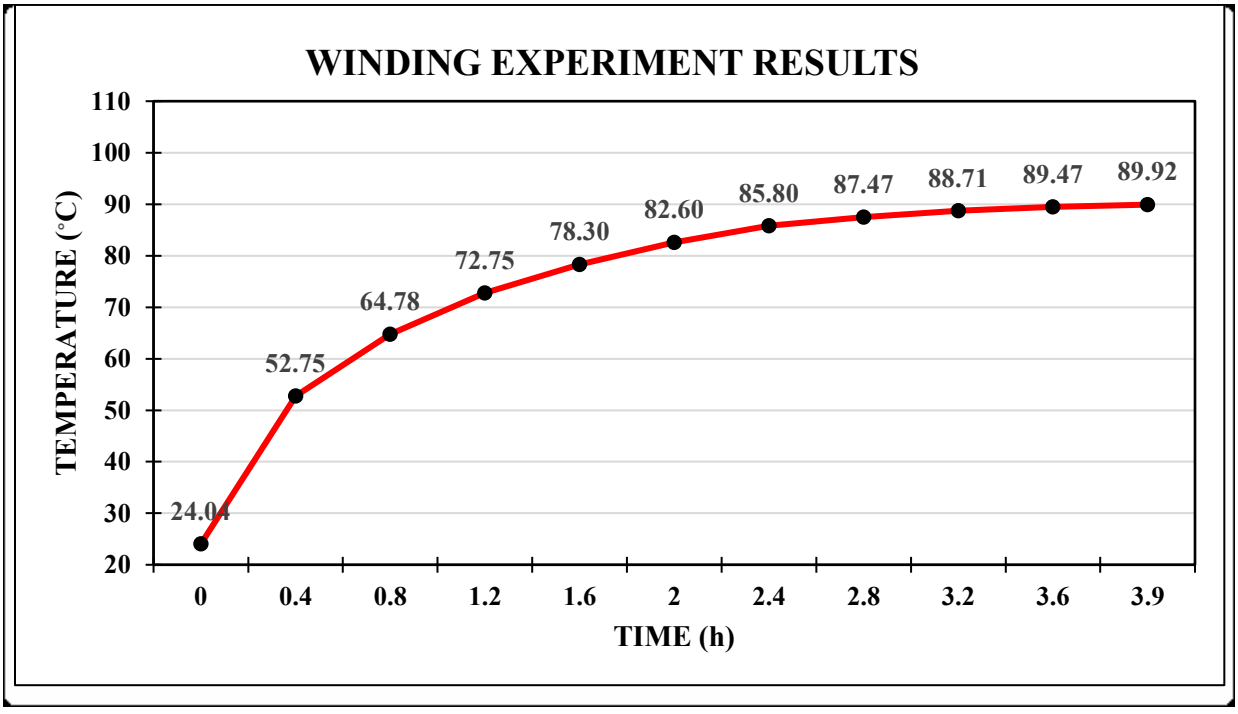

Figure 4.4. SPMSM winding experiment results.

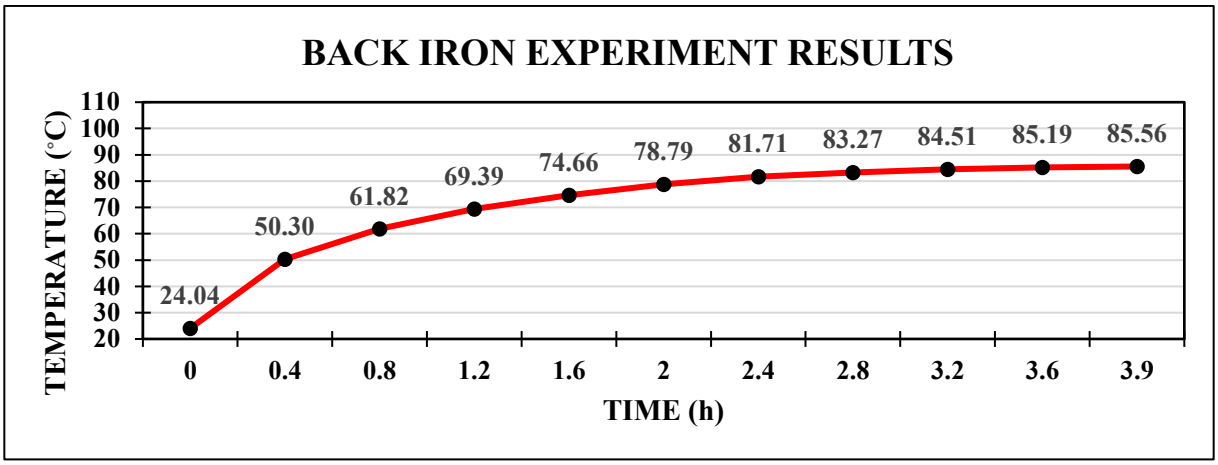

Figure 4.5. SPMSM back iron experiment results.

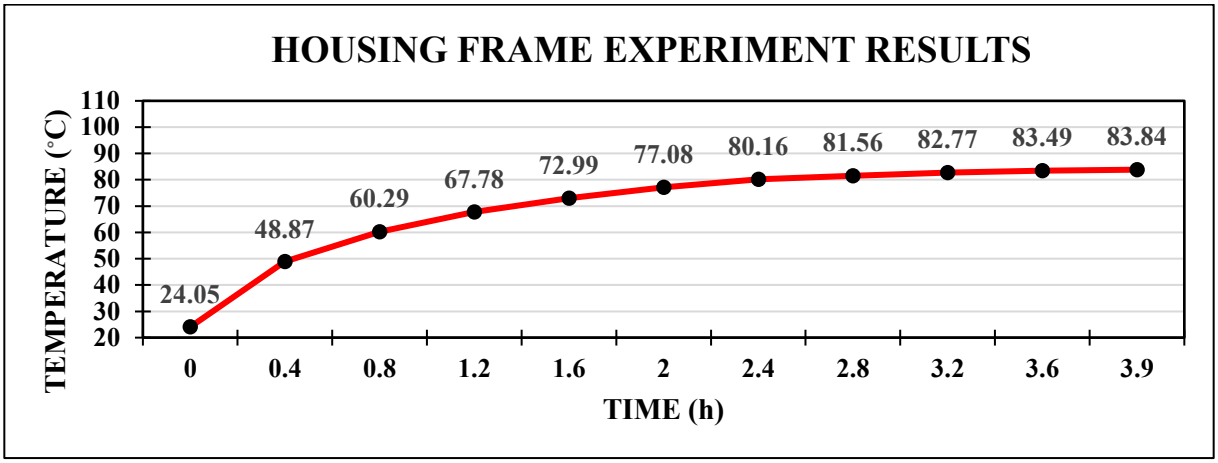

Figure 4.6. SPMSM housing frame experiment results.

4.2.2. SPMSM Simulation Temperature Results

MOTOR-CAD simulation software was used for FEA results. The reason for choosing this software for simulation is that it supports the LPTN method and provides comparisons. According to the simulation results, the temperature data obtained show a difference of 3-4 degrees compared to the experimental results. According to the simulation data, although the transient graph is similar to the experiment, it shows different values at steady state. For example, for the winding temperature, it reached approximately 93 degrees as a result of a 4-hour simulation. While the back iron temperature was 89 degrees, the housing temperature was simulated to be approximately 84 degrees.

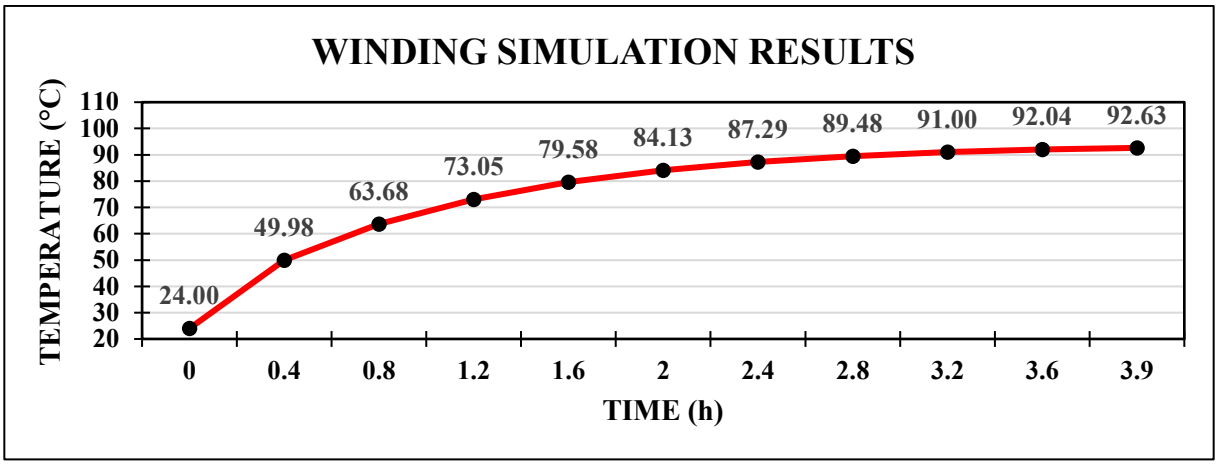

Figure 4.7. SPMSM winding simulation results.

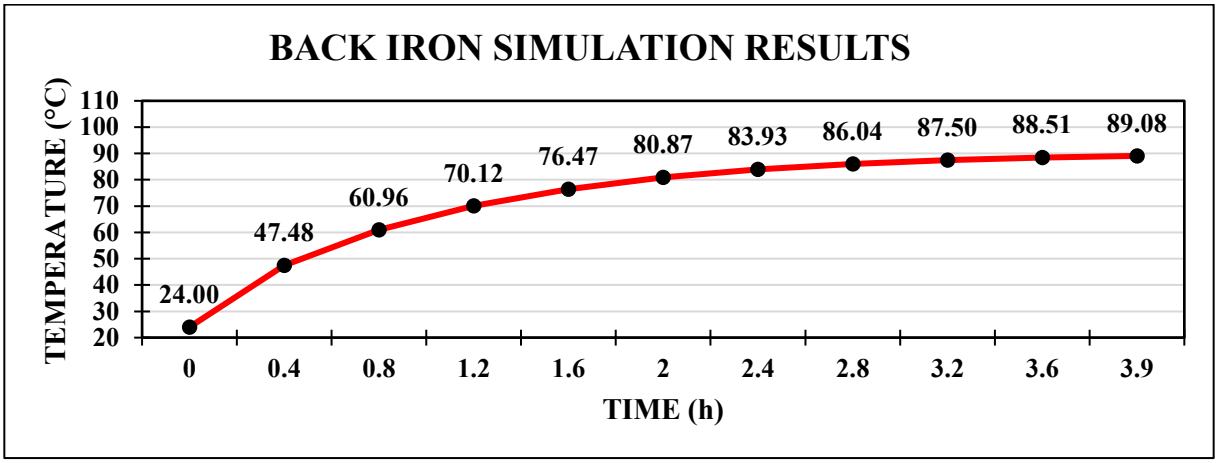

Figure 4.8. SPMSM back iron simulation results.

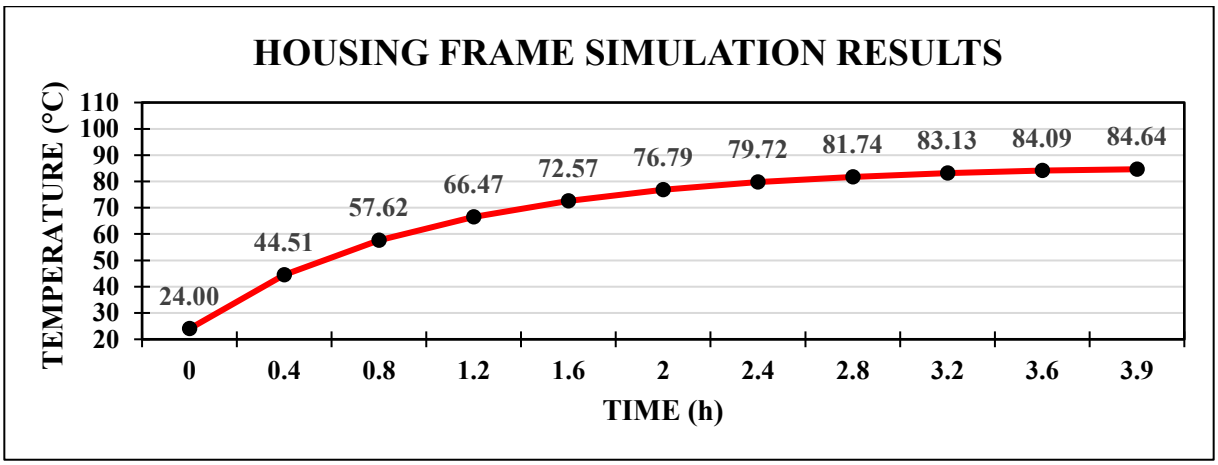

Figure 4.9. SPMSM housing frame simulation results.

4.2.3. SMC PMSM Experiment Temperature Results

After a 45-minute experiment, the system reached the specified temperature limit conditions. As expected, the winding temperature increased rapidly due to the high current applied. At the end of the experiment, it was noted that the winding temperature reached approximately 100 degrees Celsius. While the winding temperature increased by 14 degrees in the first five minutes, the temperature increase was less than 4 degrees in the last five minutes. This result can be estimated that the winding temperature will be around 120 degrees at half load and steady state. The temperature difference between the parts was observed to be high because the temperature increase was too fast and the system could not reach the steady state point. The stator back iron temperature was above 85 degrees Celsius at the end of the experiment, while the housing temperature remained below 75 degrees Celsius. When approximation is made, it is seen that the stator back iron temperature can rise above 100 degrees when the steady state is reached and it is predicted that this temperature can damage the system. In the part that is in direct contact with the ambient and radiates heat to the environment through natural convection, the housing temperature reaching 100 degrees can damage electronic components that may be around it.

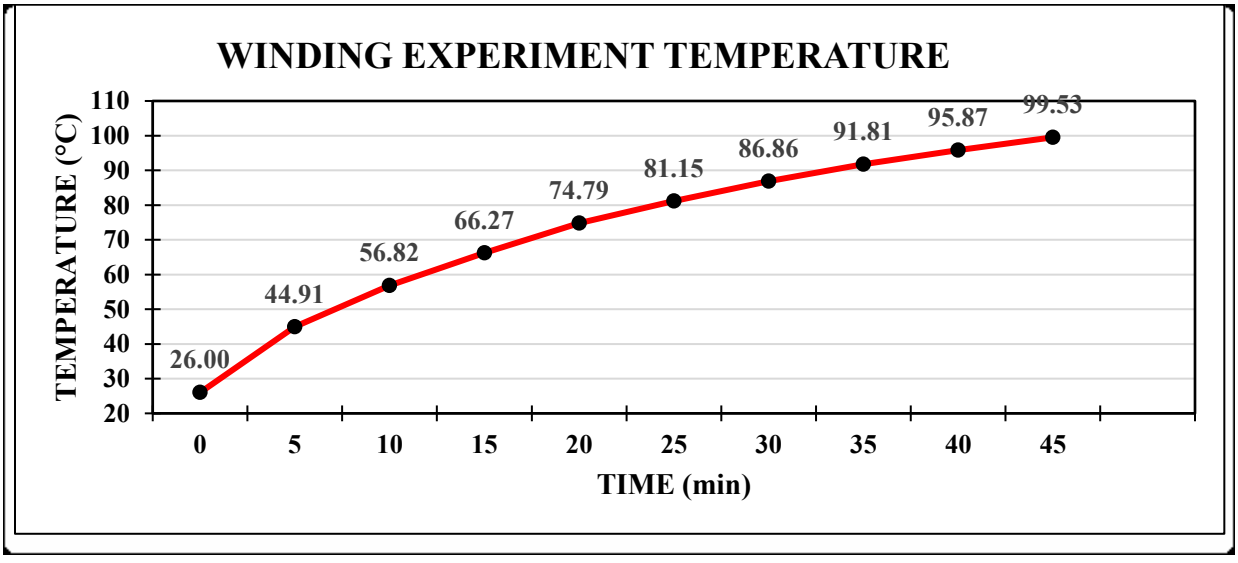

Figure 4.10. SMC PMSM winding experiment temperature results.

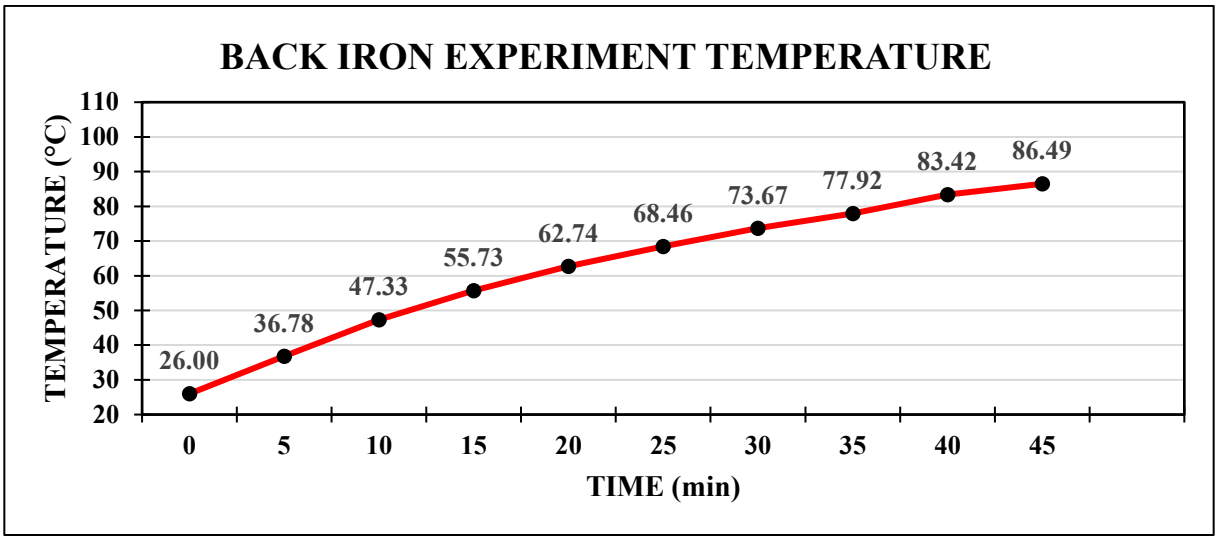

Figure 4.11. SMC PMSM back iron experiment temperature results.

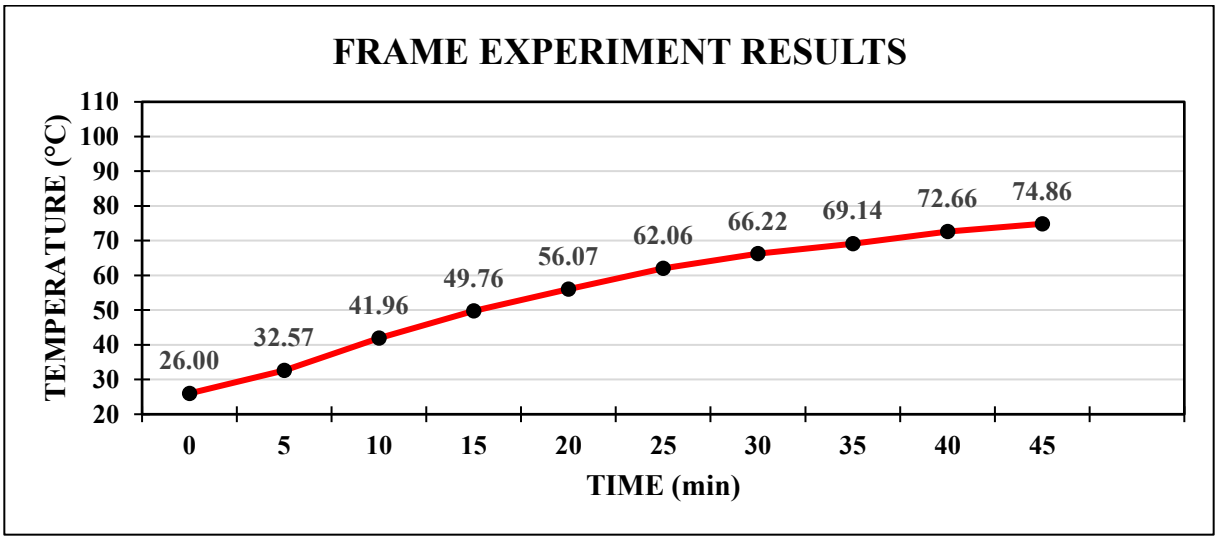

Figure 4.12. SMC PMSM housing frame experiment temperature results.

4.2.4. SMC PMSM Simulation Temperature Results

MOTOR-CAD simulation software was used for FEA results. When the simulation results were obtained, although the transient graphs were similar to the experimental data, the temperature data at the end of 45 minutes showed differences. The highest temperature value measured in the windings where the temperature increase was expected to be the highest was below 90 degrees. On the other hand, the stator back iron temperature was about 80 degrees while the housing temperature was below 75 degrees.

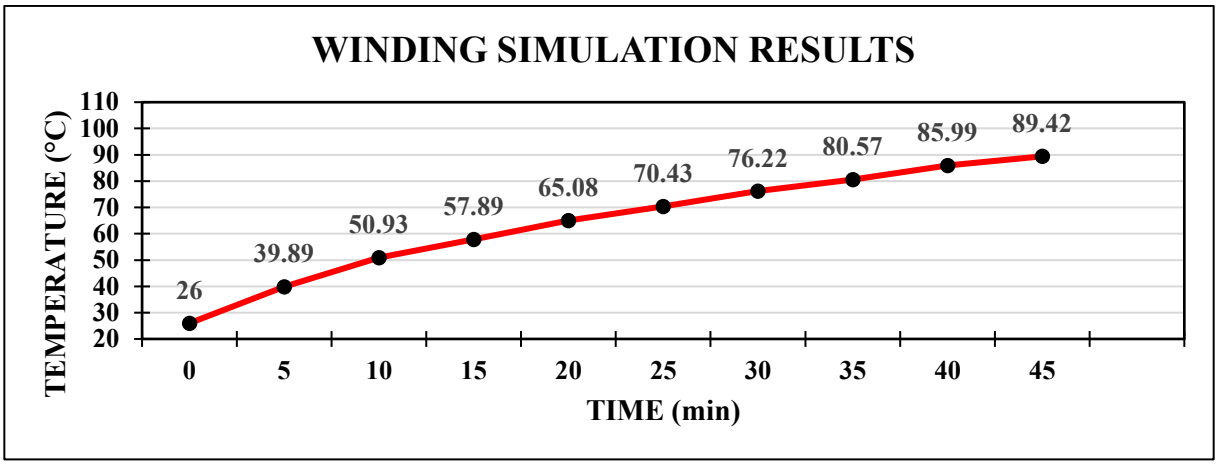

Figure 4.13. SMC PMSM winding simulation results.

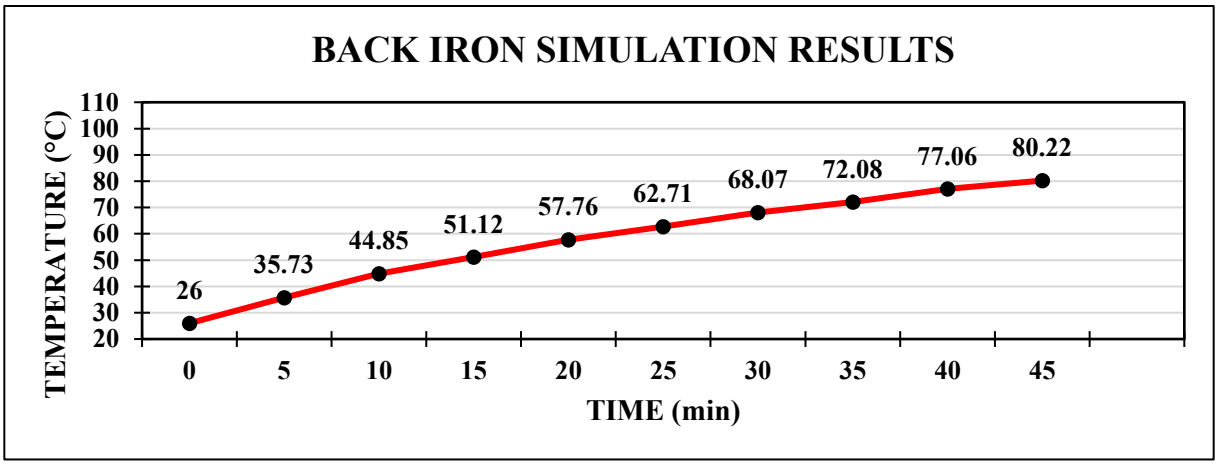

Figure 4.14. SMC PMSM back iron simulation results.

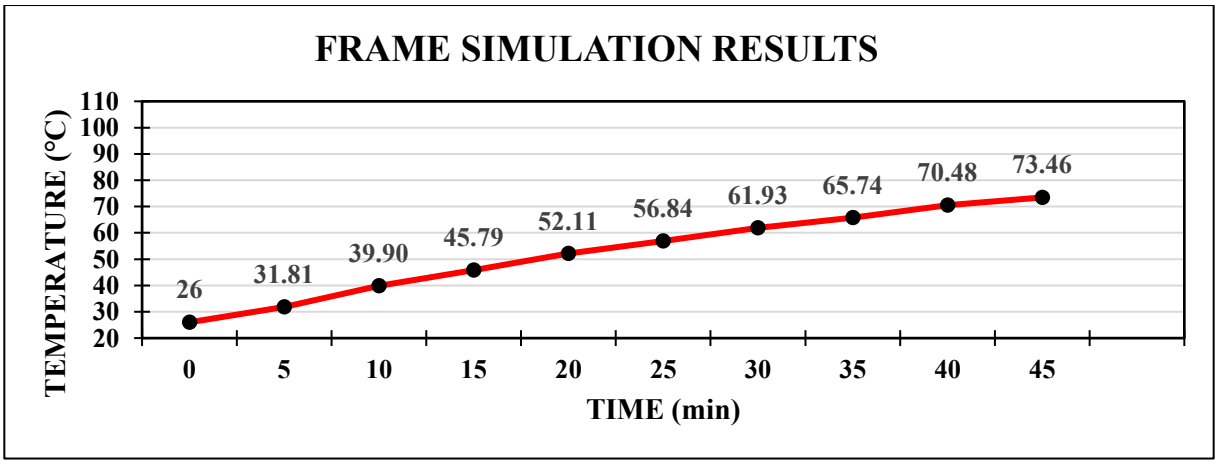

Figure 4.15. SMC PMSM housing frame simulation results.

4.3. Temperature Comparisons According to Experiment, Motor-Cad Simulation and Lumped Parameter Thermal Network (LPTN) Model Results

4.3.1. SPMSM Temperature Comparisons

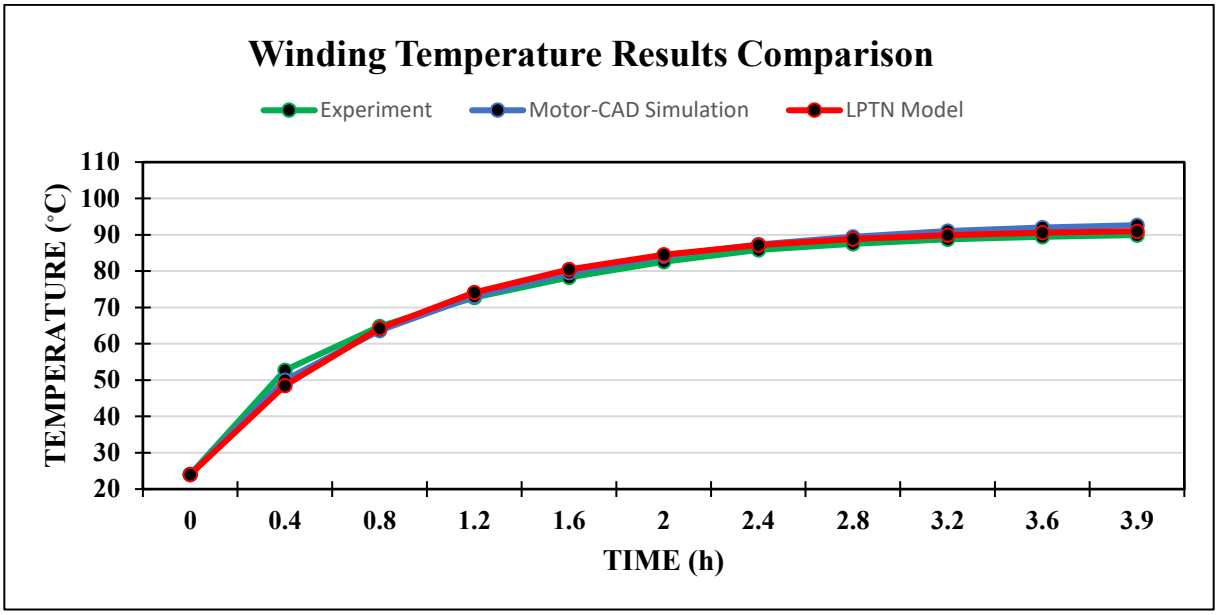

Figure 4.16. SPMSM winding temperature comparisons.

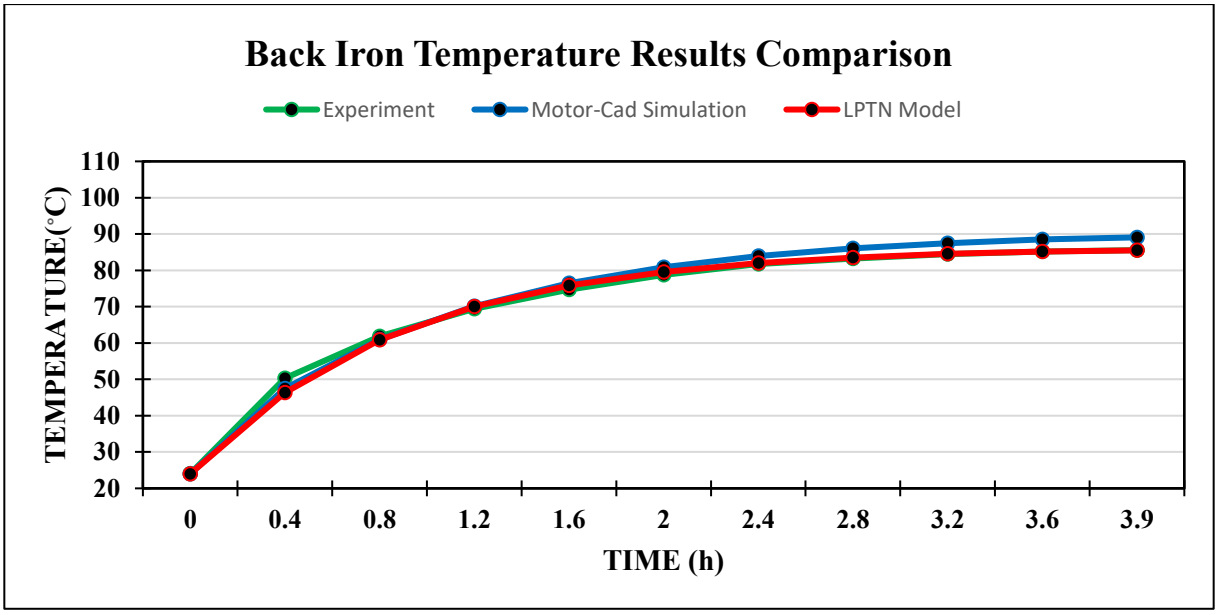

Figure 4.17. SPMSM back iron temperature comparisons.

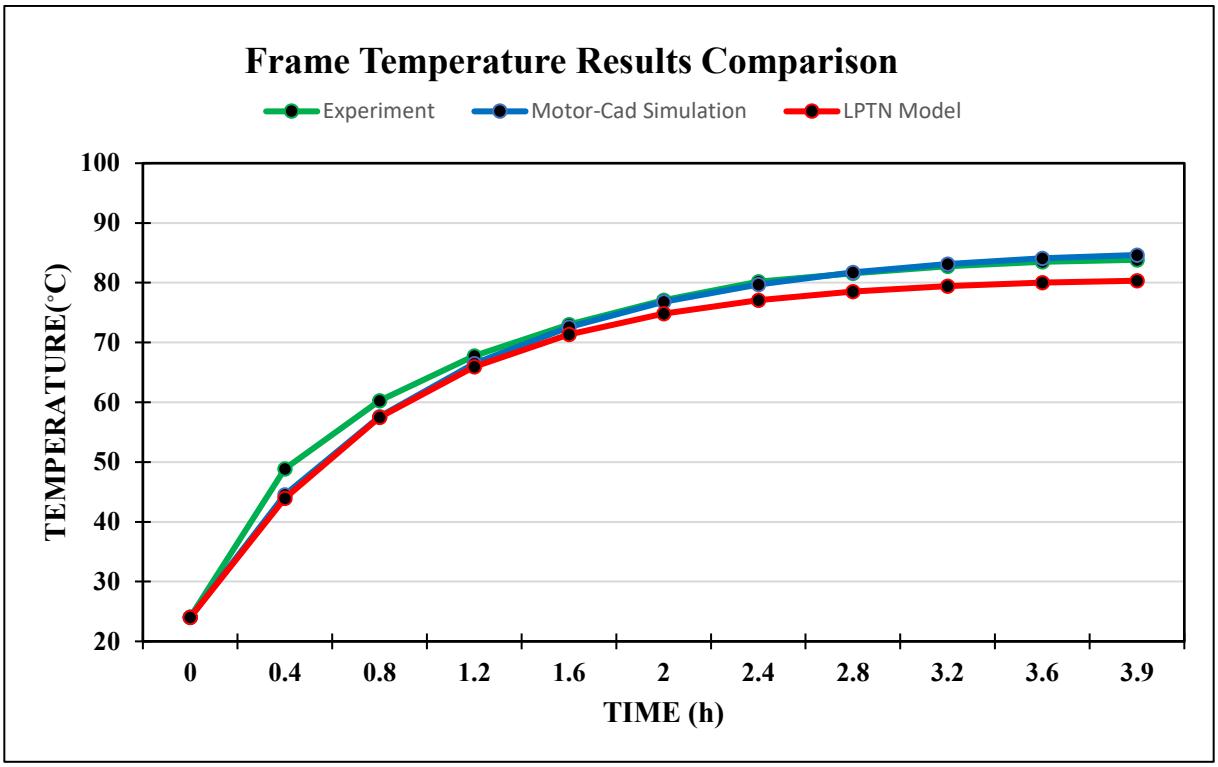

Figure 4.18. SPMSM housing frame temperature comparisons.

When the experimental, simulation and model prediction data were obtained, it was seen that all data for the SPMSM model almost matched each other. When the winding temperatures are compared, the simulation result shows a 3-percent margin of error compared to the experimental data, while the modeling result shows a lower than 2-percent error. When analyzed, the highest percentage of error was observed in stator back iron measurements. Compared to the experimental data, a simulation result showed a result of 4 percent deviation. In the analysis of temperature predictions made as a result of modeling, the highest error is in the housing region. While the margin of error was 1 percent for simulation, this rate increased to 3 percent for modeling. In summary, the maximum temperature difference according to the simulation parameters is 4 degrees, while for modeling it is 3 degrees. When the whole model is analyzed and predicted correctly, the results are acceptable. In addition, the fact that all the results match each other indicates that the modeling is correct and the theory works properly for this motor. In addition, as a result of the tests performed before comparing the simulation with the experiment, all electromagnetic parameters were matched and the real and simulation conditions were parallel to each other, which increased the accuracy of the results.

4.3.2. SMC PMSM Temperature Comparisons

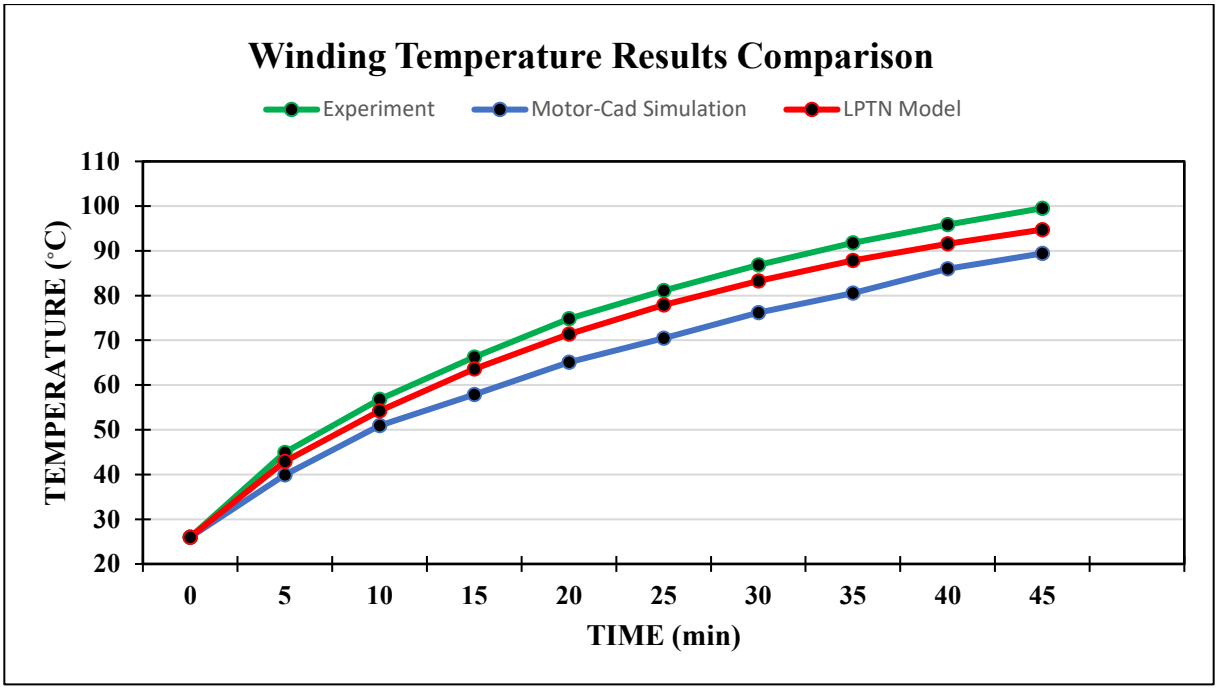

Figure 4.19. SMC PMSM winding temperature comparisons.

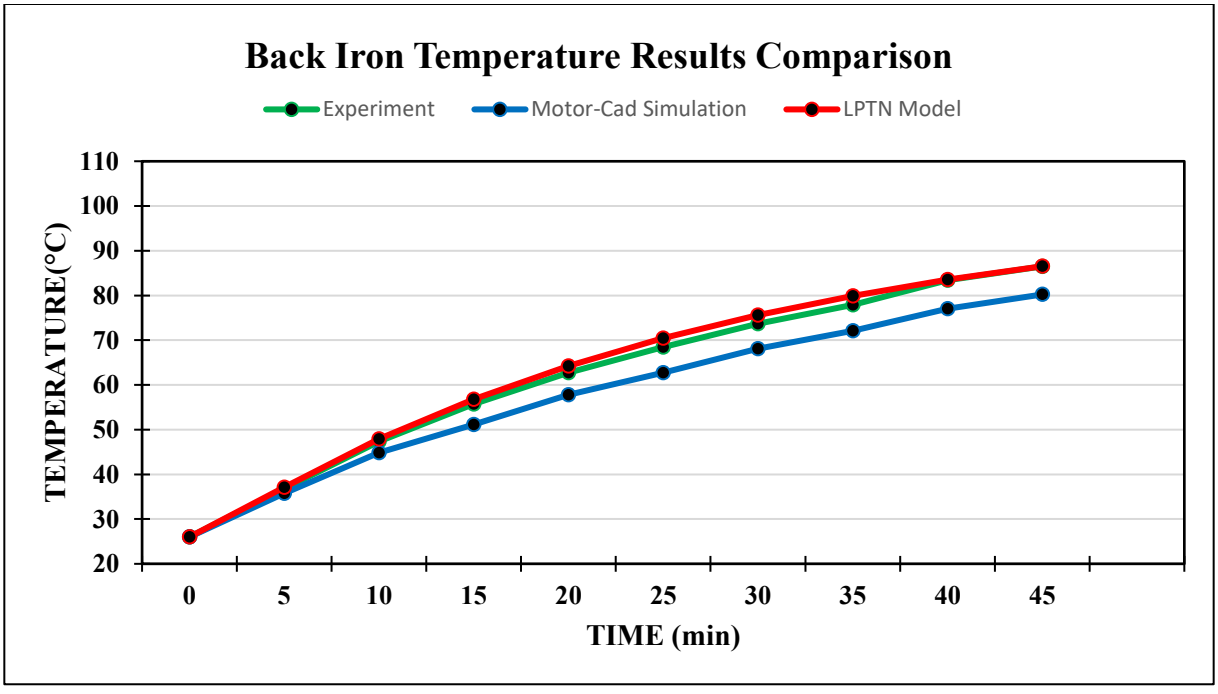

Figure 4.20. SMC PMSM back iron temperature comparisons.

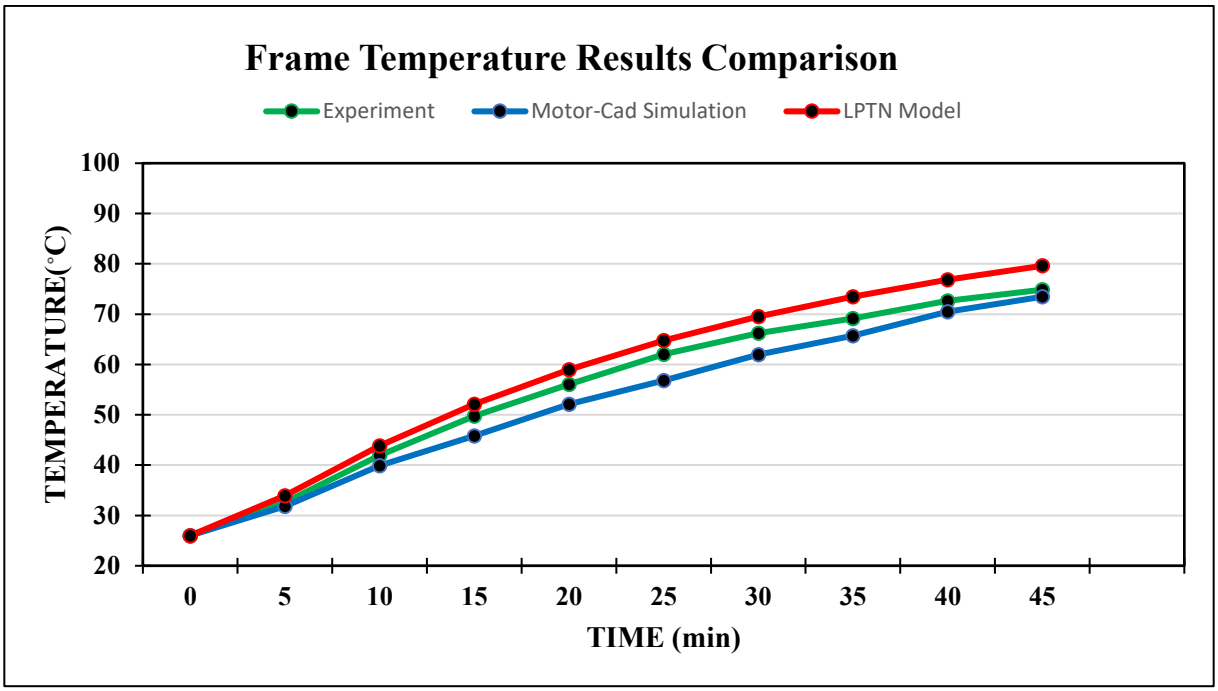

Figure 4.21. SMC PMSM housing frame temperature comparisons.

It was seen that the error rates increased in the measurements made for SMC PMSM. One of the reasons for this increase in errors is the complexity of the motor structure and the calculation difficulties caused by this complexity. When calculations are made for motor parameters, it is important that the geometric shapes are uniform. Since the SMC PMSM rotor and stator structure is very complex, some assumptions have been made on the geometry such as the average radius calculations. In addition, the interpenetration of different materials made the heat dissipation estimation difficult. On the other hand, when the motor simulations were made, an exact geometric design could not be achieved due to some design limitations. For example, the air gaps in the rotor could not be designed in the simulation. In addition, the new generation technological components used in the winding configuration do not have exact equivalents in the simulation. All these parameters were simulated with the data containing the closest results. The complex structure of the motor components has caused problems in formula solutions during analytical analysis and these problems have been solved by making some assumptions. These geometrical, analytical and electrical limitations caused an increase in the margin of error.

As can be seen in the figure, the difference between simulation data and experimental data for winding temperatures is about 10 degrees, while the result obtained from modeling differences by

5 degrees. As can be seen in the figure, the difference between simulation data and experimental data for winding temperatures is about 10 degrees, while the result obtained from modeling differences by 5 degrees. In proportion, whereas the simulation error is 10 percent, the modeling error is measured as 5 percent. For the stator back iron, the simulation gave an error of 8 percent when the modeling predicted almost the same temperature value. On the other hand, for the housing temperature, the simulation data is accurate with an error of about 2 percent, while the modeling error is approximately 5 percent. When all the parameters were calculated and compared, the modeling itself gave a more realistic result as it was calculated based on the characteristics of the real geometric structure. The accuracy factor for modeling is 5 percent or less, which is acceptable even if the error rate increases in complex motors.

4.4. Summary

This section describes the real-time experiments and simulation results for PMSM motors. For the experimental studies, the critical temperature was set as 100 C and the experiment was terminated when the system exceeded this temperature. Temperature sensors were placed inside the motors to collect temperature data and these data were analyzed during operation. In addition, simulation data and experimental data are compared and error margins are analyzed. As a result of the experiments, SPMSM reached the steady state temperature and the experiment was carried out for about 4 hours. For SMC PMSM, the critical temperature was reached in about 1 hour and the experiment was finalized. Since all data are observed the thermal model results was analyzed according to experiment and simulation results.

5. CONCLUSION

According to the data obtained as a result of all literature studies, the number of electric vehicles is increasing day by day. The benefits and drawbacks of this radical change in the transportation sector are the subject of new research. To summarize, it is obvious that the use of electric vehicles alone cannot change the transportation sector. In order to get rid of the global warming problem, we need to use the advantages that this new technology offers to humanity. The most important issue is that in addition to using electric vehicles to get rid of dependence on fossil fuels, the energy provided for these vehicles must also be clean and sustainable. In other words, it would not be very environmentally friendly option, if electricity is provided from fossil fuels such as coal and oil for electric vehicles. The fact that renewable energy sources provide the electrical energy required for electric vehicles will both increase efficiency and have a cleaner energy supply.

Chapter 1 shows how widespread the types of electric vehicles and their use in the transportation sector are. In addition, it is analyzed how the primary energy factor of electric vehicles has changed. Considering that well-to-wheels energy conversions vary between 10 percent and 50 percent, it is necessary to use the systems accurately in order to use electric vehicles more efficiently. With the development and expansion of the charging infrastructure, production, transmission and distribution losses can be prevented and efficiency can be increased with the right planning.

One of the most important details that make electric vehicles sustainable and renewable is the electric motor. With the introduction of electric motors in traction applications, more efficient, sustainable and smooth driving applications have been developed in vehicle motors. According to the results of the research, it was seen that electric motor technology is suitable for all kinds of vehicles. Electric scooters, bicycles, three wheels vehicles, cars, buses, trucks, trucks, marine industry and air industry have become widespread use of electric motors in daily life.

Studies in the field of electric motors have accelerated with the rapid development of electric vehicles. One of the most preferred models in this field today is Permanent Magnet Synchronous Motors. These motors have an important role in electric vehicle applications thanks to their high efficiency, torque and wide speed range. With the advantage of having high power density, they can provide high power in small sizes. Their small size within the vehicle structure provides an

advantage to developers in the design stages. In addition, the fact that it is suitable for all kinds of applications shows that it has a wide range of fields of practice. With the development of control mechanisms, it can be seen in almost every new electric vehicle model today. With all these features, it has become a preferred motor type for electric vehicle applications.

As seen in Chapter 1 and 2, it has been proven by researchers that PMSM motors are more efficient and have higher power density than other types. Other advantages are their ability to provide high torque at low speeds and to reach high speeds.

Along with all these advantages, the PMSM motor has brought with it some difficult problems to overcome. One of the most important issues is thermal management. Due to its complex structure and high-power density, the large amount of heat released causes the motor temperature to rise and this can lead to various problems. For example, it can reduce the lifetime of motor components in the long term or cause mechanical and electrical damage in the short term. To overcome all these problems, it is necessary to predict the thermal performance of the motor and designing suitable cooling systems accordingly. In addition to simulation programs developed to predict the motor temperature parameters, some thermal analysis methods are available. In this thesis, Lumped Parameter Thermal Network Method, one of the thermal analysis methods, is applied on the PMSM motor.

As discussed in Chapter 2, LPTN is a modeling method using thermal resistance, capacitance and heat sources. It offers the possibility of thermal analysis by designing a circuit similar to an electrical circuit. In this study, the importance of the geometric and specific properties of the material while calculating the thermal resistance and capacitance data is demonstrated.

In Chapter 3, the thermal modeling showed that two different motors have very different thermal circuits. The structural differences of these motors with two different designs and input parameters created some disadvantages. One of the problems brought by the complex structure is the increase in the number of nodes. As seen in the two different models, there are more nodes in the thermal circuit of the SMC PMSM motor than the SPMSM motor. This has increased the complexity and may cause a decrease in efficiency. It is also seen that changing the geometric structure can affect the heat transfer. Calculation and analysis of thermal parameters of interpenetrating materials became difficult and increased the number of equations.

In Chapter 4, the operational temperature predictions of two different motors are made and the results are compared with experimental and simulation results. Some differences were observed when thermal model, simulation and experimental data were compared. The results show that thermal modeling provides accurate temperature parameters with an error of less than 5 percent. In the study, the margin of error of the motor with a simple design was low, while the margin of error of the motor with a complex structure increased. This shows that increasing the complexity of the structure will bring new assumptions and the error margin of the analysis will increase. In addition, when the simulation results are compared, it is seen that while there is less than 5 percent error for SPMSM, the errors are up to 10 percent for SMC PMSM. This shows that simulation results cannot be completely reliable when designing the motor. It has shown that the complex motor structure can lead to different results. On the other hand, it has been seen how important the design of the appropriate cooling system will be. While the temperature increase in the SMC PMSM motor with high current is very fast and can reach the steady state temperature in almost an hour, it is found that the SPMSM motor with low current can reach the steady state temperature in 3 hours. This indicates the importance of designing a cooling system that can act in a shorter time for motors that reach high temperatures in a short time. In summary, thermal analysis is critical for an electric motor. Correctly performed analyses can improve motor efficiency and extend its lifetime.

5.1. Future Work

All analyses provided a basis for future studies. First of all, a suitable cooling system can be designed for these two different motors and the differences can be demonstrated. The variability of cooling capacity according to power, speed and current values can be analyzed. It can be investigated whether air cooling systems are sufficient or whether an additional liquid cooling system is needed.

Another future study could be to investigate the effects of temperature increase on mechanical or electrical parameters. For example, efficiency losses can be analyzed as the temperature increase affects the resistivity. The reason for this is that the electrical parameters change with temperature and the motor power decreases. With increasing motor losses, more heat is released and the effects on motor efficiency can be analyzed.

References

[1] Report on Paris Agreement, United Nations Framework Convention on Climate Change, 22 Oct. 2018 [Online]. Available: The Paris Agreement | UNFCCC

[2] Maantay, J., & Becker, S. (2012). The health impacts of global climate change: a geographic perspective. *Applied Geography*, *33*, 1-106.

[3] Mestre-Sanchís, F., & Feijóo-Bello, M. L. (2009). Climate change and its marginalizing effect on agriculture. *Ecological economics*, *68*(3), 896-904.

[4] Yang, W., Li, T., & Cao, X. (2015). Examining the impacts of socio-economic factors, urban form and transportation development on CO2 emissions from transportation in China: a panel data analysis of China's provinces. *Habitat International*, *49*, 212-220.

[5] World Business Council for Sustainable Development (WBCSD). (2004). Mobility: 2030: http://docs.wbcsd.org/2004/06/Mobility2030-ExSummary.pdf

[6] Thiel, C., Julea, A., Acosta Iborra, B., De Miguel Echevarria, N., Peduzzi, E., Pisoni, E., ... & Krause, J. (2019). Assessing the impacts of electric vehicle recharging infrastructure deployment efforts in the European Union. *Energies*, *12*(12), 2409.

[7] Roy, P. (2020). *Thermal Modeling of Permanent Magnet Synchronous Motors for Electric Vehicle Application* (Doctoral dissertation, University of Windsor (Canada)).

[8] Liu, W., Hu, W., Lund, H., & Chen, Z. (2013). Electric vehicles and large-scale integration of wind power–The case of Inner Mongolia in China. *Applied energy*, *104*, 445-456.

[9] Hezam, I. M., Mishra, A. R., Rani, P., Cavallaro, F., Saha, A., Ali, J., ... & Štreimikienė, D. (2022). A hybrid intuitionistic fuzzy-MEREC-RS-DNMA method for assessing the alternative fuel vehicles with sustainability perspectives. *Sustainability*, *14*(9), 5463.

[10] Tong, F., & Azevedo, I. M. (2020). What are the best combinations of fuel-vehicle technologies to mitigate climate change and air pollution effects across the United States? *Environmental Research Letters*, *15*(7), 074046.

[11] Brase, G. L. (2019). What would it take to get you into an electric car? Consumer perceptions and decision making about electric vehicles. *The Journal of psychology*, *153*(2), 214-236.

[12] Fenton, J., & Hodkinson, R. (2001). Lightweight electric/hybrid vehicle design.

[13] De Novellis, L., Sorniotti, A., Gruber, P., & Pennycott, A. (2014). Comparison of feedback control techniques for torque-vectoring control of fully electric vehicles. *IEEE Transactions on Vehicular Technology*, *63*(8), 3612-3623.

[14] Morrow, K., Karner, D., & Francfort, J. E. (2008). Plug-in hybrid electric vehicle charging infrastructure review.

[15] Sciarretta, A., & Guzzella, L. (2007). Control of hybrid electric vehicles. *IEEE control systems magazine*, *27*(2), 60-70.

[16] Maggetto, G., & Van Mierlo, J. (2001, July). Electric vehicles, hybrid electric vehicles and fuel cell electric vehicles: state of the art and perspectives. In *Annales de Chimie Science des Materiaux* (Vol. 26, No. 4, pp. 9-26). No longer published by Elsevier.

[17] Kumar, R. R., & Alok, K. (2020). Adoption of electric vehicle: A literature review and prospects for sustainability. *Journal of Cleaner Production*, *253*, 119911.

[18] Poornesh, K., Nivya, K. P., & Sireesha, K. (2020, September). A comparative study on electric vehicle and internal combustion engine vehicles. In *2020 International Conference on Smart Electronics and Communication (ICOSEC)* (pp. 1179-1183). IEEE.

[19] Taylor, A. M. (2008). Science review of internal combustion engines. *Energy Policy*, *36*(12), 4657-4667.

[20] Yildirim, M., Polat, M., & Kürüm, H. (2014, September). A survey on comparison of electric motor types and drives used for electric vehicles. In *2014 16th International Power Electronics and Motion Control Conference and Exposition* (pp. 218-223). IEEE.

[21] Cuenca, R. M., Gaines, L. L., & Vyas, A. D. (2000). *Evaluation of electric vehicle production and operating costs* (No. ANL/ESD-41). Argonne National Lab., IL (US).

[22] [Online] Available: https://www.nrdc.org/stories/electric-vs-gas-cars-it-cheaper-drive-ev . [Accessed 2023]

[23] Larson, P. D., Viáfara, J., Parsons, R. V., & Elias, A. (2014). Consumer attitudes about electric cars: Pricing analysis and policy implications. *Transportation Research Part A: Policy and Practice*, *69*, 299-314.

[24] Narasipuram, R. P., & Mopidevi, S. (2021). A technological overview & design considerations for developing electric vehicle charging stations. *Journal of Energy Storage*, *43*, 103225.

[25] Giansoldati, M., Monte, A., & Scorrano, M. (2020). Barriers to the adoption of electric cars: Evidence from an Italian survey. *Energy Policy*, *146*, 111812.

[26] Tu, H., Feng, H., Srdic, S., & Lukic, S. (2019). Extreme fast charging of electric vehicles: A technology overview. *IEEE Transactions on Transportation Electrification*, *5*(4), 861-878.

[27] Ravi, S. S., & Aziz, M. (2022). Utilization of electric vehicles for vehicle-to-grid services: Progress and perspectives. *Energies*, *15*(2), 589.

[28] Münzel, C., Plötz, P., Sprei, F., & Gnann, T. (2019). How large is the effect of financial incentives on electric vehicle sales?–A global review and European analysis. *Energy Economics*, *84*, 104493.

[29] Eberle, U., & Von Helmolt, R. (2010). Sustainable transportation based on electric vehicle concepts: a brief overview. *Energy & Environmental Science*, *3*(6), 689-699.

[30] 'What is the role of electric vehicles in clean energy transitions' [online]. Available: https://www.iea.org/energy-system/transport/electric-vehicles . [Accessed 2023]

[31] [online] Available: https://www.iea.org/reports/global-ev-outlook-2023/trends-in-electric-light-duty-vehicles . [Accessed 2023]

[32] [online] Available: https://www.statista.com/outlook/mmo/electric-vehicles/canada#unit-sales . [Accessed 2023]

[33] [online] Available: https://driving.ca/column/driving-by-numbers/10-best-selling-electric-vehicles-canada-2022. [Accessed 2023]

[34] Michaelides, E.E. (2018). Energy, the Environment, and Sustainability (1st ed.). CRC Press. https://doi.org/10.1201/b22169

[35] Elgowainy, A., Han, J., Poch, L., Wang, M., Vyas, A., Mahalik, M., & Rousseau, A. (2010). Well-to-wheels analysis of energy use and greenhouse gas emissions of plug-in hybrid electric vehicles (No. ANL/ESD/10-1). Argonne National Lab.(ANL), Argonne, IL (United States).

[36] Brinkman, N., Wang, M., Weber, T., & Darlington, T. (2005). Well-to-wheels analysis of advanced fuel/vehicle systems: A North American study of energy use, greenhouse gas emissions, and criteria pollutant emissions. EERE Publication and Product Library, Washington, DC (United States).

[37] Michaelides, E. E. (2021). Primary energy use and environmental effects of electric vehicles. World Electric Vehicle Journal, 12(3), 138.

[38] Dorrell, D. G., Knight, A. M., Popescu, M., Evans, L., & Staton, D. A. (2010, September). Comparison of different motor design drives for hybrid electric vehicles. In *2010 IEEE energy conversion congress and exposition* (pp. 3352-3359). IEEE.

[39] Jape, S. R., & Thosar, A. (2017). Comparison of electric motors for electric vehicle application. *international Journal of Research in Engineering and Technology*, *6*(09), 12-17.

[40] Patil, S. V., & Saxena, R. (2022, February). Design & Simulation of Brushless DC Motor Using ANSYS for EV Application. In *2022 IEEE International Students' Conference on Electrical, Electronics and Computer Science (SCEECS)* (pp. 1-5). IEEE.

[41] Pugliese, H., & Von Kannewurff, M. (2013). Discovering DC: A primer on DC circuit breakers, their advantages, and design. *IEEE Industry Applications Magazine*, *19*(5), 22-28.

[42] Gupta, J. B. (2009). *Theory & performance of electrical machines*. SK Kataria and Sons.

[43] Hashemnia, N., & Asaei, B. (2008, September). Comparative study of using different electric motors in the electric vehicles. In *2008 18th international conference on electrical machines* (pp. 1-5). IEEE.

[44] Mohanraj, D., Aruldavid, R., Verma, R., Sathiyasekar, K., Barnawi, A. B., Chokkalingam, B., & Mihet-Popa, L. (2022). A review of BLDC Motor: State of Art, advanced control techniques, and applications. *IEEE Access*, *10*, 54833-54869.

[45] Rahman, K. M., & Schulz, S. E. (2002). Design of high-efficiency and high-torque-density switched reluctance motor for vehicle propulsion. *IEEE Transactions on Industry Applications*, *38*(6), 1500-1507.

[46] Zabihi, N., & Gouws, R. (2016, June). A review on switched reluctance machines for electric vehicles. In *2016 IEEE 25th International Symposium on Industrial Electronics (ISIE)* (pp. 799-804). IEEE.

[47] Shi, X., & Krishnamurthy, M. (2014). Survivable operation of induction machine drives with smooth transition strategy for EV applications. *IEEE Journal of Emerging and Selected Topics in Power Electronics*, *2*(3), 609-617.

[48] Tazerart, F., Mokrani, Z., Rekioua, D., & Rekioua, T. (2015). Direct torque control implementation with losses minimization of induction motor for electric vehicle applications with high operating life of the battery. *International journal of hydrogen energy*, *40*(39), 13827-13838.

[49] Guan, Y., Zhu, Z. Q., Afinowi, I. A., Mipo, J. C., & Farah, P. (2014, October). Comparison between induction machine and interior permanent magnet machine for electric vehicle application. In *2014 17th International Conference on Electrical Machines and Systems (ICEMS)* (pp. 144-150). IEEE.

[50] Murali, N., & Ushakumari, S. (2020, November). Performance comparison between different rotor configurations of PMSM for EV application. In *2020 IEEE REGION 10 CONFERENCE (TENCON)* (pp. 1334-1339). IEEE.

[51] Hassan, W., & Wang, B. (2012, June). Efficiency optimization of PMSM based drive system. In *Proceedings of The 7th International Power Electronics and Motion Control Conference* (Vol. 2, pp. 1027-1033). IEEE.

[52] Rauth, S. S., & Samanta, B. (2020, December). Comparative analysis of IM/BLDC/PMSM drives for electric vehicle traction applications using ANN-based FOC. In *2020 IEEE 17th India Council International Conference (INDICON)* (pp. 1-8). IEEE.

[53] Zeraoulia, M., Benbouzid, M. E. H., & Diallo, D. (2006). Electric motor drive selection issues for HEV propulsion systems: A comparative study. *IEEE Transactions on Vehicular technology*, *55*(6), 1756-1764.

[54] 'Indian Railways' IRFCA. [online] Available: https://www.irfca.org/gallery/Locos/Electric/wam4x/?g2_page=2. [Accessed 2023]

[55] [online] Available: https://www.speegovehicles.com/speego-cr.php. [Accessed 2023]

[56] [online] Available: https://www.tesla.com. [Accessed 2023]

[57] [online] Available: https://www.nissan.ca. [Accessed 2023]

[58] Barman, P., Dutta, L., Bordoloi, S., Kalita, A., Buragohain, P., Bharali, S., & Azzopardi, B. (2023). Renewable energy integration with electric vehicle technology: A review of the existing smart charging approaches. *Renewable and Sustainable Energy Reviews*, *183*, 113518.

[59] Omekanda, A. M. (2013, March). Switched reluctance machines for EV and HEV propulsion: State-of-the-art. In *2013 IEEE Workshop on Electrical Machines Design, Control and Diagnosis (WEMDCD)* (pp. 70-74). IEEE.

[60] Lukic, S. M., & Emado, A. (2003, September). Modeling of electric machines for automotive applications using efficiency maps. In *Proceedings: Electrical Insulation*

Conference and Electrical Manufacturing and Coil Winding Technology Conference (Cat. No. 03CH37480) (pp. 543-550). IEEE.

[61] Xu, W., Chen, H., Zhao, H., & Ren, B. (2019). Torque optimization control for electric vehicles with four in-wheel motors equipped with regenerative braking system. *Mechatronics*, *57*, 95-108.

[62] Vražić, M., Vuljaj, D., Pavasović, A., & Pauković, H. (2014, May). Study of a vehicle conversion from internal combustion engine to electric drive. In *2014 IEEE international energy conference (ENERGYCON)* (pp. 1544-1548). IEEE.

[63] Davis, R. I., & Lorenz, R. D. (2003). Engine torque ripple cancellation with an integrated starter alternator in a hybrid electric vehicle: implementation and control. *IEEE Transactions on Industry Applications*, *39*(6), 1765-1774.

[64] Ralev, I., Qi, F., Burkhart, B., Klein-Hessling, A., & De Doncker, R. W. (2017). Impact of smooth torque control on the efficiency of a high-speed automotive switched reluctance drive. *IEEE Transactions on industry applications*, *53*(6), 5509-5517.

[65] Wang, H., & Leng, J. (2018, June). Summary on development of permanent magnet synchronous motor. In *2018 Chinese Control And Decision Conference (CCDC)* (pp. 689-693). IEEE.

[66] Marlino, L. D. (2005). Report on Toyota Prius motor thermal management. Oak Ridge National Laboratory, 11-36.Petrov, I., & Pyrhonen, J. (2012). Performance of low-cost permanent magnet material in PM synchronous machines. *IEEE transactions on Industrial Electronics*, *60*(6), 2131-2138.

[67] Li, Z., Feng, G., Lai, C., Banerjee, D., Li, W., & Kar, N. C. (2019). Current injection-based multi-parameter estimation for dual three-phase IPMSM considering VSI nonlinearity. IEEE Transactions on Transportation Electrification, 5(2), 405-415.

[68] Ibrahim, M., & Pillay, P. (2018, September). Aligning the reluctance and magnet torque in permanent magnet synchronous motors for improved performance. In *2018 IEEE Energy Conversion Congress and Exposition (ECCE)* (pp. 2286-2291). IEEE.

[69] Yan, X., & Patterson, D. (1999, July). Improvement of drive range, acceleration and deceleration performance in an electric vehicle propulsion system. In *30th Annual IEEE Power Electronics Specialists Conference. Record.(Cat. No. 99CH36321)* (Vol. 2, pp. 638-643). IEEE.

[70] Li, M., He, J., & Demerdash, N. A. (2014, June). A flux-weakening control approach for interior permanent magnet synchronous motors based on Z-source inverters. In *2014 IEEE Transportation Electrification Conference and Expo (ITEC)* (pp. 1-6). IEEE.

[71] Bilgin, B., & Emadi, A. (2014). Electric motors in electrified transportation: A step toward achieving a sustainable and highly efficient transportation system. *IEEE Power Electronics Magazine*, *1*(2), 10-17.

[72] Ali, S. N., Hanif, A., & Ahmed, Q. (2016, January). Review in thermal effects on the performance of electric motors. In *2016 International Conference on Intelligent Systems Engineering (ICISE)* (pp. 83-88). IEEE.

[73] Zhang, Z., Li, G., Qian, Z., Ye, Q., & Xia, Y. (2016, June). Research on effect of temperature on performance and temperature compensation of interior permanent magnet motor. In *2016 IEEE 11th Conference on Industrial Electronics and Applications (ICIEA)* (pp. 411-414). IEEE.

[74] Zhang, B., Song, Z., Liu, S., Huang, R., & Liu, C. (2022). Overview of integrated electric motor drives: Opportunities and challenges. *Energies*, *15*(21), 8299.

[75] Akram, S., Wang, P., Nazir, M. T., Zhou, K., Bhutta, M. S., & Hussain, H. (2020). Impact of impulse voltage frequency on the partial discharge characteristic of electric vehicles motor insulation. *Engineering Failure Analysis*, *116*, 104767.

[76] [online] Available: https://electrical-engineering-portal.com. [Accessed 2023]

[77] Ost, W., & De Baets, P. (2005). Failure analysis of the deep groove ball bearings of an electric motor. *Engineering Failure Analysis*, *12*(5), 772-783.

[78] Wallscheid, O., Huber, T., Peters, W., & Böcker, J. (2014, October). Real-time capable methods to determine the magnet temperature of permanent magnet synchronous motors—A review. In *IECON 2014-40th Annual Conference of the IEEE Industrial Electronics Society* (pp. 811-818). IEEE.

[79] Schützhold, J., & Hofmann, W. (2013, September). Analysis of the temperature dependence of losses in electrical machines. In *2013 IEEE Energy Conversion Congress and Exposition* (pp. 3159-3165). IEEE

[80] Desai, C., & Pillay, P. (2019). Back EMF, torque–angle, and core loss characterization of a variable-flux permanent-magnet machine. *IEEE Transactions on Transportation Electrification*, *5*(2), 371-384.

[81] Schmitz, D., Sadowski, N., Nau, S. L., Batistela, N. J., & Bastos, J. P. A. (2014). Three-phase electromagnetic device for the evaluation of the magnetic losses in electric motors' stators. *IEEE Transactions on energy conversion*, *30*(2), 515-521.

[82] Muthusamy, M., & Pillay, P. (2021, October). Design of an Outer Rotor PMSM with Soft Magnetic Composite Stator Core. In *2021 IEEE Energy Conversion Congress and Exposition (ECCE)* (pp. 3987-3992). IEEE.

[83] Ilina, I. D. (2011, May). Experimental determination of moment to inertia and mechanical losses vs. speed, in electrical machines. In *2011 7th International Symposium on Advanced Topics in Electrical Engineering (ATEE)* (pp. 1-4). IEEE.

[84] Boglietti, A., Cavagnino, A., Staton, D., Shanel, M., Mueller, M., & Mejuto, C. (2009). Evolution and modern approaches for thermal analysis of electrical machines. *IEEE Transactions on industrial electronics*, *56*(3), 871-882.

[85] Nategh, S. (2013). *Thermal analysis and management of high-performance electrical machines* (Doctoral dissertation, KTH Royal Institute of Technology).

[86] Roy, P. (2020). Thermal Modeling of Permanent Magnet Synchronous Motors for Electric Vehicle Application (Doctoral dissertation, University of Windsor (Canada)).

[87] Bergman, T. L., Lavine, A. S., Incropera, F. P., & DeWitt, D. P. (2011). *Introduction to heat transfer*. John Wiley & Sons.

[88] Kirchgässner, W., Wallscheid, O., & Böcker, J. (2023). Thermal neural networks: Lumped-parameter thermal modeling with state-space machine learning. *Engineering Applications of Artificial Intelligence*, *117*, 105537.

[89] Madonna, V., Giangrande, P., Gerada, C., & Galea, M. (2019). Thermal analysis of fault-tolerant electrical machines for aerospace actuators. *IET Electric Power Applications*, *13*(7), 843-852.

[90] Kačenka, A., Pop, A. C., Vintiloiu, I., & Fodorean, D. (2019, October). Lumped parameter thermal modeling of permanent magnet synchronous motor. In *2019 Electric Vehicles International Conference (EV)* (pp. 1-6). IEEE.

[91] Wang, X., Li, B., Gerada, D., Huang, K., Stone, I., Worrall, S., & Yan, Y. (2022). A critical review on thermal management technologies for motors in electric cars. *Applied Thermal Engineering*, *201*, 117758.

[92] Boglietti, A., Cavagnino, A., & Staton, D. (2008). Determination of critical parameters in electrical machine thermal models. *IEEE transactions on Industry Applications*, *44*(4), 1150-1159.

[93] Nerg, J., Rilla, M., & Pyrhonen, J. (2008). Thermal analysis of radial-flux electrical machines with a high power density. *IEEE Transactions on industrial electronics*, *55*(10), 3543-3554.

[94] Tam, A. C., & Sontag, H. (1986). Measurement of air gap thickness underneath an opaque film by pulsed photothermal radiometry. *Applied physics letters*, *49*(26), 1761-1763.

[95] He, H., & Yu, Z. (2018). Effect of air gap entrapped in firefighter protective clothing on thermal resistance and evaporative resistance. *Autex Research Journal*, *18*(1), 28-34.

[96] Anderssson, B. (2013). Lumped parameter thermal modelling of electric machines.

[97] Yang, Y., Bilgin, B., Kasprzak, M., Nalakath, S., Sadek, H., Preindl, M., ... & Emadi, A. (2017). Thermal management of electric machines. *IET Electrical Systems in Transportation*, *7*(2), 104-116.

[98] Muthusamy, M., Hendershot, J., & Pillay, P. (2022). Design of a Spoke Type PMSM With SMC Stator Core for Traction Applications. IEEE Transactions on Industry Applications, 59(2), 1418-1436.

[99] Boylestad, R. L. (2010). Introductory circuit analysis. Prentice Hall Press.

APPENDIX

In this thesis, a different method was used to measure temperature parameters. As we know that copper resistance increases sensitively to temperature, winding resistance was measured during motor operation to estimate the temperature. According to the results, it was observed that the winding resistance increased as the operational temperature increased. Since it is necessary to stop the motor and cut off the power to read the resistance value during the experiment, the motor rapidly cooled down during this process and therefore it is not a suitable method for measuring temperature. Even so, seeing that the resistance value increased proved that losses will increase if the motor temperature increases.

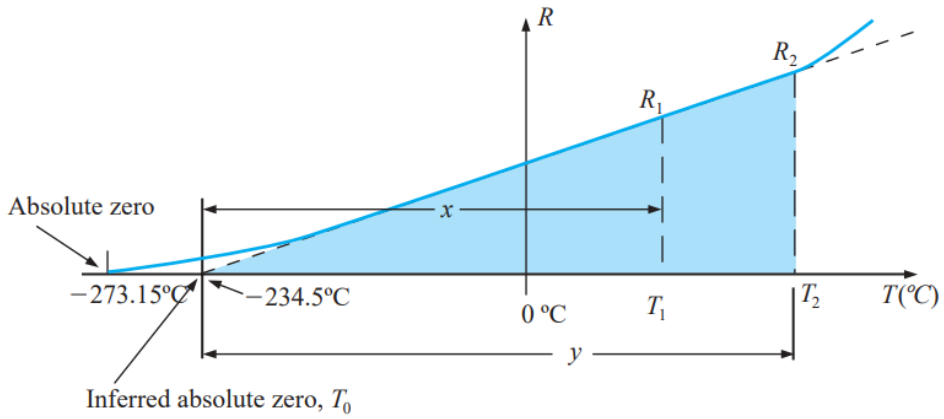

Figure 0.1A. Temperature and copper resistance relationship graph [99].

As seen in Figure 1A, copper resistivity increases depending on the temperature. So, the final temperature can be calculated when the initial values are known for two different cases. The formula is;

$$\frac{234.5 + T_1}{R_1} = \frac{234.5 + T_2}{R_2} \qquad (A.1)$$

-234.5 °C is inferred absolute temperature of copper. R1 is the initial resistance of copper and T1 is the initial temperature of the copper. So, if we now the resistance data we can calculate the

temperature. According to this information, a temperature graph was created for SPMSM after about 5 hours of experimentation. Although accurate results are obtained at low temperatures, it is not an effective method as the motor cools rapidly at high temperatures.

Table 0-1A. Resistance measurement table.

Rab (ohm)	Time (min)	Copper Temperature °C
0.486	0	23.8
0.511	30	35.8
0.52	60	41.88
0.524	90	44
0.526	120	45.07
0.528	150	46.13
0.528	180	46.13
0.529	210	46.66
0.529	240	46.66
0.53	270	47.19

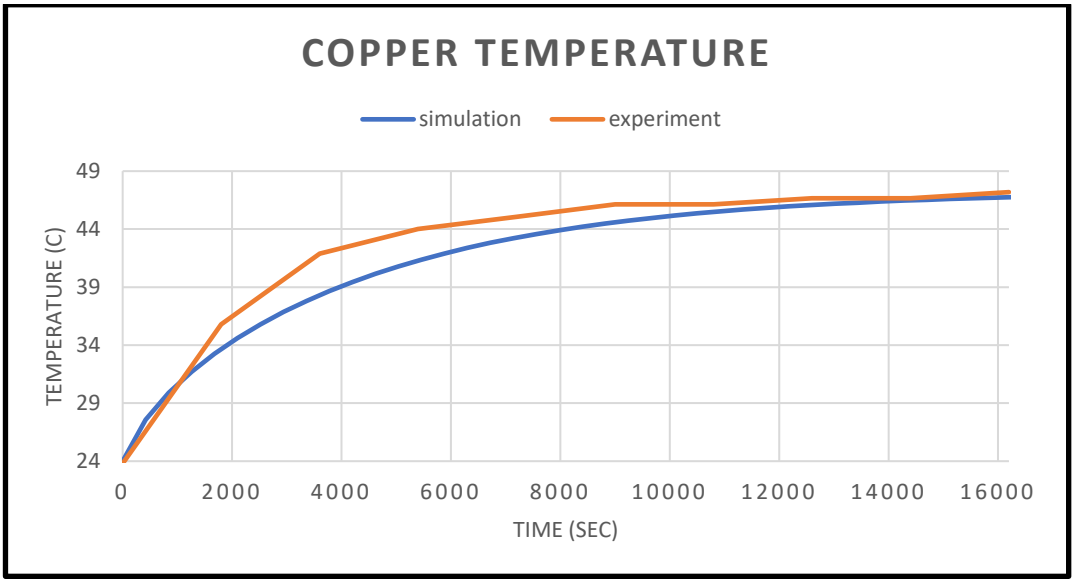

Figure 0.2A. Copper temperature graph.